CHARACTERIZATION OF *DROSOPHILA* NEMO KINASE, A CONSERVED MODULATOR OF WNT AND TGFβ SIGNAL TRANSDUCTION

by

Yi (Arial) Zeng
M.Sc., Jinan University, China 2000

THESIS
SUBMITTED IN PARTIAL FULFILLMENT OF
THE REQUIREMENTS FOR THE DEGREE OF
DOCTOR OF PHILOSOPHY

In the Department
of
Molecular Biology and Biochemistry

SIMON FRASER UNIVERSITY
Summer 2005

APPROVAL

Name:	**Yi Arial Zeng**
Degree:	Doctor of Philosophy (Science)
Title of Thesis:	Characterization of *Drosophila* Nemo kinase, a conserved modulator of Wnt and TGFβ signal transduction
Examining Committee:	
Dr. Barry Honda	**Chair** Professor, Department of Molecular Biology and Biochemistry, Simon Fraser University
Dr. Esther Verheyen	**Senior Supervisor** Associate Professor, Department of Molecular Biology and Biochemistry, Simon Fraser University
Dr. Nicholas Harden	**Supervisor** Associate Professor, Department of Molecular Biology and Biochemistry, Simon Fraser University
Dr. Nancy Hawkins	**Supervisor** Assistant Professor, Department of Molecular Biology and Biochemistry, Simon Fraser University
Dr. Bruce Brandhorst	**Internal Examiner** Professor, Department of Molecular Biology and Biochemistry, Simon Fraser University
Dr. William Brook	**External Examiner** Associate Professor, Department of Biochemistry and Molecular Biology, University of Calgary
Date Approved:	**July 26th, 2005**

SIMON FRASER UNIVERSITY

PARTIAL COPYRIGHT LICENCE

Abstract

The development of muticellular organisms requires precisely regulated cell-cell communication mediated by numerous signal transduction pathways. Regulatory "crosstalk" is essential in integrating the many inputs and stimuli that each cell receives, and ensuring that a cell responds appropriately.

Drosophila nemo (*nmo*) is the founding member of an evolutionarily conserved family of serine/threonine protein kinases kinases that are involved in several Wnt signal transduction pathways. Consistent with these findings, the detailed genetic analyses of the role of Nemo in *Drosophila* wing development support the proposed antagonistic role for Nemo in Drosophila Wingless (Wg) signaling pathway. In addition, I provide evidence that transcription of *nmo* is induced by high levels of Wg signaling in the developing wing disc. Our results indicate that Nemo acts as an intracellular feedback inhibitor of Wg during wing development and that it is a novel Wg target gene.

In this study, a novel function for Nemo in inhibition of Drosophila Bone Morphogenetic Protein (BMP) signalling is also revealed. Genetic interaction studies demonstrate that *nmo* can antagonize BMP signaling and can inhibit the expression of BMP dependent target genes during wing development. Nemo can bind to and phosphorylate the BMP effectors Mad and Medea. In cell culture, phosphorylation by Nemo blocks the nuclear translocation of Mad. Mutation of a single Nemo phosphorylation site in Mad relieves the inhibition of nuclear translocation, and causes ligand-independent nuclear translocation. This is the first example of inhibition of Drosophila BMP signaling by a MAPK and also represents an original mechanism of

Smad inhibition through phosphorylation of a conserved Serine residue within the MH1 domain of Mad.

In *Drosophila* wing imaginal disc development, Wg signalling pathway organizes the dorsal–ventral (DV) axis, while BMP signaling pathway is required to pattern the anterior-posterior (AP) axis. In the analyses of the roles of Nemo in Wg and BMP signaling pathways, a novel crosstalk between Wg and Dpp signaling is unveiled, in which Wg-dependent gene expression is suppressed by ectopic Dpp signaling. In addition, Arm and Mad compete for the binding of dTCF in cell culture. Consistently, in vivo, supplement of dTCF is able to rescue the suppression of Wg-dependent gene expression caused by ectopic Mad. Our results suggest a novel mechanism that Dpp represses Wg target gene by influencing the binding of Arm and dTCF.

Dedication

To Dad

Acknowledgements

I wish to express my utmost gratitude to my senior supervisor and my mentor, Dr. Esther Verheyen, for giving me the opportunity to study in her lab, and being extremely supportive over the last four years. Words cannot describe my appreciation to her. I am grateful to Dr. Nicholas Harden and Dr. Nancy Hawkins, both members of my committee, for their helpful suggestion and their kind words of encouragement.

I would like to extend my sincerest thanks and appreciation to members of the Verheyen and the Harden laboratories, past and present, for their assistance and support throughout my studies. I am grateful to Sheila MacLean, Adrian Ally and Darrell Bessette for teaching me various techniques at the beginning of my study. I thank Bryan Andrews for all his help with the bioinformatics. I thank Wendy Lee and Wolanyo Sosu-Sedzorme for their unconditional support and being wonderful friends. I thank Maryam Rahnama for her technical assistance and her hard work in making many constructs. I thank Bari Zahedi and Minna Roh for their friendship and support in times of difficulty. I thank Ryan Conder and Simon Wang for always being ready to help.

I am also grateful to members of Michel Leroux laboratory for the generosity with their equipments, without which my cell culture studies in this thesis would not have been possible. In particular, I would like to thank Muneer Esmail and Junchul Kim for all of their experimental advice and helpful discussion.

A special thanks goes to my friend, Yang Ying. She has been the cornerstone on which I can always find support in difficult times.

My heartfelt gratitude goes to my parents for their unfailing love and financial support throughout my education. I am also indebted to Wengang He for his immense support, commitment and sacrifice over the past years.

Table of Contents

List of Figures

Chapter 1

General Introduction

1.1 Signal transduction pathways

Cell behavior is regulated by a complex network of intracellular and extracellular signal transduction pathways. A signal transduction pathway is a cascade of information relayed from the plasma membrane to the nucleus in response to an extracellular stimulus in living organisms. Specifically, an extracellular signaling molecule binds to a specific transmembrane receptor, and initiates the signal pathway. Cell-cell communication regulated by signal transduction pathways is essential for many biological processes ranging from developmental patterning to the regulation of cell proliferation and cell death.

In the past two decades, many studies have rapidly increased our understanding of molecular mechanisms that mediate intercellular signal transduction. To date, many components in signal transduction have been identified and regulatory mechanisms have

been modeled. We are now beginning to understand how such pathways are initiated, controlled, and communicate with each other.

1.2 *Drosophila* wing development as a model system for studying signal transduction

Drosophila melanogaster has been used extensively as a model system in experimental studies of genetics, development and signal transduction due to its short life cycle, ease of manipulation and extensive genetic characterization. Moreover, the substantial functional conservation between human and *Drosophila* genes makes it possible to extend the insight gained from *Drosophila* gene research to its human orthologs.

Drosophila wing development is an excellent model for the study of epithelial morphogenesis and signal transduction. The wing is non-essential, therefore wing development is amenable to genetic analyses, as witnessed by the vast amount of homozygous viable wing mutations. The *Drosophila* adult wing shows a rather simple pattern of five longitudinal and two transverse veins (Fig. 1.1A). The large size of wing facilitates the process of genetic screening and scoring of mutant phenotypes. The wing is also attractive from the developmental and cell biological perspective. Wing morphogenesis is a relatively simple process involving the conversion of a single layered columnar epithelium to a flattened bilayer where the basal surfaces of dorsal and ventral epithelia are in close contact (Brabant et al., 1996; Fristrom et al., 1993).

The *Drosophila* imaginal disc comprises ~20 cells when it is formed during embryonic development. These cells proliferate during the three larval stages (the first,

second instar and third instar) to generate ~75,000 cells in the late third instar larva (Klein, 2001). The disc is considered as a monolayered epithelium, therefore pattern formation occurs in a two-dimensional layer. Two major patterning centres are formed at the beginning of the third instar larval stage. They are the boundaries of the dorsoventral (DV) and anteroposterior (AP) compartments (Fig. 1.1B). By the late third instar, with the help of appropriate molecular markers, one can already observe the major elements, future hinge, blade and margin (Fig. 1.1B). Also during the third larval instar, vein formation is initiated in the wing imaginal disc. Gene expression in veins is initiated as a series of parallel stripes (Fig. 1.1C) (Klein, 2001). During the early pupal stage, the monolayer of wing disc cells protrudes out and folds into a bilayer along a line which become the future margin of the wing. The stripes of longitudinal vein primodia bend back and the dorsal and ventral vein cells communicate with one another during pupal development via various inductive signals in order to align precisely. Cross-veins are also formed during the pupal stage (Bier, 2000b).

Where and how vein cells appear and differentiate is determined by the ordered contribution of mutiple cell signal transductions and subsequently transcriptional regulation. Many conserved signaling pathways converge and integrate during wing development. These pathways including Notch (N), Wingless (Wg), TGFβ/BMPs, Hedgehog (Hh) and EGF exert their effects on both global and localized patterning. Although many of the components of these pathways have been identified, how they are integrated to establish precise positional information during development is not well understood.

Figure 1.1 *Drosophila* wings

(A) Wild type *Drosophila melanogaster* wing showing the longitudinal veins (L1-L6) and the transverse veins, anterior cross vein and posterior cross vein (acv, pcv). A indicates antiror compartment and P indicates posterior compartment of the adult wing.

(B) Major elements of the wing highlighted by Wg (red) and Dpp (green) expression in late third instar wing disc. Wg is expressed in two ring-like domains in the hinge region and along the DV boundary dividing the wing blade. The inner ring domain frames the wing blade. The domain along the DV boundary corresponds to the future wing margin. Wg is also expressed in the dorsal part of the disc, which will become the notum of the fly. Dpp is expressed along the AP boundary.

(C) The positions of vein primordia corresponding to longitudinal veins L2-L5 are indicated.

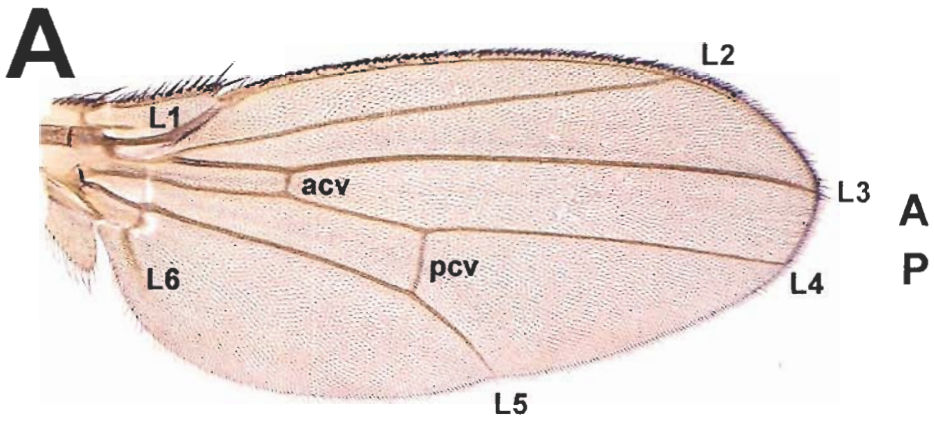
A
L1
L2
L3
L4
L5
L6
acv
pcv
A
P

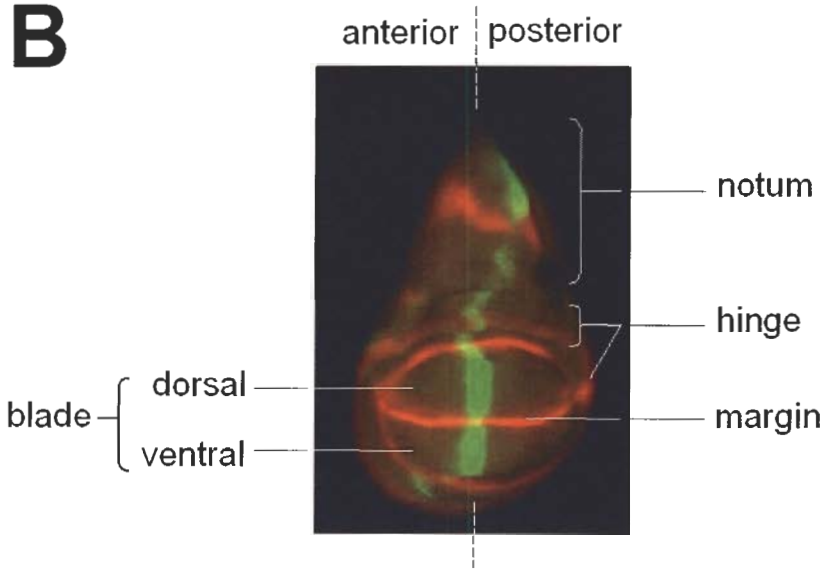
B
anterior
posterior
notum
hinge
margin
blade
dorsal
ventral

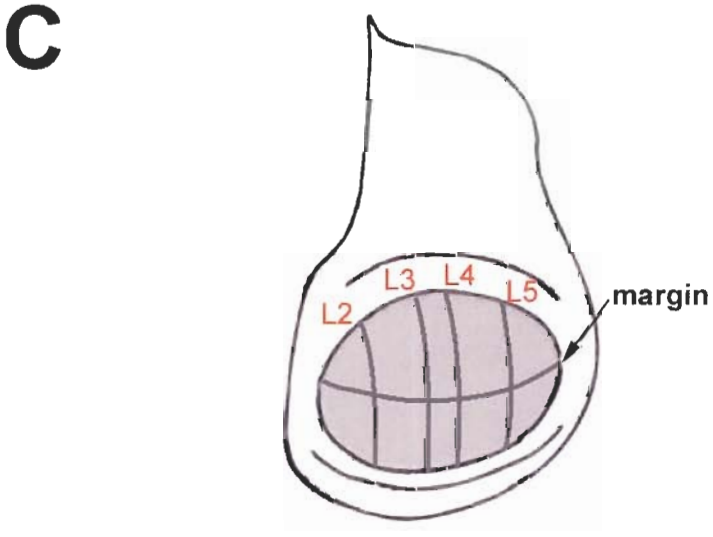
C
L2
L3
L4
L5
margin

1. 3 Drosophila Nemo

Drosophila nemo (*nmo*) was first identified as a gene required for epithelial planar polarity (EPP) during ommatidial development, a process known to involve the Frizzled (Fz) receptor, which is proposed to signal through a noncanonical Wnt pathway (Choi and Benzer, 1994; Mlodzik, 2002). Subsequent analysis has shown that Nemo functions in multiple tissues and has diverse roles in development. In addition to its effect on eye polarity, previous research from our lab have suggested that disruption of *nmo* results in changes in wing shape and size, wing vein specification, fertility and viability (Verheyen et al., 2001). *nmo* is essential for embryonic development as loss of maternal and zygotic *nmo* results in embryonic lethality characterized by patterning defects in the head and ventral denticle belts as well as disruption of apoptosis (Mirkovic et al., 2002).

Nemo is the founding member of an evolutionarily conserved family of proline-directed serine/threonine protein kinases. The predicted amino acid sequence of Nemo has 37–41% homology to Extracellular-signal regulated kinases/mitogen activated protein kinases (Erk/MAPKs) and cyclin-directed kinases (Cdks), and is thus more closely related to these kinases than to other families of kinases (Choi and Benzer, 1994). Nemo differs from the Erk/MAPKs and Cdks in its longer carboxy-terminal regions and the amino acid sequence (TQE) in the phosphorylation lip in the conserved kinase domain is unlike that of either the Erk/MAPKs or Cdks (Choi and Benzer, 1994). Most typical MAP kinases possess a TxY motif that is dually phosphorylated at threonine and tyrosine. The Nemo TQE site contains a glutamic acid instead of a tyrosine and such an amino acid substitution often mimics a phosphorylated residue. This sequence suggests

that Nemo may be partially active and may require only phosphorylation on the threonine (T) residue in order to be fully activated. Based on its sequence, Nemo therefore appears to be a member of an extended family of Erk/MAPK-like and Cdk-like kinases (Brott et al. 1998).

My graduate study has been focused on characterizing *Drosophila* Nemo in Wg and TGFβ signaling pathways. Through detailed genetic and biochemical analyses, novel roles of Nemo in these two pathways have been established. Furthermore, insights gained from studies of Nemo lead to the discovery of a previously unidentified mechanism of Wg and TGFβ signaling crosstalk.

Chapter 2

Nemo is an inducible antagonist of Wingless signaling during *Drosophila* wing development

2.1 Introduction

2.1.1 Wnt and Drosophila Wingless signaling pathway

Wnt proteins were first identified by their association with mammary tumors in mice (Nusse and Varmus, 1982). Wnt signals are pleiotropic, with effects that include mitogenic stimulation, cell fate specification, and differentiation in many organisms, from the nematode *C. elegans* to mammals (Cadigan and Nusse, 1997; Logan and Nusse, 2004). Components of Wnt signal transduction pathways are highly conserved in evolution and can participate in either canonical or non-canonical pathways (the Wnt homepage: http://www.stanford.edu/~rnusse/wntwindow.html). The noncanonical pathways, which do not involve β-catenin or Wnt ligands, have been implicated in tissue polarity or epithelial planar polarity (EPP) signaling. My studies mainly focused on Wnt

signaling through its receptors (Frizzleds) to β-catenin, which is often called the canonical pathway.

wingless (*wg*), which participates in the canonical signaling pathway, is the best-characterized of the seven *Drosophila* Wnt genes. A simple outline of the current model of Wg signal transduction is presented in Figure 2.1.1. Pathway activation occurs when the secreted Wg protein is received by the Frizzled (Fz)/ low density lipoprotein (LDL) receptor-related protein (LRP) complex at the cell surface. This, in turn, leads to activation of Dishevelled, which inhibits the action of a protein complex including glycogen synthase kinase 3β (GSK3 or *Drosophila* Zw3), Axin and APC (reviewed by Cadigan and Nusse, 1997). In the absence of Wg signaling, cytoplasmic β-catenin (*Drosophila* Armadillo, Arm) levels are normally kept low through continuous proteasome-mediated degradation, which is controlled by a complex containing Zw3/APC/Axin. (Aberle et al., 1997; Willert et al., 1999; Yost et al., 1996; Logan and Nusse, 2004). Wg signaling results in down regulation of Zw3 kinase activity which allows Arm to escape degradation and accumulate in the cytoplasm. Subsequently, Arm can proceed into the nucleus where it forms a complex with dTCF, a member of the lymphoid enhancer factor 1 (LEF1)/T-cell factor (TCF) family of transcription factors, and participates in transcriptional activation of Wg target genes (Brunner et al., 1997; van de Wetering et al., 1997).

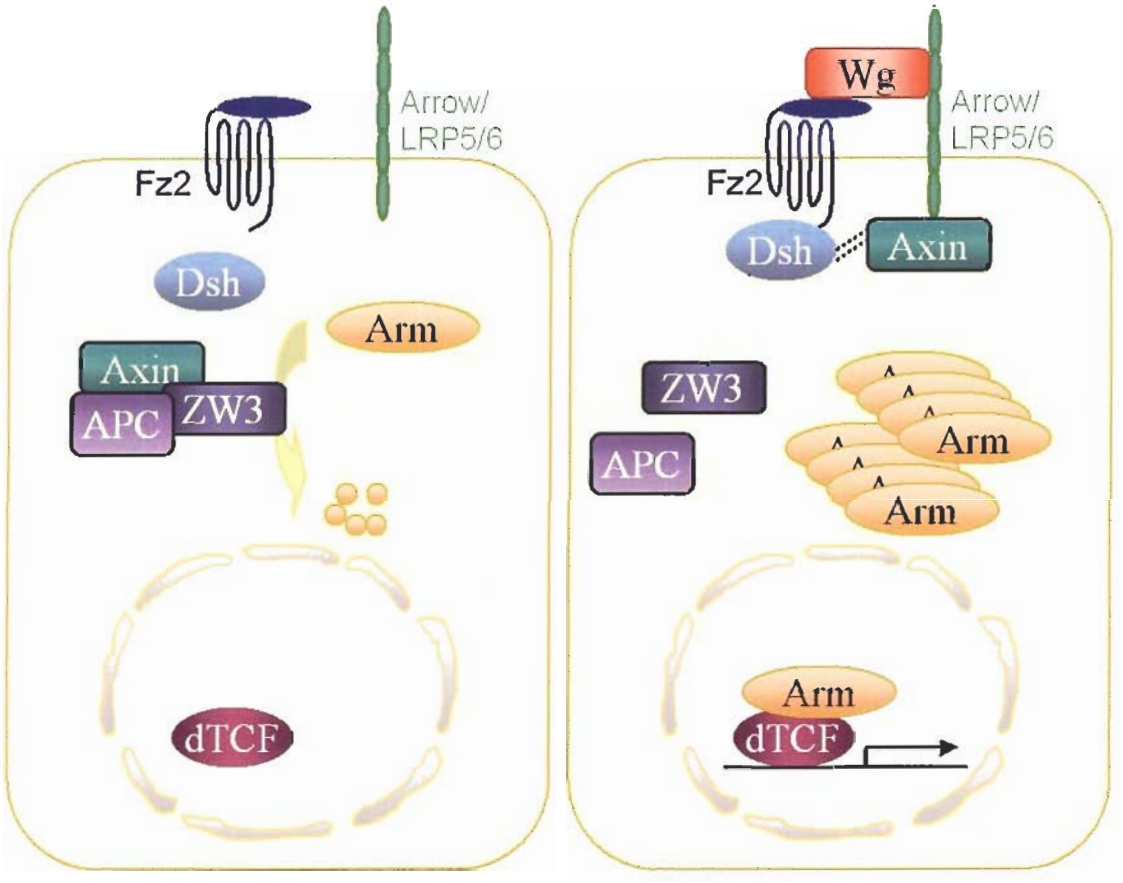

Figure 2.1.1 The canonical Wnt signaling pathway.

In the absence of Wnt signal (*left panel*), Arm is degraded through interactions with Axin, APC, and Zw3. Upon Wg signaling (right panel), Wg protein binds to the Frizzled/LRP receptor complex at the cell surface. These receptors transduce a signal to Dishevelled (Dsh) and to Axin, which may directly interact (*dashed lines*). As a consequence, the degradation of Arm is inhibited. Arm thus accumulates in the cytoplasm and proceeds into the nucleus and interacts with TCF to control target gene transcription. Negative regulators are outlined in black.

Wg function is required throughout *Drosophila* development in a wide range of patterning events (Cadigan and Nusse, 1997). Mutations disrupting *wg* result in lethality and defects in patterning as displayed by the loss of naked cuticle in the ventral epidermis of the embryo (Bejsovec and Martinez, 1991). During wing development, Wg signaling plays at least two distinct roles. Early reductions of *wg* result in wing-to notum transformations, indicating a requirement for Wg in defining the wing blade (Morata and Lawrence, 1977; Ng et al., 1996). Later reductions cause wing margin notching due to tissue loss, indicating the subsequent role of Wg in specifying the margin and organizing wing development (Couso et al., 1994; Diaz-Benjumea and Cohen, 1995; Rulifson and Blair, 1995). In late third larval instar wing imaginal discs, Wg is expressed in a narrow stripe of three to six cells straddling the dorsoventral (DV) boundary of the future wing blade (Baker, 1988; Couso et al., 1994; Williams et al., 1993). Directly adjacent to the stripe, Wg regulates the expression of high threshold (or short-range) target genes, including *achaete* (*ac*) and *neuralized* (*neur*) (Phillips and Whittle, 1993; Couso and Arias, 1994; Zecca et al., 1996). In addition to these targets of Wg signaling, *Distal-less* (*Dll*) is expressed in a Wg-dependent manner in a wider domain radiating from the thin DV stripe (Zecca et al., 1996).

2.1.2 TCF, β-catenin families and their interactors

The founding members of the TCF/ LEF family of transcription factors, TCF-1 and LEF-1, were identified in screens for T cell-specific transcription factors (van de Wetering *et al.,* 1991; Oosterwegel *et al.,* 1991; Travis *et al.,* 1991; Waterman *et al.,* 1991). Subsequently, two additional family members were identified in mammals: *TCF-3* and *TCF-4* (Korinek et al., 1998). The *Drosophila* genome only contains one TCF gene,

called *dTcf* or *pangolin* (*pan*) (Brunner et al., 1997; van de Wetering et al., 1997). Similarly, a single gene resides in the genome of the nematode *Caenorhabditis elegans, pop-1* (Lin et al., 1995). Proteins of the TCF/LEF family contain a sequence-specific high mobility group (HMG) box that binds DNA as monomers (van de Wetering et al., 1991) (Fig. 2.1.2A). The TCF consensus recognition sequence is remarkably conserved between the family members and comprises AGATCAAAGGG (van de Wetering *et al.,* 1991; Giese *et al.,* 1991; van Beest *et al.,* 2000). TCF/LEF family members by themselves do not regulate transcription.

β-catenin is the first protein found to interact with TCF/LEF factors (Behrens et al., 1996; Molenaar et al., 1996). All members of the TCF family can bind β-catenin through a conserved N-terminal stretch of 55 amino acids. β-catenin thus functions as a classical coactivator of transcription. The primary structure of β-catenin consists of acidic amino and carboxyl termini, and a highly basic central region containing 12 imperfect sequence repeats that are known as Armadillo repeats (Arm repeats) (Fig. 2.1.2B). The amino terminus of β-catenin is known to be important for regulating the stability of β-catenin (Barth et al., 1997; Munemitsu et al., 1996; Yost et al., 1996), whereas the carboxyl terminus functions as a transcriptional activation domain when fused to the GAL4 DNA-binding domain (van de Wetering et al., 1997). The Arm repeats pack against each other to form a positively charged groove (Huber et al., 1996). The Arm repeat domain provides binding sites for APC, Axin, E-cadherin (E-cad), and TCF4 (Fig. 2.1.2B). APC, E-cadherin and TCF4 are known to bind competitively to β-catenin, despite lack of significant sequence homology (Hulsken et al., 1994; Omer et al., 1999). These interactors bind to largely overlapping regions of the positively charged groove of

β-catenin (Eklof Spink et al., 2001; Graham et al., 2001; Graham et al., 2000; Huber and Weis, 2001; Xing et al., 2003). Legless (Lgs), identified as a presumptive adaptor protein of β-catenin, requires the first four Arm repeats for binding to Arm (Hoffmans and Basler, 2004; Kramps et al., 2002). Lgs mediates signalling activity by recruiting the transcriptional activator Pygopus (Pygo) (Townsley et al., 2004).

In 1997, two labs independently cloned the fly homologue of TCF, *dTcf* (van de Wetering *et al.*, 1997; Brunner *et al.*, 1997). dTCF binds a TCF DNA motif and, together with the fly β-catenin homologue Armadillo, transactivates transcription of reporter genes. In *Drosophila*, the CREB-binding protein (CBP) interacts with the HMG box domain of dTCF and acetylates a conserved lysine in the Armadillo-binding domain of TCF. This acetylation lowers the affinity of dTCF for Arm (Waltzer and Bienz, 1998). Furthermore, in both *C. elegans* and mammalian cells, the Nemo-like kinases LIT-1 and NLK, respectively, phosphorylate LEF-1/TCF. Phosphorylation inhibits LEF-1/TCF signaling by disruping DNA binding (Ishitani, 1999) and by inducing redistribution of POP-1 from the nucleus to the cytoplasm (Rocheleau, 1999).

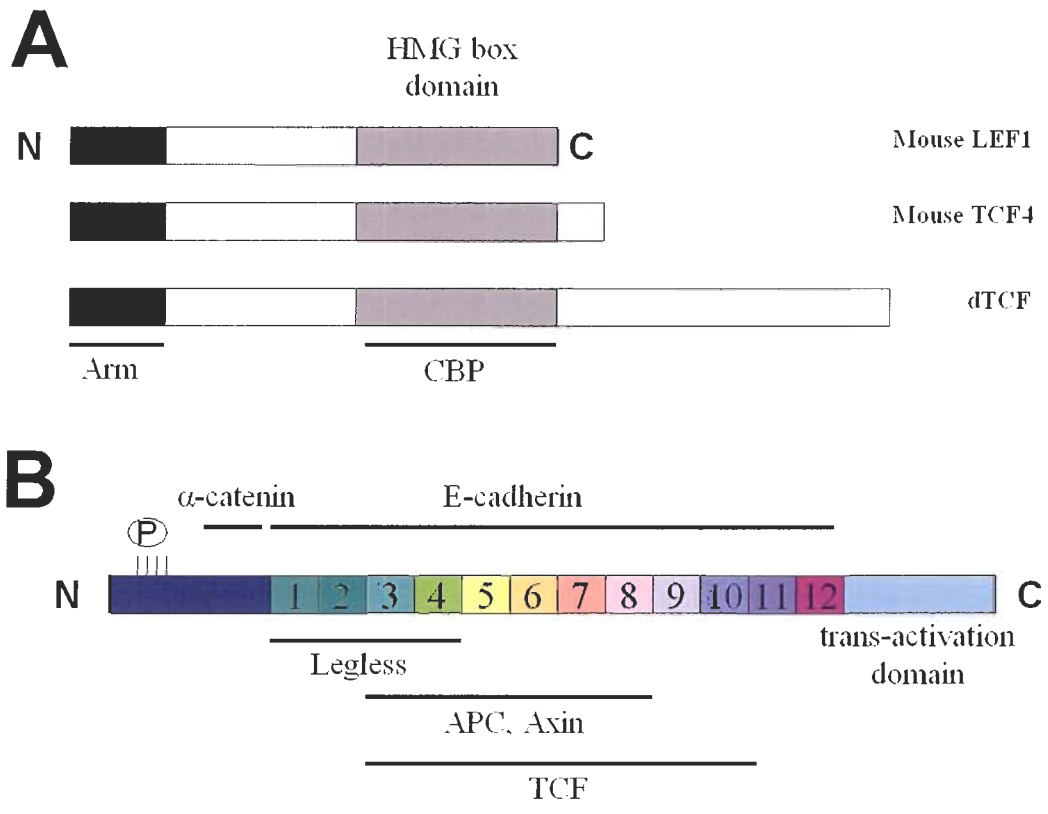

Figure 2.1.2 Schematic representation of TCF and the β-catenin protein

(A) TCFs contain sequence-specific high mobility group (HMG) box that binds DNA. Black lines outline the binding domains of dTCF interaction partners, Arm and CBP.

(B) The Arm repeats are marked by different colours and numbered 1-12. Black lines represent the binding domains of β-catenin interaction partners. P marks the phosphorylation sites used by the degradation complex. The C terminus is the trans-activation domain.

2.1.3 Feed back inhibitors of Wg signaling

In addition to extrinsic regulatory factors, inducible feedback loops have been found for most conserved signal transduction pathways controlling development (Freeman, 2000). In *Drosophila*, two inducible inhibitors of Wg signaling have been described that target distinct steps in the pathway. *naked cuticle* (*nkd*) encodes a cytoplasmic protein that binds to Dsh and blocks accumulation of Arm in response to Wg signaling during embryonic patterning and eye development (Rousset et al., 2001; Zeng et al., 2000). Conversely, *wingful* (*wf*) encodes a secreted extracellular feedback inhibitor that acts non-autonomously during larval imaginal disc development to inhibit Wg (Gerlitz and Basler, 2002).

2.1.4 Nemo-like kinases (Nlks)

Nemo homologs (referred to as Nemo-like kinases, NLKs) have been studied in many other model organisms, including the murine and human Nemo-like kinases (Nlk), *C. elegans* LIT-1, *Fugu rubripes* NLK and *Xenopus* xNLK (Brott et al., 1998; Harada et al., 2002; Hyodo-Miura et al., 2002; Kehrer-Sawatzki et al., 2000; Meneghini et al., 1999; Rocheleau et al., 1999). NLKs can exert an inhibitory effect on the gene regulation activity of TCF/LEF transcription factors (Ishitani et al., 1999; Rocheleau et al., 1999; Shin et al., 1999). Nlk mediates phosphorylation of TCF and inhibits the DNA-binding ability of the TCF/β-catenin complex (Ishitani et al., 1999). In a *C. elegans* non-canonical pathway, activation of the LIT-I kinase requires WRM-1, a β-catenin-like protein, and

leads to phosphorylation of LIT-1 and WRM-1 and subsequent phosphorylation and inhibition of a nematode TCF, POP-1 (Rocheleau et al., 1999).

NLKs have been found to participate in both canonical and non-canonical Wnt pathways. In *C. elegans*, LIT-1 has been found to play roles in cell polarity and cell fate decisions, two processes regulated by distinct Wnt pathways (Ishitani et al., 1999; Meneghini et al., 1999; Rocheleau et al., 1999). Analysis of NLK function in *Xenopus* oocyte axis formation assays has shown that injection of murine *Nlk* and *xNLK* mRNAs can block axis formation and can rescue the axis duplication induced by β-catenin or Wnt (Hyodo-Miura et al., 2002; Ishitani et al., 1999).

Consistent with these findings, genetic and phenotypic analyses in *Drosophila* support the proposed role for Nemo in both canonical and non-canonical Wnt signaling pathways. In addition to its role in the non-canonical Fz pathway regulating epithelial planar polarity (EPP) in the eye, wing and abdomen (Choi and Benzer, 1994; Strutt et al., 1997; Verheyen et al., 2001), preliminary evidence has previously been reported that modulating levels of *nmo* results in phenotypes consistent with a role as a Wg-antagonist (Verheyen et al., 2001).

2.1.5 Summary of the chapter

In this chapter, I present a thorough study of the role of Nemo in *Drosophila* canonical Wg signaling. Through detailed genetic analysis it is observed that *nmo* is an antagonist of Wg during larval wing disc development and that Nemo can negatively influence Wg-dependent gene expression. Nemo associates and phosphorylates dTcf and Arm in cell culture. In addition, I present evidence that transcription of *nmo* is induced by

high levels of Wg signaling in the developing wing disc. Finally, I show that cellular levels of Armadillo protein can be controlled by Nemo, such that ectopic Nemo leads to reductions in stabilized Arm. Our results indicate that Nemo is an intracellular inducible feedback antagonist of the Wingless signaling pathway that is involved with refining the Wg activity gradient during wing development.

2.2 Results

2.2.1 *nmo* expression in wing imaginal discs flanks the Wg expression domain

The *nmo* gene plays a role in the development of the wing. Homozygous *nmo* mutant flies display abnormal wing patterning characterized by alterations in wing size and shape and the presence of extra vein material along the longitudinal veins and emanating from the posterior crossvein (see Fig. 2.2.2D) (Verheyen et al., 2001). During pupal wing development, *nmo* is expressed in intervein regions of the wing blade, where it presumably acts to suppress vein development (Verheyen et al., 2001). To better understand the role of *nmo* in earlier patterning events, we determined its localization pattern in larval wing imaginal discs in the nmo^{P} enhancer trap line, *nmo-lacZ* (Fig. 2.2.1A-C) (Choi and Benzer, 1994). The expression of *nmo* is quite dynamic during larval development. Staining of second instar larval discs reveals very weak expression at the anterior and posterior periphery of the wing disc (Fig. 2.2.1A). Early in the third larval stage, staining at the DV boundary becomes evident (Fig. 2.2.1B) and the intensity of the staining increases with age. In late third instar discs, *nmo* is expressed in two thin stripes flanking the DV boundary (Fig. 2.2.1C). These two stripes of staining are weaker at the point where the anteroposterior (AP) boundary intersects the DV boundary. *nmo* expression is also seen in a ring encircling the future wing pouch in a tissue corresponding to the future proximal wing hinge, with the expression in the dorsal ring appearing darker than the ventral ring. Staining is also seen in the primordia of longitudinal wing veins 3, 4 and 5, beginning in the late third instar stage (arrowheads in

Fig. 2.2.1C). Finally, *nmo* expression is also detected in spots on the wing imaginal discs that represent sites of sensory organ formation on the future notum (arrow in Fig. 2.2.1C). Consistent with such an expression pattern, we have previously shown a role for *nmo* in macrochaete bristles, as demonstrated by genetic interactions with *Hairless* (Verheyen et al., 2001).

Whole-mount RNA in situ hybridization carried out by Dr. E.M. Verheyen confirms that this enhancer trap insertion accurately represents the expression of *nmo* (Fig. 2.2.1D). In addition to the localized staining seen in the enhancer trap, low level ubiquitous staining is detected throughout the disc. This ubiquitous staining is also apparent when anti-β-galactosidase antibody is used to detect the *nmo-lacZ* expression pattern (see Fig. 2.2.1E, F).

The *nmo-lacZ* pattern is reminiscent of the Wg expression pattern in imaginal discs (Rulifson et al., 1996). To examine the relationship between the two expression patterns, we performed double staining for β-galactosidase and Wg protein. This staining reveals that *nmo* expression at the DV boundary flanks the Wg protein domain in late third instar wing discs (Fig. 2.2.1E-G). Wg protein is detected in a narrow stripe along the presumptive wing margin (Fig. 2.2.1G) and *nmo* is seen in the cells directly adjacent to the Wg-expressing cells (Fig. 2.2.1E). In addition, *nmo* is detected in the ring domain overlapping with the Wg inner ring expression domain that encircles the wing pouch (Fig. 2.2.1F). Such a localization for *nmo* is also consistent with the observed defect in adult flies in which the wing is held away from the body at an angle and may reflect a hinge defect (Verheyen et al., 2001).

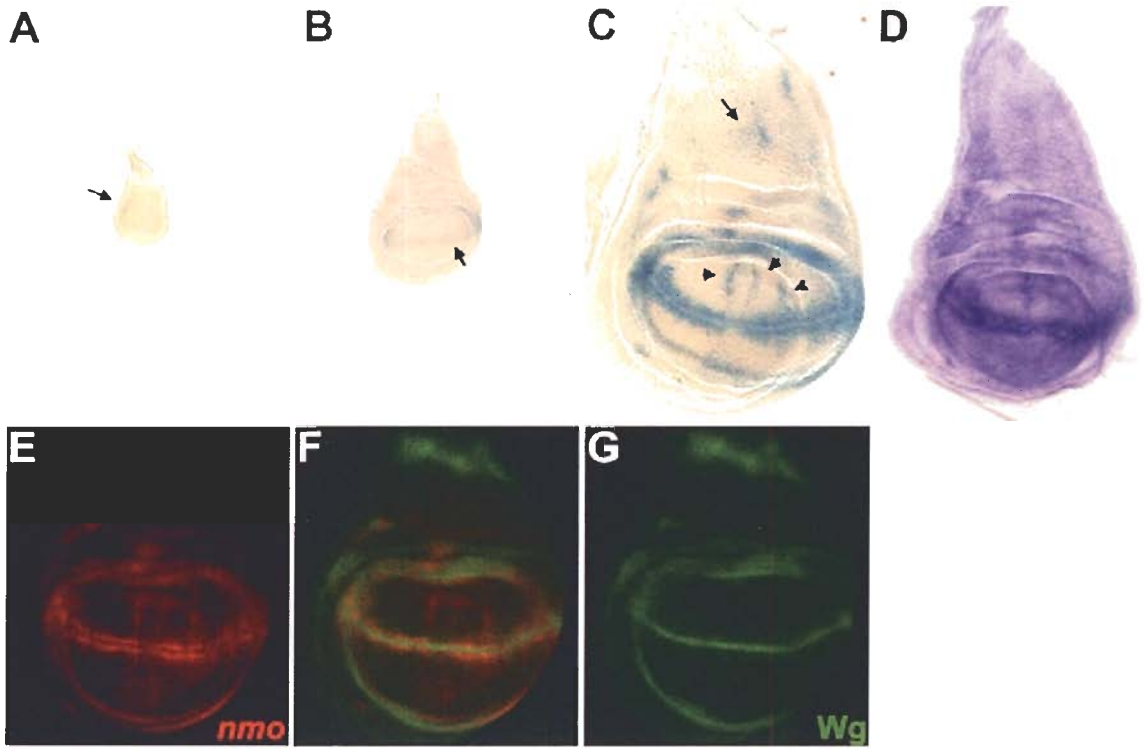

Figure 2.2.1 *nmo* expression in the wing imaginal disc

nmo expression was examined in *nmo-lacZ* flies . (A) In second instar discs, weak *nmo* expression is seen at the periphery of the future wing pouch (arrow). (B) In early third instar discs low level expression is at the DV boundary (arrow) and encircling the wing pouch. (C) In late third instar, high levels of *nmo* expression are seen in two stripes flanking the DV boundary and in a ring around the pouch. *nmo* is also seen in the L3, L4 and L5 vein primordia (arrowheads) and in several spots in the presumptive notum (arrow). (D) In situ hybridization using an antisense *nmo* RNA probe. (E-G) Co-localization with Wg. Discs were double stained with (E) anti-β-gal and (G) anti-Wg antibodies and the images were merged to show overlap (F). Wing imaginal discs are orientated anterior to the left, dorsal side up.

2.2.2 *nmo* antagonizes Wg signaling during wing development

Based on the expression pattern of *nmo* and data suggesting a role in Wnt signal transduction, we investigated the role of Nemo in Wg signaling using a combination of approaches, involving ectopic expression, mutant analysis, somatic loss-of function clones and ectopic flip-out misexpression clones (Brand and Perrimon, 1993; Ito et al., 1997; Xu and Rubin, 1993). Wg is expressed along the presumptive wing margin where it is required for proneural *achaete-scute* (*AS-C*) complex gene expression and for the formation of margin bristles. Loss of Wg signaling along the wing margin leads to loss of these margin bristles and the appearance of notches along the wing margin (Couso et al., 1994; Phillips and Whittle, 1993; Rulifson et al., 1996). Ectopic expression of *UAS-nmo* in the wing using either *scalloped-Gal4* (referred to as *sd>nmo*) or *omb-Gal4* also produces such a wing notching effect (Fig. 2.2.2B, and data not shown), suggesting Nemo plays an antagonistic role in the pathway. A similar wing notching phenotype is seen when either *71B-Gal4* or *69B-Gal4* is used to drive expression of the Wg inhibitor Daxin (Hamada et al., 1999; Willert et al., 1999). The observed wing margin loss seen in *sd>nmo* flies is completely suppressed when flies are heterozygous for the $zw3^{m11}$ loss-of-function allele (Fig. 2.2.2C), consistent with the antagonistic role that Zw3 plays in Wg signaling and with the speculation that the effect of *nmo* is due to blocking the action of Wg.

To extend this study, we examined whether loss of *nmo* or ectopically expressed Nemo is able to suppress defects caused by overexpression of Wg pathway components. Ectopic expression of Dfz2N, a dominant-negative form of the *Drosophila* Frizzled 2 receptor (Zhang and Carthew, 1998) using the *sd-Gal4* driver induces a tiny wing

phenotype characterized by loss of the wing margin and significant amounts of wing blade (Fig. 2.2.2E). Flies homozygous for nmo^{DB24}, a putative null allele of *nmo*, have a broader, shorter wing than wild type and ectopic vein material near longitudinal vein 2 and 5 and emanating from the posterior cross vein (Fig. 2.2.2D) (D. Bessette and E.M.V., unpublished). The *sd>Dfz2N* phenotype is significantly suppressed when flies are homozygous for nmo^{DB24}, resulting in restoration of most wing margin structures as well as wing blade tissue (Fig. 2.2.2F). Furthermore, we found that nmo^{DB24} also suppresses the effects of Daxin in a dose-sensitive manner (Fig. 2.2.2G-L). *sd>Daxin* causes wing-to-notum transformations (Fig. 2.2.2G) that can be rescued to a small wing by heterozygosity for nmo^{DB24} (Fig. 2.2.2H). Stronger suppression is detected in homozygous nmo^{DB24} flies, in which the ectopically produced nota are completely suppressed and the wing blade is partially restored, particularly in the anterior wing margin (Fig. 2.2.2I). The same dose-sensitive suppression is observed when the dorsally expressed *ap-Gal4* driver was used to drive Daxin. *ap>Daxin* induces a tiny blistered wing pouch (Fig. 2.2.2J). Heterozygosity for nmo^{DB24} in this background partially rescues the pouch defect (Fig. 2.2.2K), while nmo^{DB24} homozygosity strongly rescues the wing blisters and abnormal appearance (Fig. 2.2.2L). These data suggest that the block in Wg signaling caused by ectopic Daxin can be suppressed by the absence of *nmo* function.

Additional evidence supporting the involvement of Nemo as a negative player in the Wg pathway comes from examining interactions with Arm. *UAS-fluΔarm* encodes an N-terminally truncated, constitutively active form of Arm (Tolwinski and Wieschaus, 2001; Zecca et al., 1996). Using *71B-Gal4* to drive *UAS--fluΔarm* causes a very abnormal wing (Fig. 2.2.2M) characterized by excess margin bristles throughout the wing blade,

loss of veins and a smaller crumpled wing blade, similar to the abnormal wing seen with ectopic expression of LEF-1 (Riese et al., 1997). While *71B>nmo* induces no visible wing defects (Fig. 2.2.2N), ectopic expression of *nmo* is able to suppress the *71B>-flu*Δ*arm* wing phenotype by restoring the size of the wing blade, reducing ectopic bristles and wing blistering (Fig. 2.2.2O).

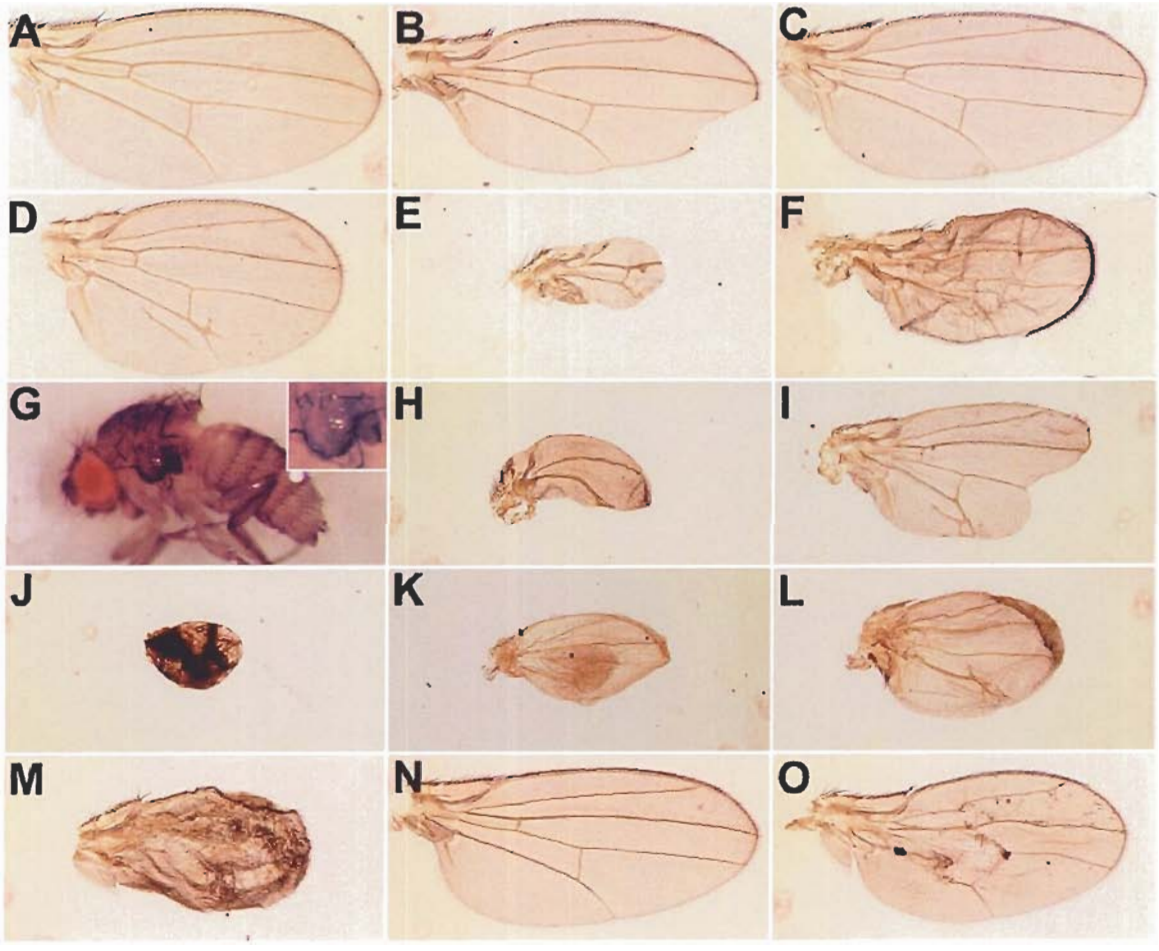

Figure 2.2.2 *nmo* antagonizes Wg signaling during wing development.

(A) A wildtype adult wing. (B) *sd-Gal4>UAS-nmo*. (C) $zw3^{m11\text{-}1}$/ *sd-Gal4; UAS-nmo/+*. (D) The null allele nmo^{DB24}. (E) *sd-Gal4>UAS-DFz2N*. (F) Loss of *nmo* in *sd-Gal4>UAS-Fz2N;* nmo^{DB24}/nmo^{DB24} flies rescues the severe wing defect seen in (E). (G) *sd-Gal4> UAS-Daxin* causes a wing-to-notum transformation (see inset). (H, I) Reductions in *nmo* rescue in a dose dependent manner in (H) *sd-Gal4/+; UAS-Daxin,* nmo^{DB24}/+ and (I) *sd-Gal4/+; UAS-Daxin,* nmo^{DB24}/nmo^{DB24}. (J) *ap-Gal4/+; UAS-Daxin* . Reductions in *nmo* rescue this phenotype in a dose-dependent manner. (K) *ap-Gal4/+; UAS-Daxin,* nmo^{DB24}/+ and (L) *ap-Gal4/+; UAS-Daxin,* nmo^{DB24}/nmo^{DB24}. (M) *71B-Gal4>fluΔarm* . (N) *71B-Gal4>nmo*. (O) *UAS-fluΔarm/ UAS-nmo; 71B-Gal4/+*.

2.2.3 Nemo plays a role in specification of macrochaete bristles on the adult notum

In addition to interactions in wing patterning, *nmo* antagonizes Wg signaling in the sensory bristles of the notum. *ap>nmo* flies display a loss of notum bristles (Fig. 2.2.3B). This phenotype is opposite to that seen upon ectopic activation of Wg signaling (Phillips et al., 1999; Riese et al., 1997; Simpson and Carteret, 1989). The *ap>nmo* bristle loss phenotype is suppressed by heterozygosity for $zw3^{m11}$ (Fig. 2.2.3C) and enhanced by co-expression of *Daxin,* resulting in loss of all scutellar bristles (Fig. 2.2.3D). *ap>nmo* flies also display an abnormal wing phenotype in which the wing blades do not appose properly, forming a large blister (Fig. 2.2.3E). Heterozygosity for $zw3^{m11}$ suppresses this effect, resulting in a significant rescue of wing morphology (Fig. 2.2.3F). All of these genetic data provide convincing evidence that Nemo can interfere with canonical Wg signaling. Both the loss and gain of *nmo* produces phenotypes consistent with the idea that Nemo acts to down regulate Wg signaling during wing development.

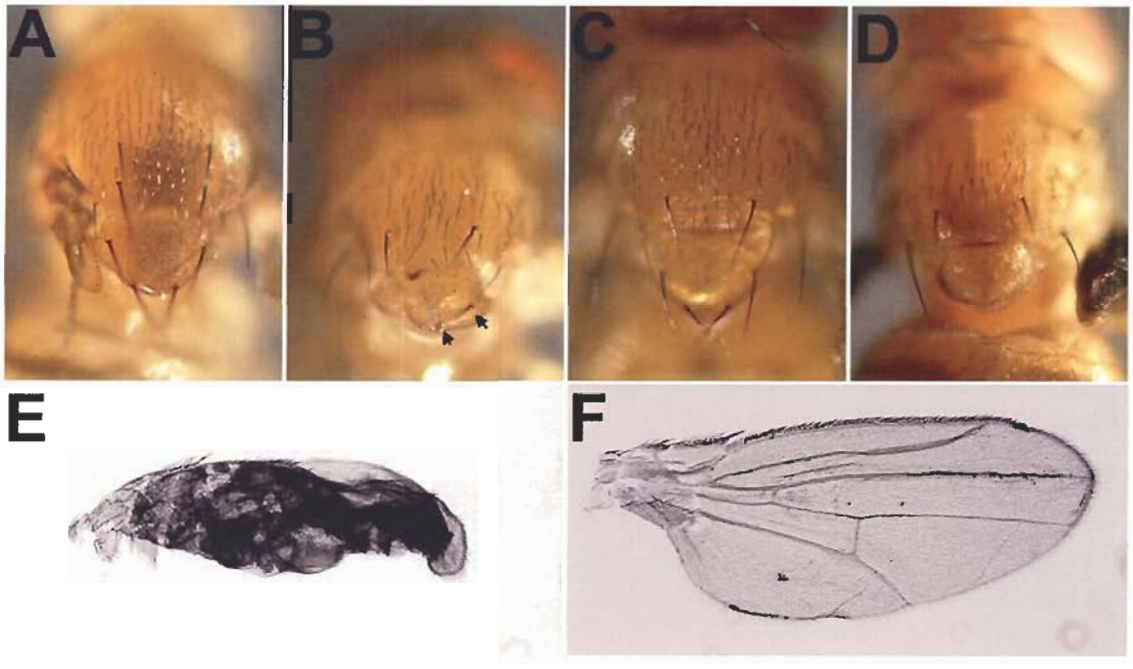

Figure 2.2.3 Nemo plays a role in specification of macrochaete bristles on the adult notum.

(A) A wildtype notum. (B) *ap>nmo* flies show loss of macrochaetes on the notum. A few scuttelar bristles remain (arrows in B). (C) *zw3*$^{m11\text{-}1}$*/+; ap>nmo.* (D) Ectopic expression of Daxin enhances the phenotype in *ap-Gal4, UAS-nmo/+; UAS-Daxin/+* flies. (E) *ap>nmo* wing. (F) *zw3*$^{m11\text{-}1}$*/+; ap>nmo.*

2.2.4 *nmo* autonomously suppresses Wg-dependent gene expression

In the wing disc, Wg signaling positively regulates *Distal-less* (*Dll*) expression (Zecca et al., 1996). Dll is expressed in a domain overlying but wider than the Wg DV expression domain and can be induced by ectopic Wg signaling (Fig. 2.2.4A) (Zecca et al., 1996). Thus the normal pattern of Dll is governed by Wg signaling and Dll expression can be used to monitor the activity of the Wg pathway. As the genetic analysis strongly indicates that Nemo antagonizes Wg signaling, I examined whether modulation of Nemo could affect Dll expression. In nmo^{DB24} clones (Fig. 2.2.4B, C), which are located inside of, or overlapping with, the *Dll* endogenous domain, enhanced expression of *Dll* is detected (Fig. 2.2.4C, D). This effect is cell autonomous as the expression in wild-type cells neighboring the clones is not changed. Clones located outside of the *Dll* endogenous domain do not show any ectopic induction of *Dll* expression (data not shown). This result is not surprising as *nmo* most probably acts to block the activity of dTCF and Arm. Thus, I do not expect an effect outside of their zone of activity which is competent to induce Dll expression.

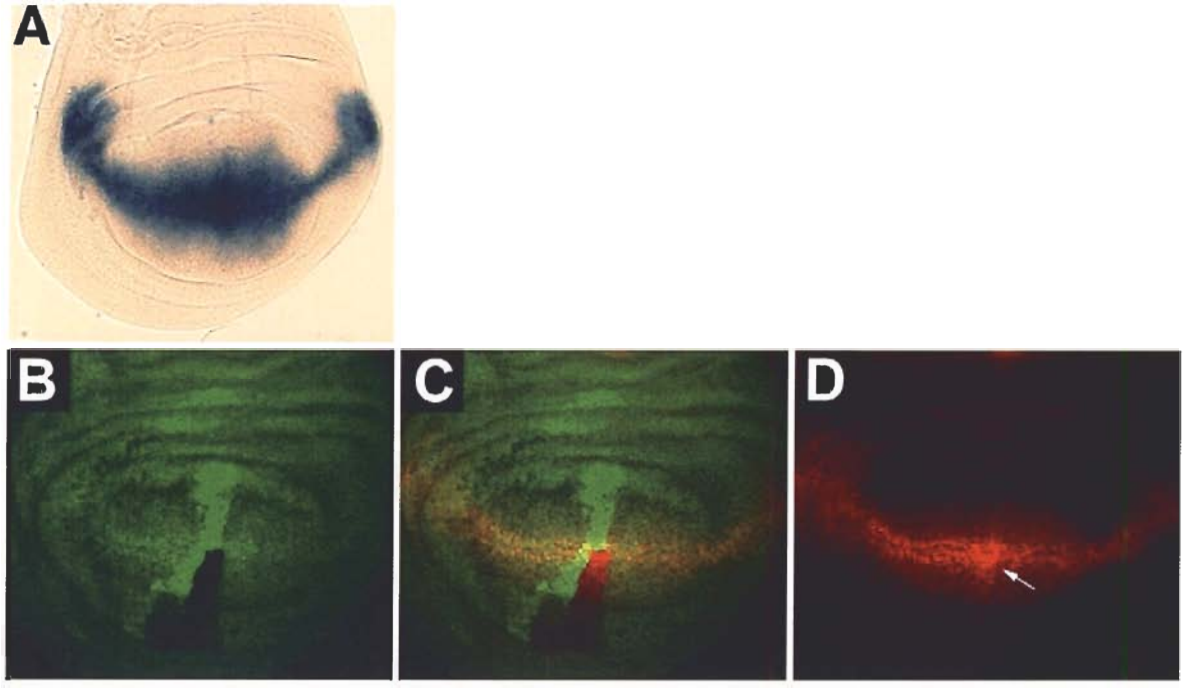

Figure 2.2.4 Loss of *nmo* affects Wg-dependent gene expression.

(A) Dll-lacZ expression is seen in a broad domain centered on the DV boundary with areas of increased expression at the anterior and posterior edges of the DV boundary. (B-D) Dll expression is enhanced in nmo mutant clones. (B, C) nmo^{DB24} clones (marked by the absence of GFP, green). (C, D) Expression of Dll-lacZ (anti β-gal, red) is also increased in nmo^{DB24} clones (arrowhead in D).

2.2.5 *wg* gene expression is not regulated by *nmo*

As Nemo inhibits Wg-dependent gene expression, I was interested in whether Nemo played any negative role in regulating *wg* expression itself. In embryos, *wg* gene expression is positively regulated in an autocrine fashion in response to Wg signaling (Hooper, 1994), whereas in wing discs Wg acts to repress *wg* expression in neighboring cells (Rulifson and Blair, 1995). Wg expression in *nmo* mutant somatic clones was examined and no change of Wg protein staining was detected (Fig. 2.2.5A-C). I also generated somatic flip-out clones ectopically expressing *nmo* in wing discs. Similar to what was found in mutant clones, no alterations in Wg expression were observed in flipout clones in wing discs ectopically expressing Nemo (Fig. 2.2.5D,F).

As Wg expression is also positively regulated by Notch at the wing margin (Neumann and Cohen, 1996), and we previously described genetic interactions between *nmo* and Notch (Verheyen et al., 2001; Verheyen et al., 1996), I also investigated whether *nmo* could be influencing Wg signaling indirectly through an interaction with the Notch pathway. Notch patterns the wing margin through transcriptional regulation of *wg* and *cut* (Neumann and Cohen, 1996). I examined the expression of the Notch target gene *cut* in *ap>nmo* wing discs. No changes in *cut* expression were observed (data not shown), suggesting that Nemo does not affect Notch signaling, and therefore its effect on Wg is most probably not mediated indirectly through Notch. From these experiments, I conclude that the antagonistic role of Nemo in Wg signaling does not include a role in the regulation of *wg* gene expression.

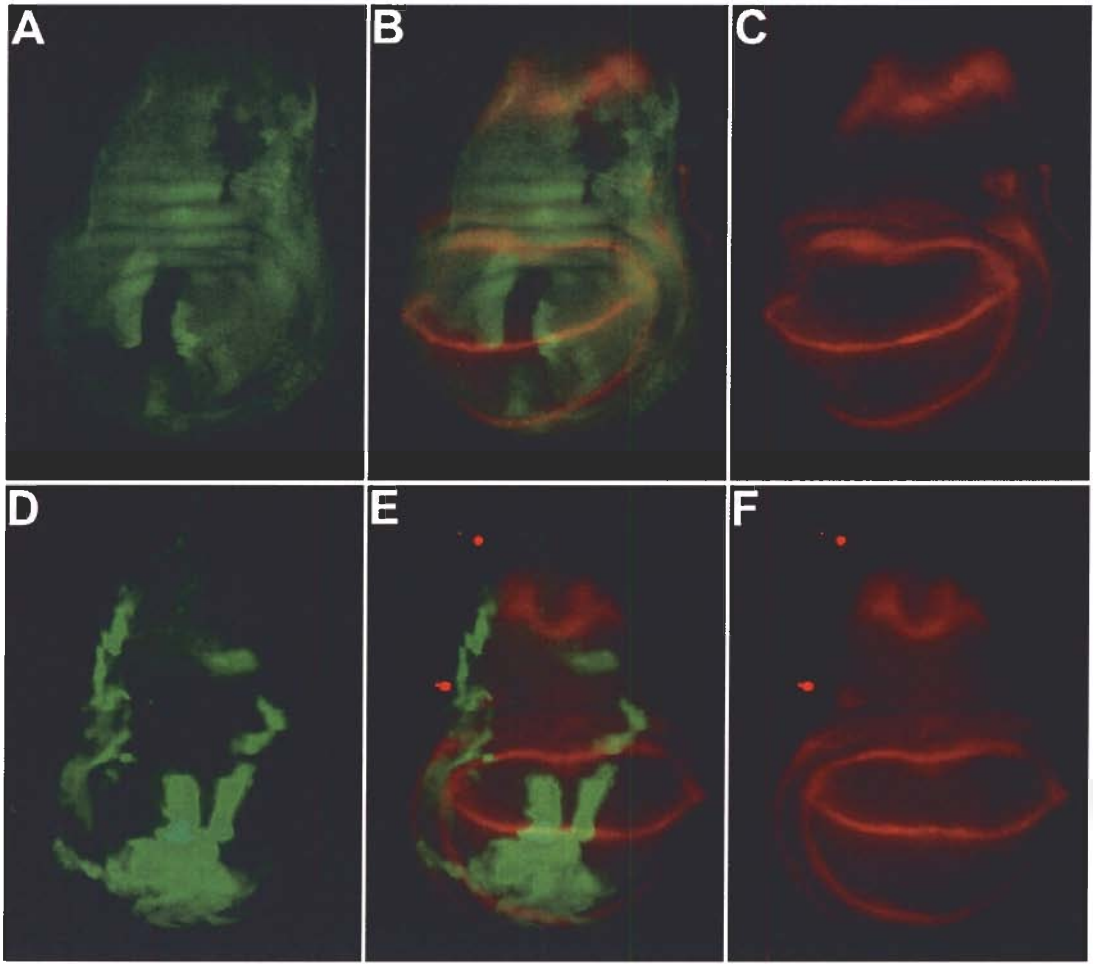

Figure 2.2.5 Neither reduction of *nmo* nor ectopic *nmo* can affect *wg* expression.

Both somatic nmo^{DB24} clones (A, B; marked by the absence of GFP, green) and flip out clones ectopically expressing UAS-nmo were induced (D, E; marked by the areas of brighter GFP staining, green). The discs were stained for Wg protein to determine whether modulation of nmo could affect the Wg expression pattern (anti-Wg antibody, red in B, C, E, F). Anti-Wg stain reveals a wild type pattern in both reduced and ectopic Nemo.

2.2.6 *nmo* is a novel Wg target gene

Considering that the expression pattern of *nmo* flanks that of Wg in wing imaginal discs, I speculated that the expression of *nmo* may be regulated by Wg signaling. I first examined the effect of ectopic Wg pathway activation on *nmo-lacZ* staining. Expression of activated *UAS-fluΔarm* using *vg-Gal4* causes high levels of Wg pathway activation and leads to ectopic *nmo-lacZ* expression along the *vg-Gal4* expression domain (Fig. 2.2.6A,B) (Zecca et al., 1996). The two DV boundary stripes become less defined and appear to expand (Fig. 2.2.6B, compare to Fig. 2.2.1C). Similarly, *dpp>fluΔarm* induces *nmo-lacZ* expression along the AP boundary (Fig. 2.2.6C). These results indicate that activation of the Wg pathway can lead to *nmo* gene expression. Next, we generated somatic flip-out clones that ectopically express *UAS-fluΔarm*. In these clones, ectopic *nmo-lacZ* expression is autonomously induced (Fig. 2.2.6D-F). The induction is observed outside of the regions of high endogenous *nmo* expression and suggests that stabilized Arm is sufficient to autonomously induce *nmo* expression.

To determine whether loss of Wg signaling activity could also affect *nmo* expression, I generated *UAS-Axin* flip-out clones and examined the effects on *nmo-lacZ* staining. In such clones, marked by GFP staining (Fig. 2.2.6G,H), *nmo* expression is suppressed (Fig. 2.2.6H,I) in both regions of high (arrow in Fig. 2.2.6I) and low (arrowhead in Fig. 2.2.6I) expression. I then examined somatic clones homozygous mutant for *disheveled* (Fig. 6J,K) and a cell-autonomous inhibition of *nmo* expression was found (Fig. 2.2.6K,L). In all cases, I observe inhibition of not only the high levels of DV boundary *nmo* but also the low level ubiquitous staining within the wing pouch. I also examined the effect of ectopic expression of *UAS-Fz2N* and found that *vg>Fz2N*

wing discs display a loss of *nmo* staining at the DV boundary which is similar to the inhibitory effect of *UAS-Fz2N* on other Wg downstream genes such as the DV boundary marker *vg-lacZ* (data not shown) (Zhang and Carthew, 1998). All of these results taken together confirm that activation of endogenous Wg signaling results in *nmo* expression, and that *nmo* is a bona fide Wg target gene.

Figure 2.2.6 Wg signaling positively regulates the expression of *nmo*.

(A) *vg-Gal4* is expressed along the DV boundary in *vg>UAS-lacZ*. (B) *nmo* expression in *vg-Gal4/ UAS-fluΔarm; nmo-lacZ/+* mid third instar larval discs is greatly expanded, especially in the posterior periphery. (C) *dpp>fluΔarm* causes ectopic nmo expression along the AP boundary. (D-F) *nmo-lacZ* expression (E-F; anti β-gal, red) in *fluΔarm* flip-out clones (D, E; marked by the areas of brighter GFP staining). (H-I) Flip-out clones ectopically expressing *UAS-Daxin* (G-H) also result in decreased nmo expression (H-I). (J-L) In dsh^{v26} somatic clones (J, K; marked by the absence of GFP, green) *nmo-lacZ* expression is reduced cell autonomously (K, L; anti β-gal, red).

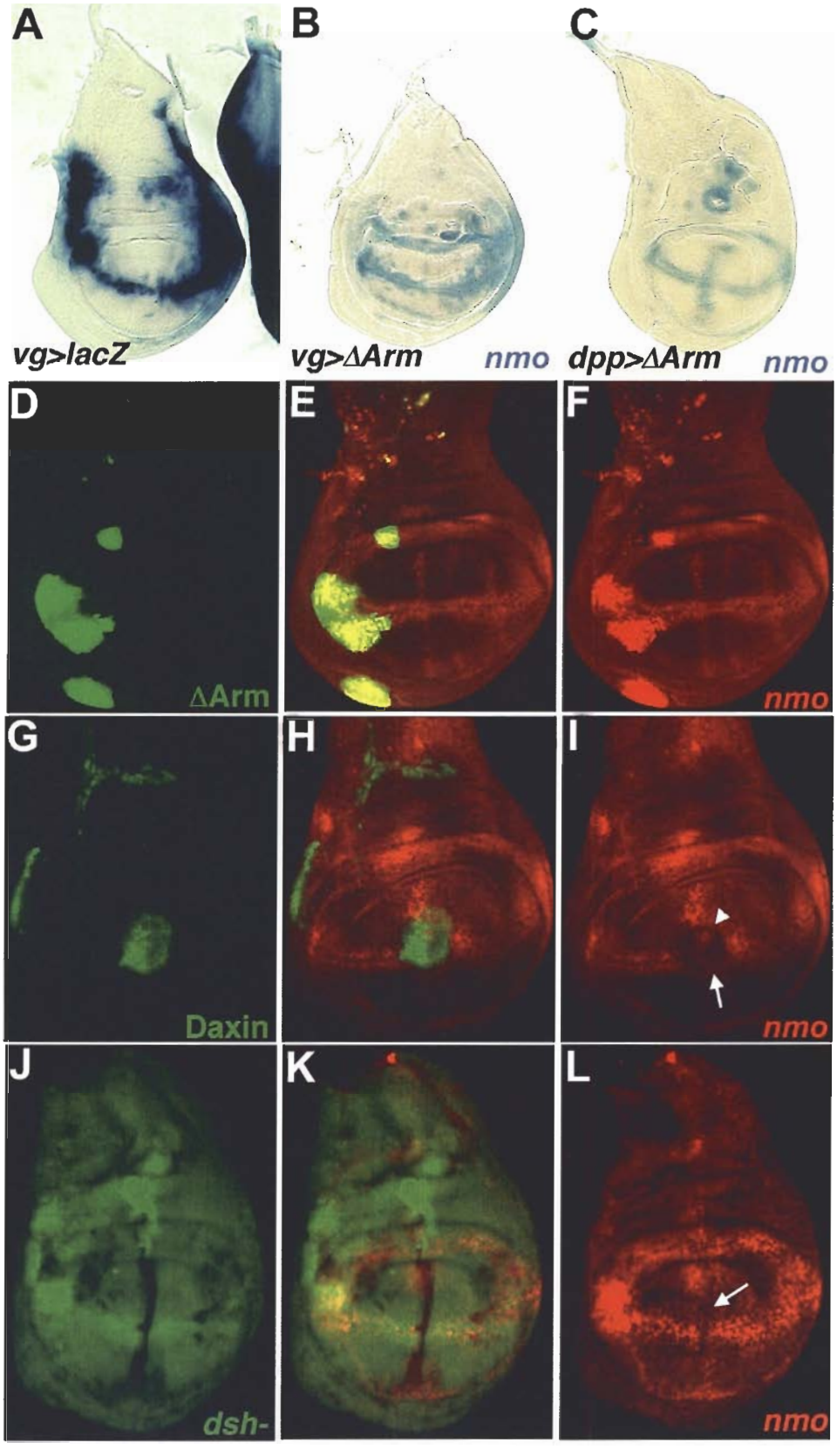
A
B
C
vg>lacZ
vg>ΔArm
nmo
dpp>ΔArm
nmo
D
E
F
ΔArm
nmo
G
H
I
Daxin
nmo
J
K
L
dsh-
nmo

2.2.7 Nemo can affect Arm stabilization

The localization of *nmo* in third instar wing discs is very reminiscent of the pattern of stabilized Arm protein observed after Wg pathway activation (Peifer et al., 1991; Mohit et al., 2003). To examine this more closely, I carried out double staining to detect *nmo* gene expression and Arm protein stabilization. First, I observed that *nmo* and stabilized Arm co-localize in the central region of the wing margin (Fig. 2.2.7A-C). In addition, it was noted that in the anterior region of the wing margin where *nmo* expression is elevated, Arm protein levels are lower, relative to the rest of the margin. Third, I find that Nemo staining is reduced in the region where the DV and AP boundaries intersect and that this region shows more stabilized Arm protein.

To determine whether these observations reflected a possible mechanism for the inhibitory effect of Nemo on in the Wg signaling, I determined whether ectopic Nemo could destabilize Arm protein, thus indicating an inhibition of Wg signal transduction. In flip-out clones ectopically expressing Nemo (Fig. 2.2.7D,E), the stabilization of Arm protein appears reduced in a cell autonomous manner (Fig. 2.2.7E,F). This most probably reflects more degradation of Arm. In an attempt to address this further, I examined the stability of Arm in nmo^{adk1} somatic clones. In this genetic background, I was unable to observe alterations in Arm stability (data not shown).

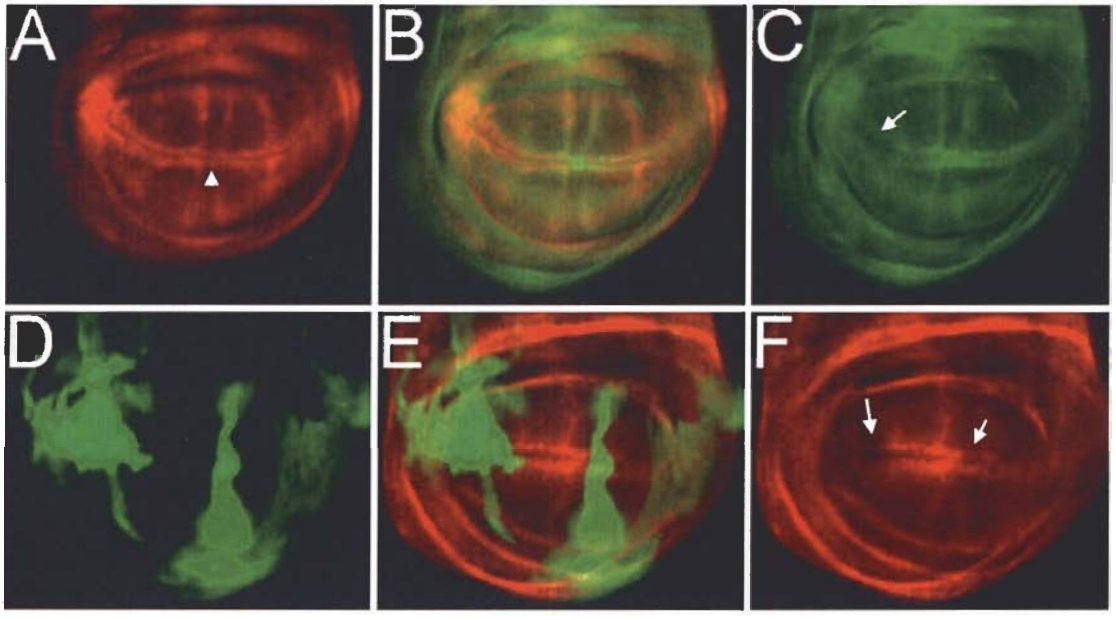

Figure 2.2.7 Nemo can influence Arm stabilization.

(A, B) *nmo* gene expression (as monitored by *nmo-lacZ*, anti β-gal, red) overlaps with (B, C; anti-Arm, green) stabilized Arm protein in third instar discs. There are distinct regions in which higher *nmo* expression in A excludes high levels of Arm (arrow in C) and in which high levels of Arm seen in C coincide with reduced *nmo* (arrowhead in A). In flip-out clones ectopically expressing Nemo (D, E; marked by the areas of brighter GFP staining), the stabilization of Arm protein appears reduced in a cell autonomous manner (E, F; anti-Arm, red; arrows in F).

2.2.8 Nemo binds dTCF and Arm

NLKs have been shown to target TCF and affect the DNA binding ability of the TCF/β-Catenin complex. In an attempt to address the mechanism of how Nemo antagonizes Wg signaling, a biochemical characterization of the interaction of Nemo, dTCF and Arm was carried out. (Human embryonic kidney) HEK293 cells were transfected with both Flag-tagged Nemo and Myc-tagged dTCF and immunoprecipitations were performed to determine whether the proteins interacted with each other. Reciprocal immunoprecipitations from cell lysates both resulted in the co-immunoprecipitation of Nemo and dTCF (Fig. 2.2.8A).

I next tested Arm, since in nematodes it was shown that the Nemo homolog Lit-1 needed to interact with a β-catenin in order to be active (Rocheleau, 1999). To assess whether Nemo could bind to Armadillo, ^{35}S-labeled Nemo was generated and incubated with GST-Arm and GST as a control. It was found that Nemo selectively bound to GST-Arm (Fig. 2.2.8B, lane 3). To confirm that this interaction occurs in vivo, HEK 293 cells were tranfected with Flag-tagged Nemo and HA-tagged Arm. Nemo and Arm were found to co-immunoprecipite from cell lysates (Fig. 2.2.8C).

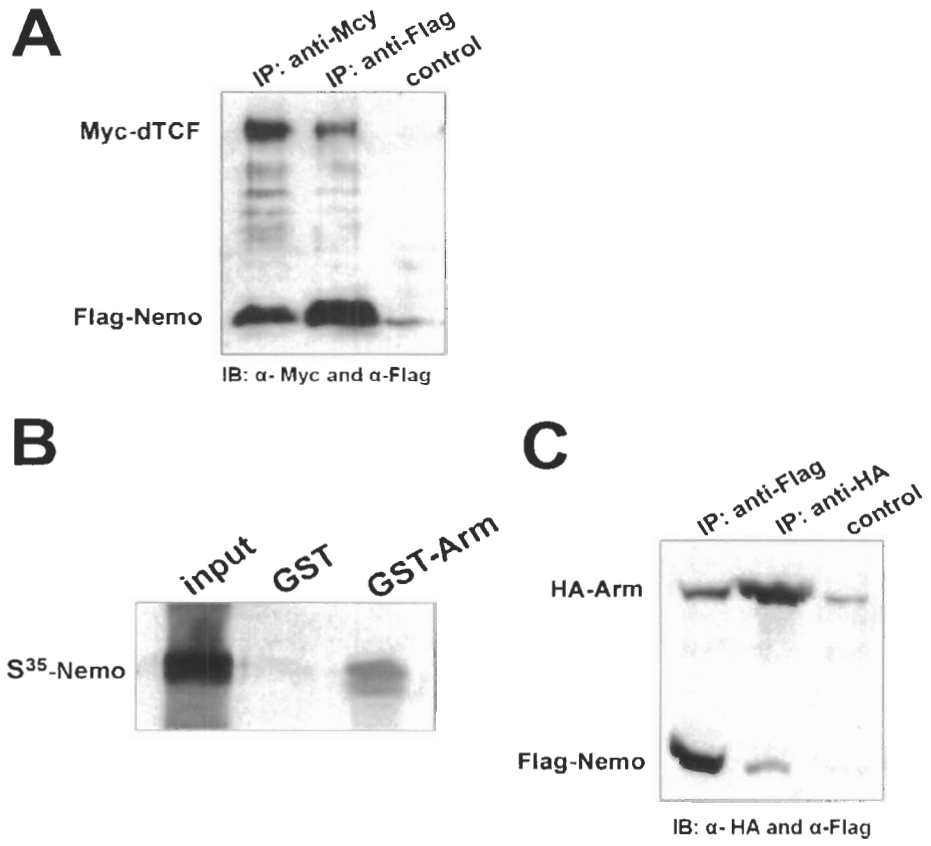

Figure 2.2.8 Nemo binds both dTCF and Arm.

(A) Association of Nemo and dTCF. pXJ-Flag-nemo and pCMV-Myc-dTCF were co-transfected into HEK293 cells. Cell lysates were immunoprecipitated with anti-Myc, anti-Flag or IgG (control). Immunoblotting was performed with anti-Myc and anti-T7 antibodies. (B) *in vitro* binding of Nemo and Arm. GST and GST-Arm were incubated with S^{35} labeled in vitro translated Nemo. Phosphor image was used to detect the association. (C) co-IP of Nemo and Arm. pXJ-Flag-Nemo and pCMV-HA-Arm were co-transfected into HEK293 cells. Cell lysates were immunoprecipitated with anti-Flag, anti-HA or IgG (control). Immunoblotting was performed with anti-HA and anti-Flag antibodies.

2.2.9 Nemo phosphorylates dTCF in its N terminus and phosphorylates Arm in its C terminus

I next addressed whether dTCF and Arm could serve as substrates for Nemo. In vitro kinase assays were performed on transfected cell lysates and Nemo was found to phosphorylate both dTCF and Arm, as well as autophosphorylate (Fig. 2.2.9A). This was dependent on Nemo's kinase activity, as a dominant negative Nemo (K69M) construct in which the lysine residue in the ATP-binding domain was changed to methionine showed neither phosphorylation of dTCF, Arm, nor Nemo autophosphorylation (Fig. 2.2.9A).

To map the domain in which the target residue was located, carboxy terminal truncated dTCF and Arm proteins were generated (Fig. 2.2.9B). These proteins, dTCF ΔC1 (partial deletion of the C terminus) and dTCF ΔC (Fig. 2.2.9B), were still phosphorylated by Nemo (Fig. 2.2.9C), indicating that the target sites were contained within the N terminus and HMG domain. However, HMG domain does not possess potancial Nemo phosphorylation sites (SP or TP) (Fig. 2.2.10A). Therefore, the target sites are located in the N terminus. This is consistent with the sites where Nlk phosphorylates TCF family, which are also located in N terminus of LEF-1 and TCF-4 (Ishitani, 2003b).

In vitro kinase assay was also performed using wild type Arm and Arm ΔC proteins. Arm ΔC was no longer phosphorylated by Nemo (Fig. 2.2.9D), indicating that the target site was contained within the deleted fragment. Within the deleted C terminal fragment there are three putative Nemo target sites (Fig 2.2,10B). Further expriments are on going to examine where the exact Nemo target sites are located.

Figure 2.2.9 Nemo phosphorylates both dTCF and Arm.

(A) Nemo phosphorylates dTCF and Arm. HEK293 cells were transfected with expression vectors as indicated. Immunoprecipitated complexes with indicated antibodies were subjected to in vitro kinase assays and analyzed by autoradiography. The immunoprecipitates were also immunoblotted with indicated antibodies to confirm loading. (B) A schematic diagram of the full length dTCF and Arm and various deletion constructs. (C) Nemo does not phosphorylate dTCF in the C terminus. In vitro kinase assays performed with wildtype dTCF, dTCF ΔC1 (partial deletion of the C terminus) and dTCF ΔC, demonstrate that Nemo targets N terminus or HMG domain of dTCF. The immunoprecipitates were also immunoblotted with indicated antibodies to confirm loading. (D) Nemo phosphorylates Arm in the C terminus. In vitro kinase assays performed with wildtype Arm and Arm ΔC, demonstrate that Nemo targets C terminus of Arm. The immunoprecipitates were also immunoblotted with indicated antibodies to confirm loading.

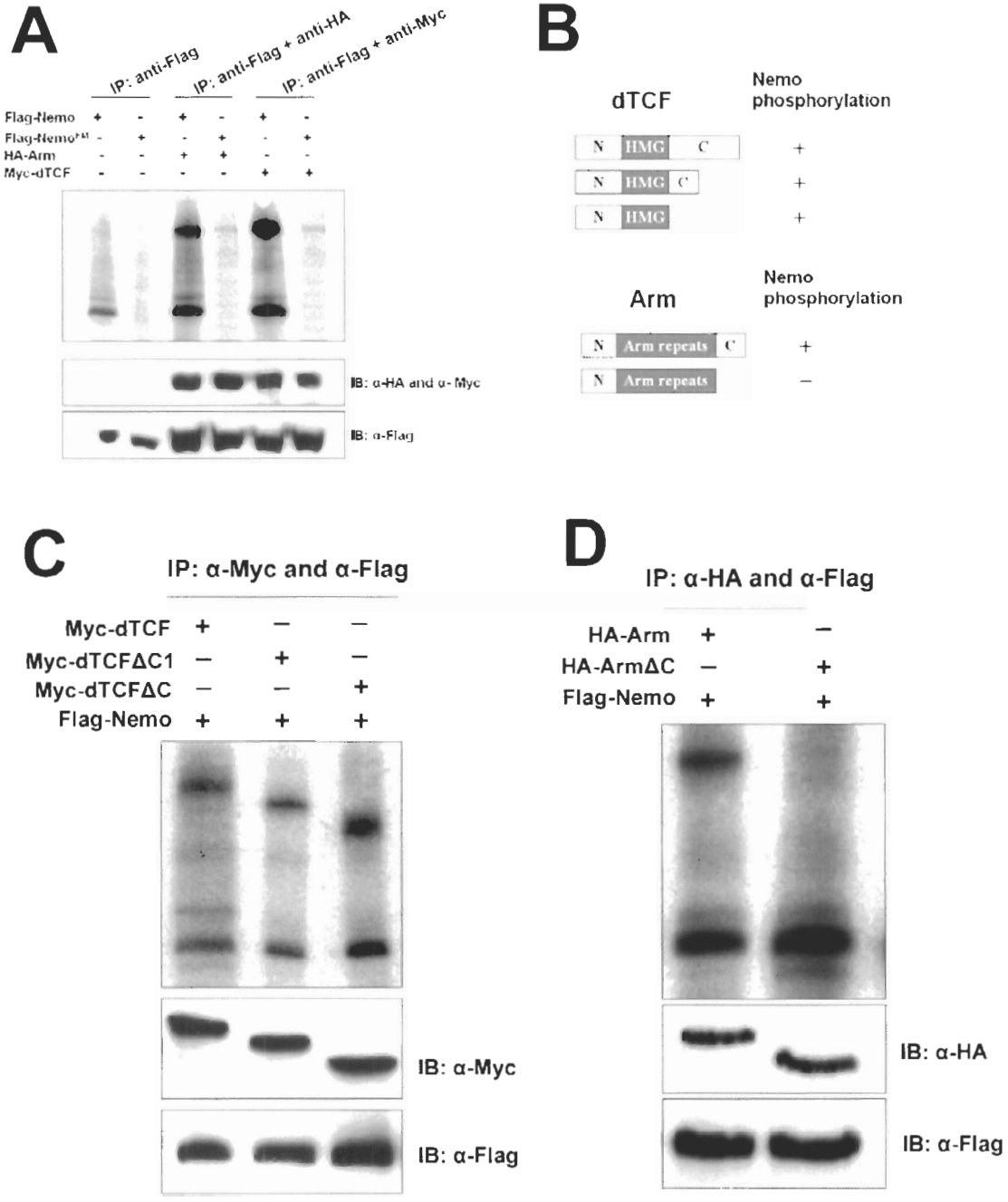
A
IP: anti-Flag
IP: anti-Flag + anti-HA
IP: anti-Flag + anti-Myc
Flag-Nemo + - + - + -
Flag-Nemo^ΔN - + - + - +
HA-Arm - - + + - -
Myc-dTCF - - - - + +
IB: α-HA and α-Myc
IB: α-Flag
B
dTCF
Nemo phosphorylation
N HMG C +
N HMG C +
N HMG +
Arm
Nemo phosphorylation
N Arm repeats C +
N Arm repeats –
C
IP: α-Myc and α-Flag
Myc-dTCF + – –
Myc-dTCFΔC1 – + –
Myc-dTCFΔC – – +
Flag-Nemo + + +
IB: α-Myc
IB: α-Flag
D
IP: α-HA and α-Flag
HA-Arm + –
HA-ArmΔC – +
Flag-Nemo + +
IB: α-HA
IB: α-Flag

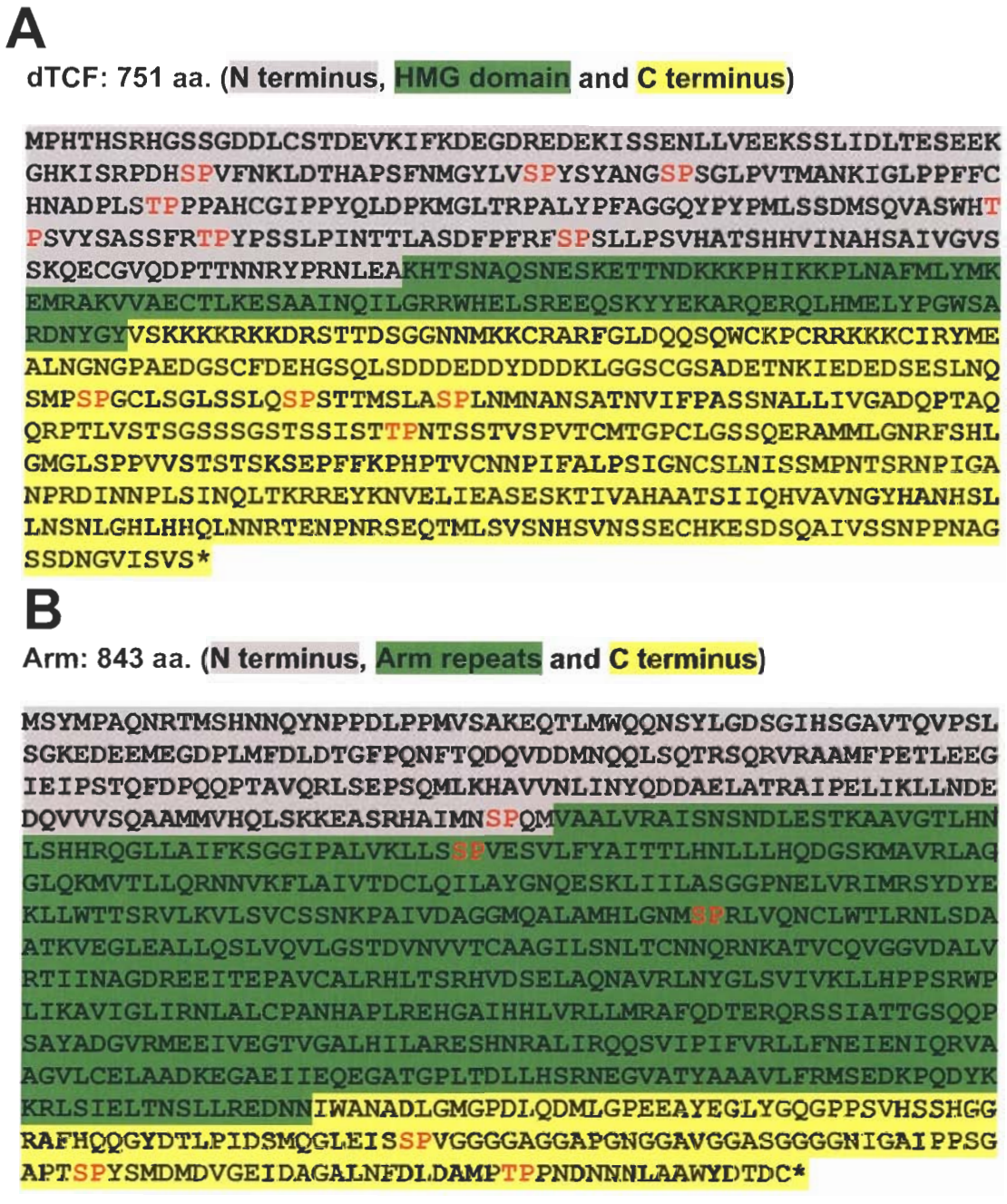

Figure 2.2.10 amino acid sequences of dTCF and Arm

dTCF contains 751 amino acids, including N terminus, HMG domain and C terminus labled by different colors. The potancial Nemo target SP and TP sites are maked by red. (B) Arm contains 843 amino acids, including N terminus, Arm repeats and C terminus labled by different colors. The SP and TP sites are maked by red.

2.3 Discussion

2.3.1 Feedback inhibition of Wg signaling

Widespread use of feedback loops makes them important mechanisms for regulating signaling pathways during development (Anderson and Ingham, 2003; Freeman, 2000; Perrimon and McMahon, 1999). For example, a number of positive and negative feedback loops regulate the *Drosophila* EGFR, TGFβ, JNK and JAK/STAT signaling pathways to both refine and potentiate signaling. Negative feedback occurs when a signaling pathway induces expression of its own inhibitor and thereby leads to pathway downregulation. In addition, both autonomous and non-autonomous mechanisms exist to negatively regulate signaling pathways.

The canonical Wnt pathway also makes use of negative feedback mechanisms. In murine Wnt signaling, the feedback loops primarily target the activity of β-catenin. For example, *Tcf1* is a target gene for β-catenin/Tcf4 in epithelial cells and is proposed to act as a repressor that counteracts β-catenin/Tcf4-mediated gene expression (Roose et al., 1999). Spiegelman et al. (Spiegelman et al., 2000) have provided evidence that the β-TrCP protein, the expression of which is induced by β-catenin/TCF signaling, targets β-catenin for ubiquitination and subsequent degradation (Spiegelman et al., 2000). It has also been shown that expression of Axin2, one of the scaffold proteins in the inhibitory APC/GSK3 complex, is also induced by Wnt signaling (Jho et al., 2002).

In *Drosophila*, several examples of Wg feedback inhibition have been identified. First, it has been shown that Wg downregulates its own transcription in the wing pouch to narrow the RNA expression domain at the DV boundary (Rulifson et al., 1996). Second,

Wg signaling can repress the expression of its receptor Dfz2 in *wg*-expressing cells of the wing disc. Wg regulation of Dfz2 creates a negative feedback loop in which newly secreted Wg is stabilized only once it moves away from the DV boundary to cells expressing higher levels of *Drosophila* Fz2 (Cadigan et al., 1998). Third, the Wg target gene *naked cuticle* (*nkd*) acts through Dsh to limit Wg activity (Rousset et al., 2001; Zeng et al., 2000). Fourth, Wingful (Wf), an extracellular inhibitor of Wg, is itself induced by Wg signaling (Gerlitz and Basler, 2002).

2.3.2 Nemo is an inducible inhibitor of Wg

My research adds Nemo to this list of inducible antagonists participating in Wg signaling (Fig. 2.3.1). I show that Nemo antagonizes the Wg signal in wing development, as evidenced by phenotypic rescue, suppression of Wg-dependent gene expression in discs ectopically expressing *nmo*, and ectopic expression of a Wg-dependent gene in *nmo* mutant clones.

As both *wf* and *nmo* expression are positively regulated by Wg signaling in the wing, their expression patterns are relatively similar to that of Wg (Fig. 2.2.1C) (Gerlitz and Basler, 2002; Zeng et al., 2000). Even though *nkd* also has a similar pattern to Wg in the larval wing disc, unexpectedly, it has no detectable role in wing development. As an intracellular antagonist, Nkd regulates embryonic Wg activity in a cell-autonomous manner by acting directly with Dsh to block accumulation of Arm in response to Wg signaling (Rousset et al., 2001; Zeng et al., 2000). Wf apparently has no role during embryogenesis, although both Wf and Nkd can inhibit Wg signaling throughout development when overexpressed (Gerlitz and Basler, 2002; Zeng et al., 2000). Wf is an

extracellular protein that functions non-autonomously to regulate Wg signaling (Gerlitz and Basler, 2002). This mechanism of inhibition parallels that of Argos, a secreted feedback antagonist in the EGFR pathway.

The effect of Nemo on the Wg-dependent reporter gene *Dll* is confined to regions of endogenous gene expression. In the absence of *nmo* expression, ectopic *Dll* expression is only seen at elevated levels within the endogenous expression domain, thus being dependent on Wg activity. This is in contrast to inhibition of the Dpp pathway by Brinker (Campbell and Tomlinson, 1999; Jazwinska et al., 1999; Minami et al., 1999). Brinker acts independently of Dpp in its repression of Dpp target genes, such that in the absence of both *brk* and Dpp the target genes are expressed ectopically (Campbell and Tomlinson, 1999). We speculate that the role of Nemo in the Wg pathway is analogous to the role of Daughters against Dpp (Dad) in Dpp signaling (Tsuneizumi et al., 1997). Dpp induces the expression of *dad*, which in turn antagonizes the pathway through an as yet undefined mechanism. These might include either interactions with the intracellular transducer Mothers against Dpp (Mad) or with TGFβ receptors.

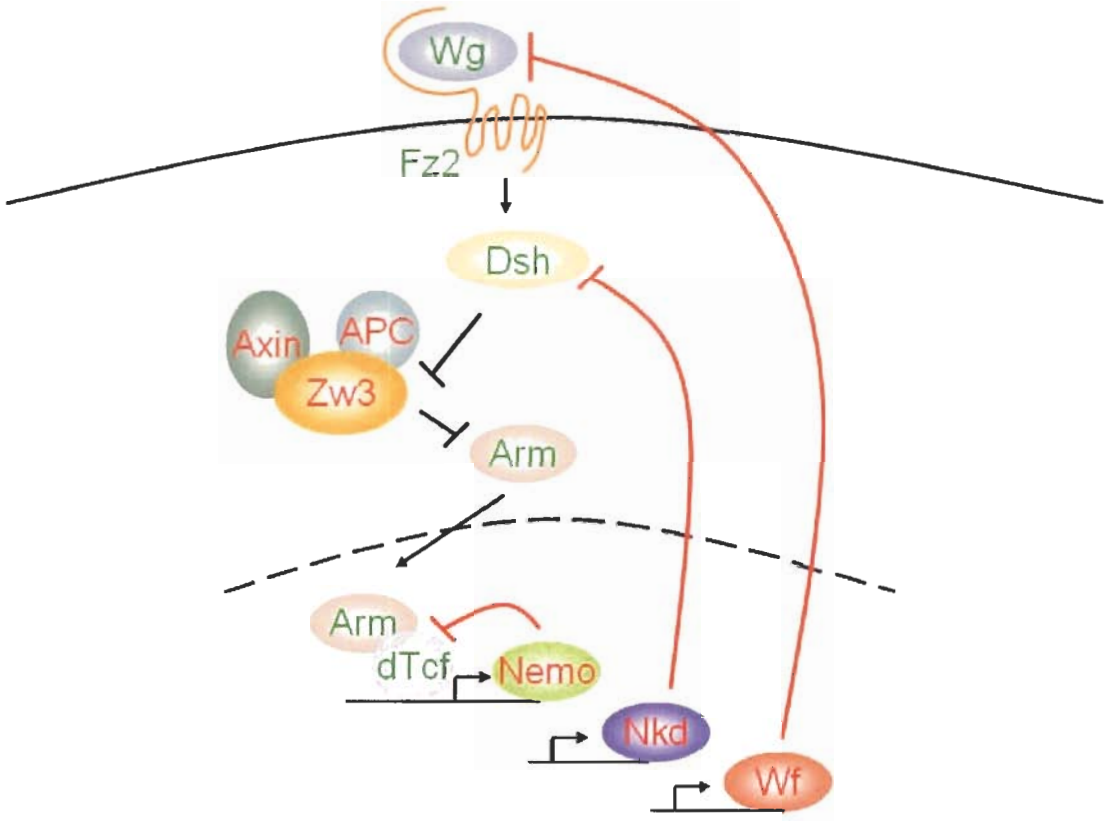

Figure 2.3.1 The role of negative feedback inhibitors in Wg signaling

Drosophila Wg signaling is controlled by a number of induced inhibitors including Nkd and Wf. We show that Wg also regulates Nemo expression and that Nemo in turn can antagonize Wg during wing patterning.

2.3.3 Nemo does not participate in the self-refinement of Wg expression

It is intriguing that Nemo does not play a role in regulating *wg* expression; however, this is most probably because of the point of action of Nemo within the Wg pathway. The self-refinement of *wg* expression in the wing is dependent on Dsh but independent of Arm (Rulifson et al., 1996). Recent work has raised some questions about the factors involved in Wg self refinement, specifically postulating a role for dTCF in this process (Schweizer et al., 2003). dTCF (*pan*) somatic clones were shown to have elevated Wg protein, suggesting that TCF plays an active role in repressing Wg gene expression. The authors, however, indicate that they fail to distinguish between increased *wg* gene expression and stabilized Wg protein. Another recent paper examined regulation of Wg signaling by Twins (*tws*), a protein phosphatase subunit, and found that it is required for Arm stabilization (Bajpai et al., 2004). Modulation of *tws* resulted in aberrant Wg signaling, as monitored by Dll expression, that are not accompanied by alterations in *wg* gene expression. Our data are consistent with the findings of Bajpai et al. and suggest that the mechanism of *wg* refinement most probably does not involve Arm or dTCF. Our genetic analyses support the placement of Nemo at or below the level of Arm within the pathway. The apparent absence of a role for Nemo in regulating *wg* expression contrasts with the other inducible feedback inhibitors. Modulation of either the extracellular inhibitor Wf or the Dsh-antagonist Nkd can influence *wg* gene expression in wing discs and embryos, respectively (Gerlitz and Basler, 2002; Zeng et al., 2000). As stated above, neither loss of nor ectopic expression of *nmo* during imaginal disc development has an effect on the pattern of Wg expression.

2.3.4 *nmo* expression is induced by high levels of Wg signaling

The developing wing is bisected by a narrow stripe of Wg expressing cells. Wg protein has a short half-life near the DV boundary, which causes a rapid decrease in Wg concentration and forms a steep symmetric gradient of the Wg protein (Cadigan et al., 1998). Radiating out from the source of Wg, there are three concentric domains of Wg-dependent gene expression (reviewed by Martinez Arias, 2003). First, a very narrow domain of cells adjacent to the highest concentration of Wg expresses *achaete* (*ac*). Second, Dll is expressed in a median range domain of Wg and third, a long-range domain expresses *vg*. Our results suggest that *nmo* is a short-range target, like *ac*, the activation of which is limited by the high threshold of Wg signal. This may be the explanation for the very narrow pattern of enriched *nmo* expression at the DV boundary and the ring domain and the cell autonomous induction of *nmo* in the ectopic *fluΔArm* clones.

If higher levels of Wg protein induce *nmo* expression, it raises the question of why *nmo* is not expressed in DV boundary cells. One possibility is that there are genes that are expressed between the two stripes of *nmo* that prevent its expression. In Fig. 2.2.6B, *vg-Gal4*, which is mainly expressed at the DV boundary, drives *UAS-fluΔarm* to induce ectopic *nmo* expression. In this case, the ectopic expression of *nmo* fills the gap between the two endogenous bands. This observation supports a model in which there is a suppressor(s) located along the DV boundary to silence *nmo* expression. The balance between the Wg signal and the suppressor(s) would refine *nmo* expression into two thin stripes flanking the DV boundary. In the case of ectopic *UAS fluΔarm*, the Wg signal

may overpower the suppressor, thereby allowing *nmo* to be expressed at the boundary. In a similar mechanism, it has been shown that Wg can direct the expression of *ac* at the margin but that this expression is prevented, at least partially, by the activity of Cut (Couso et al., 1994).

Although the wing margin, ring expression and low level ubiquitous staining of *nmo* in imaginal wing discs reflects regulation by Wg signaling, the other developmental expression patterns, such as staining in primordia of wing veins, may reflect regulation by other signaling pathways. For example, the staining in the wing vein primordia that emerges in late third instar and the gene expression pattern observed in pupal wings reflects the later role of *nmo* in wing vein patterning (Verheyen et al., 2001), which may involve interactions with EGFR and TGFβ signaling.

In further support that Wg signaling regulates the transcription of *nmo*, we find several dTCF consensus binding sites in the 5'region of the *nmo* gene which may represent enhancer elements (B. Andrews and E.M.V., unpublished). Indeed, two sites match 9 out of 11 bp (GCCTTTGAT) of the T1 site (GCCTTTGATCT) in the *dpp* BE enhancer that has been shown both in vitro and in vivo to bind and respond to dTCF (Yang et al., 2000). The presence of these sites suggests that the observed transcriptional regulation of *nmo* by Wg may involve direct binding to the *nmo* DNA sequence by dTCF.

2.3.5 Nemo may target Arm for degradation

As a result of comparing the endogenous expression pattern of *nmo* with stabilized Arm, we noticed that the highest levels of Nemo excluded Arm stabilization, while high levels of Arm were present in cells in which *nmo* levels were lower. As Arm

protein stabilization is a direct consequence of Wg pathway activation, we sought to examine whether Nemo may function to inhibit Wg by promoting Arm destabilization and subsequent breakdown. Indeed, ectopic expression of Nemo can lead to cell-autonomous reduction in Arm protein levels. This preliminary result suggests a mechanism in which Nemo may contribute to the destabilization of Arm that involves the Axin/APC/GSK3 complex. One explanation to account for such a finding would concern the interaction with TCF in the nucleus and the role of dTCF as an anchor for Arm (Behrens et al., 1996; Tolwinski and Wieschaus, 2001). Given what is known about NLKs, it is likely that Nemo may act on the ability of the dTCF/Arm complex to bind DNA and activate transcription (Ishitani et al., 1999). Tolwinksi and Wieschaus (Tolwinksi and Wieschaus, 2001) propose that dTCF acts as an anchor for Arm in the nucleus. It remains to be determined how efficient this anchor is and whether there are conditions in which the interaction may become compromised, such as we see with elevated Nemo. NLKs have been shown to affect the DNA-binding ability of TCF/β-catenin (Ishitani et al., 1999). Perhaps in the absence of DNA binding, this complex is less stable and Arm could be free to shuttle to the cytoplasm where it could associate with Axin or APC and become degraded (Henderson and Fagotto, 2002). I propose that the ectopic *nmo* in our assay is leading to destabilization of the dTCF/Arm/DNA complex and thus causing Arm to exit the nucleus and be degraded through interaction with Axin, APC and GSK3. The observation that ectopic expression of full-length Arm cannot induce any activated Wg phenotypes (Orsulic and Peifer, 1996) have been explained by the hypothesis that even these high levels of protein are not sufficient to overcome the degradation machinery (Tolwinski and Wieschaus, 2001). Thus, the finding that there is

no elevated Arm in *nmo* clones is consistent with an inability to overcome the endogenous degradation machinery; even though less Nemo could lead to more stabilized DNA interactions, this would not lead to higher levels of stabilized Arm than is normally found.

2.3.6 Model for Nemo function in Wg signaling

Studies of homologs of Nemo in other species have provided clues to its function. Murine Nlk can autophosphorylate and when active can phosphorylate TCF proteins bound to β-catenin and inhibit the complex from associating with DNA (Brott et al., 1998; Ishitani et al., 2003b; Ishitani et al., 1999). It was recently shown that vertebrate Nlk forms a complex with β-catenin in a TCF/LEF-1-dependent manner (Ishitani et al., 2003b). *C. elegans* Lit-1 does not autophosphorylate and seems to depend on an interaction with the β-catenin homolog WRM-1 for its activity (Rocheleau et al., 1999). Active Lit-1 can then phosphorylate the TCF homolog POP-1 and lead to its cytoplasmic translocation (Rocheleau et al., 1999). In both scenarios, the end effect is inhibition of TCF activity.

Our genetic studies establish that *Drosophila* Nemo does in fact play a negative regulatory role in canonical Wg signaling. Although *nmo* was originally identified as playing a role in the non-canonical Fz pathway that regulates tissue planar polarity, its precise role in that pathway has not been further defined (Brown and Freeman, 2003; Choi and Benzer, 1994; Strutt et al., 1997).

In addition to the findings of the interaction of Nemo with dTCF and Arm, in collaboration with L. Smit and H. Clevers, we found that Nemo inhibits the TCF-

dependent gene expression in a vertebrate cell line called AzuII. The genetic and biochemical analyses, all together, suggest that *Drosophila* Nemo, like its homologs, functions to inhibit canonical Wnt signaling though interaction with TCF.

The protein-protein interactions involved in this mechanism share some features, but not all, with NLK signaling found in both vertebrates and nematodes. Nemo can bind to and phosphorylate the *Drosophila* β-catenin Armadillo and dTCF. This interaction and phosphorylation leads to downregulation of Wg signaling and reduced target gene expression, as is observed both in vivo and through the use of a TCF-responsive reporter construct. While the exact biochemical mechanisms used between species may not be exactly conserved, it appears that the end result, namely inhibition of TCF/LEF function is a conserved feature of NLKs. All of these data illustrate that the analysis of Nemo function in *Drosophila* will shed light on mechanisms used across species and may provide greater insight into the regulation of Wnt signaling in general.

Chapter 3

Drosophila Nemo kinase antagonizes BMP signalling by phosphorylation of Mad and inhibition of its nuclear localization

3.1 introduction

3.1.1 TGFβ and *Drosophila* BMP signaling

The transforming Growth Factor beta (TGFβ) superfamily is a large group of secreted growth factors, grouped into three families: the TGFβs, the Activins and the BMPs. TGFβ1 is the founding member of the family, which was identified as a regulator of mesenchymal growth and antimitogen in epithelial cells. Activins were identified as endocrine regulators of pituitary function and as inducers of mesoderm in frogs. Bone morphogenetic proteins (BMPs) were identified as bone repair factors and independently, as dorsalizing factor in *Drosophila* (reviewed in Massague, 1998).

TGFβ signalling is initiated when a secreted ligand of the TGFβ, BMP or Activin family binds to a type II serine/threonine (S/T) kinase receptor (reviewed in Attisano and

Wrana, 2002; von Bubnoff and Cho, 2001). This receptor then recruits and phosphorylates a type I S/T kinase receptor. The type I receptor, through the help of an anchor protein, SARA (Smad Anchor for Receptor Activation), recruits and phosphorylates a receptor-regulated member of the receptor regulated Smad (R-Smad) family of proteins. The phosphorylated R-Smad releases from the receptor, binds a common mediator Smad (Co-Smad), and translocates to the nucleus where it can form complexes with transcription factors on the promoters of target genes. Association of Inhibitory Smad (I-Smads) with activated type I receptor, inhibits phosphorylation of R-Smad, thereby preventing complex formation with R-Smad and translocation to the nucleus (reviewed in Massague, 1998).

Drosophila TGFβ superfamily signaling is carried out by at least three related BMPs, Decapentaplegic (Dpp), Screw (Scw) and Glass bottom boat (Gbb), and the Activin named Baboon (Arora et al., 1994; Brummel et al., 1999; Doctor et al., 1992; Padgett et al., 1987; Wharton et al., 1991). Dpp has been the best characterized and is found to act as a morphogen during the patterning of multiple tissues during embryonic and imaginal disc development (reviewed in Raftery and Sutherland, 1999). Gbb demonstrates complex relationships with Dpp in different tissues or even within the same tissue (Chen et al., 1998; Haerry et al., 1998; Khalsa et al., 1998; Ray and Wharton, 2001; Wharton et al., 1999). Screw function appears to be limited to the embryo, where it functions in a heterodimer with Dpp (Arora, 1994). Dpp and Gbb activate the Punt receptor, which in turn phosphorylates Thickveins (Tkv), leading to the activation of the Smad family of proteins (Fig. 3.1.1). The Smad1 homologue, Mothers against Dpp (Mad), is phosphorylated by activated Tkv; it then associates with the Co-Smad (Smad4)

homologue Medea (Med) and translocates to the nucleus, either alone or in association with a DNA-binding subunit, where it activates target genes by binding to specific promoter elements (Moustakas et al., 2001; Shi and Massague, 2003; ten Dijke and Hill, 2004).

In the wing imaginal discs, Dpp signaling regulates the expression of several genes, such as *optomoter blind (omb), spalt major (salm)* and *vestigial-quadrant enhancer* (vg^{Q}) (Burke and Basler, 1996; Grimm and Pflugfelder, 1996a; Kim et al., 1997; Lecuit et al., 1996; Lecuit and Cohen, 1998; Nellen et al., 1996). The I-Smad homologue, *daughters against dpp* (*dad*), is also a Dpp target gene that acts in a negative feedback loop to inhibit Dpp signaling (Tsuneizumi et al., 1997). A number of extracellular proteins also act as regulators of BMP signaling. The Crossveinless-2 (Cv-2) and Tolloid (Tld) proteins potentiate signaling (Conley et al., 2000; Marques et al., 1997) while the Chordin homologue Short gastrulation (Sog) inhibits the BMP ligands (Francois et al., 1994; Yu et al., 1996).

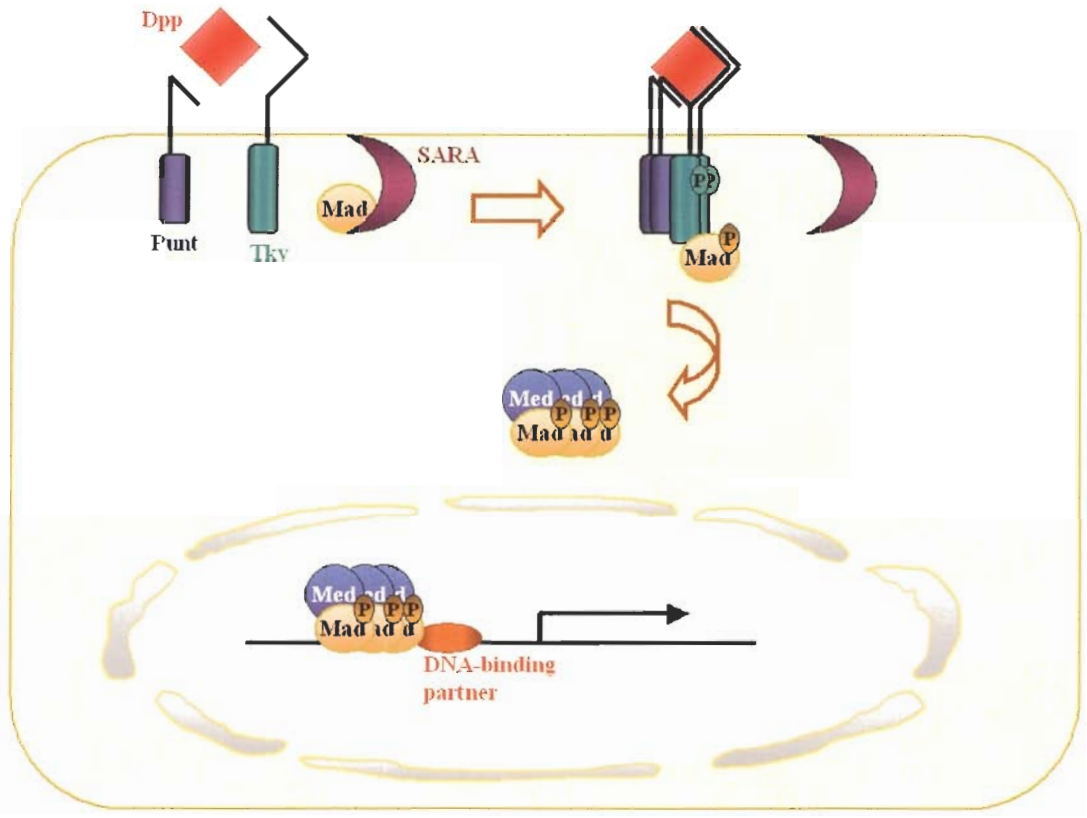

Figure 3.1.1 The Dpp signaling pathway

Binding of Dpp ligand to a type II receptor Punt in concert with a type I receptor Tkv leads to formation of a receptor complex and phosphorylation of Tkv. Tkv subsequently phosphorylates Mad, which allows it to associate with Med and move into the nucleus. In the nucleus, the Smad complex associates with a DNA-binding partner, and then binds to specific enhancer in target gene, activating transcription.

3.1.2 Nlk kinase cascade in TGFβ signaling

There is accumulating evidence that the action of NLKs is not restricted to the Wnt pathway, rather they have the ability to target the activity of a number of different proteins. Among these are additional members of the HMG-domain containing protein family, such as xSox11 and HMG2L1 (Hyodo-Miura et al., 2002; Yamada et al., 2003), as well as other transcriptional regulators such as CBP/p300, Stat3 and Myb (Kanei-Ishii et al., 2004; Ohkawara et al., 2004; Yasuda et al., 2004).

NLKs are proposed to be a part of a kinase cascade composed of Nemo-like mitogen-activated protein kinases (MAPK), the MAPKK, HIPK2 (Kanei-Ishii, 2004) and the MAPKKK Tak1 (TGFβ-activated kinase). Extensive studies in vertebrate cell culture systems have shown that Tak1 participates in many different signaling processes and cellular events, including TGFβ signaling, apoptosis and the NfκB pathway (Ninomiya-Tsuji et al., 1999; Shibuya et al., 1996; Takaesu et al., 2000; Takaesu et al., 2003; Yamaguchi et al., 1995). Tak1 has been implicated in the activation of JNK, p38 and NLK MAPKs (Shirakabe et al., 1997) (Wang et al., 2001) (Ishitani, 1999; Rocheleau, 1999). In addition to activating numerous pathways, Tak1 activity can be induced by a number of extracellular stimuli, among them TGFβ, Activin, Interleukin-1 and more recently Wnts themselves (Ohkawara et al., 2004) (Golan et al., 2004; Ishitani et al., 2003a; Kanei-Ishii et al., 2004; Smit et al., 2004; Yamaguchi et al., 1995). Although Tak1 and the NLKs have been implicated to play roles in TGFβ superfamily, mainly being activated by TGFβ signaling, much remains to be learned.

3.1.3 Structure and function of Smads

The Smad family plays pivotal roles in TGFβ signalling. The Smads typically consist of conserved N-terminal Mad homology 1 (MH1) and a C-terminal Mad homology 2 (MH2) domains which are separated by a poorly conserved proline-rich linker region (Christian and Nakayama, 1999) (Fig. 3.1.2). The MH1 domain is highly conserved in R-Smads and Co-Smads but not in I-Smads. In the basal unstimulated state, the MH1 domain inhibits the functions of MH2 domain. However, the MH1 domain possesses other function as well; it has a nuclear localization signal (NLS) and DNA-binding motif. The DNA-binding activity of MH1 domain is suppressed by the presence of the MH2 domain, suggesting that the MH1 and MH2 domains may inhibit each other's function in the absence of TGFβ (reviewed in Massague, 1998). I-Smads do not have MH1 domain.

The Smad MH2 domain is involved in several important protein-protein interactions (Fig. 3.1.2). The MH2 domain of the R-Smad contains receptor phosphorylation sites (SSXS indicated in Fig 3.1.2; Macias-Silva et al., 1996); mediates the association with type I receptor (Macias-Silva et al., 1996), interacts with Co-Smad MH2 domain upon receptor mediated phosphorylation (Hata et al., 1997) and binds to other transcription factors, such as Fast-1 (Chen et al., 1996) and *Drosophila* Schnurri (Arora et al., 1995; Grieder et al., 1995). Co-Smad and I-Smad do not possess receptor phosphorylation sites.

The linker region is highly variable in size and sequence. In R-Smads, the linker region contains MAPK phosphorylation sites. There is evidence that phosphorylation of

these sites in response to Erk MAPK activation inhibits nuclear translocation of Smads (Kretzschmar et al., 1997). The PY motif of a proline-rich sequence in the linker region of R-Smads is important for interacting with the WW motif of Smurf (Smad ubiquitination regulatory factors) (Massague and Chen, 2000). Smurfs are a group of ubiquitination ligases that bind specifically to R-Smads and target them for proteosome-mediated ubiquitination and subsequent degradation (Ebisawa et al., 2001; Tajima et al., 2003).

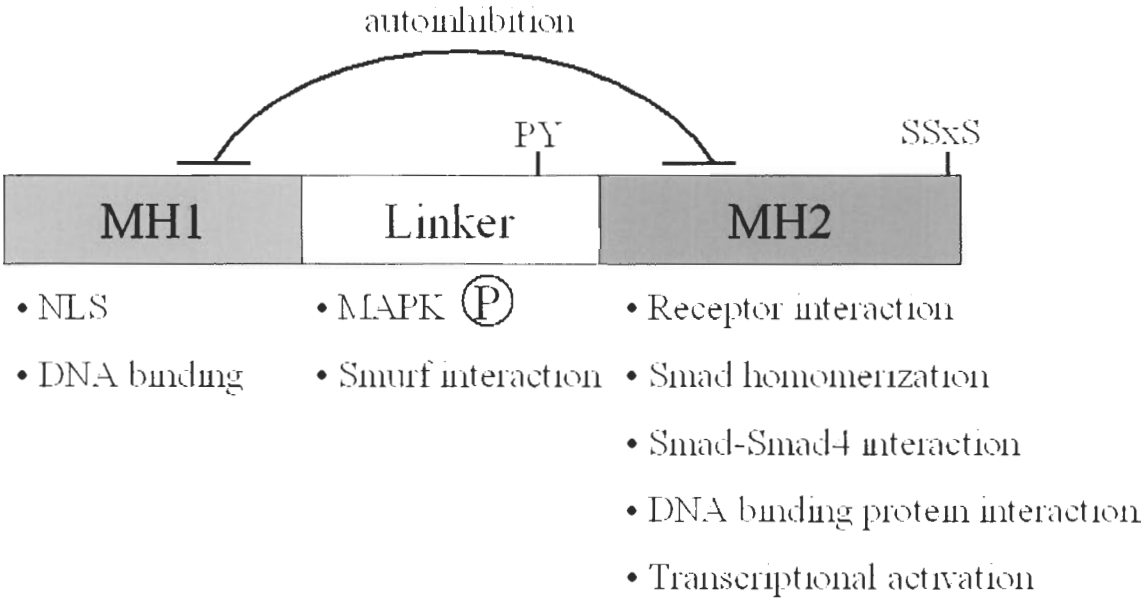

Figure 3.1.2 Smad domains and their functions

MH1 and MH2 domains inhibit each other in the absence of signal. MH1 domain is important for binding to DNA, and is missing in I-Smads which also have a longer linker region. Nuclear localization signal (NLS) in both R- and Co-Smads enhance their nuclear import.

Upon signaling, activated receptor phosphorylates R-Smad on the C-terminal distal serine residues. R-Smads associate with Co-Smad (Smad4) and with DNA-binding protein via the MH2 domain. MH2 domain also participates in transcriptional activation.

MAPK phosphorylate some Smads in the linker region, inhibiting Smad accumulation in the nucleus. The PY motif in the linker region of R-Smads is important for interacting with the WW motif of Smurf.

3.1.4 Smad nuclear translocation is signal dependent

When Smad proteins are overexpressed in culture cells, regulated nuclear translocation is a key event for induction of gene expression (reviewed in Raftery and Sutherland, 1999). In the basal state, Smads exist as monomers (Inoue et al., 1998; Kawabata et al., 1998) or homo-trimers (Shi et al., 1997). Upon ligand activation of the receptor complex, the type I receptor kinase phosphorylates the specific R-Smad in the very C-terminus SSXS domain. These R-Smads then form hetero-hexamers with Co-Smads and move into nucleus. Nuclear translocation of R-Smad does not require Co-Smad as determined by using Smad4-defective cells (Liu et al., 1997). Co-Smad also translocates into the nucleus in response to TGFβ signaling and this translocation requires the presence of R-Smad (Das et al., 1998; Wisotzkey et al., 1998).

Other signals also modulate TGFβ family signal activity through regulation of Smad nuclear translocation. MAPK-mediated phosphorylation of Smad in the linker domain can negatively regulate BMP signals through blocking Smad nuclear accumulation (Kretzschmar et al., 1997). Given the possibility that other extracellular signals may interfere the Smad subcellular localization, characterization of novel players and studies of the crosstalk of TGFβ with other signaling pathways would be valuable.

3.1.5 Dpp in *Drosophila* wing development

Dpp signalling plays several distinct roles during larval and pupal wing development (Segal and Gelbart, 1985; Spencer et al., 1982). During larval disc development, Dpp participates in the initiation phase of vein specification as well as overall patterning of the wing. Dpp is expressed along the AP boundary of the disc in response to Hedgehog signaling (Tanimoto et al., 2000). Hh signaling acts at short range to pattern the central (L3 to L4) region independently of inducing Dpp expression (Mullor et al., 1997; Strigini and Cohen, 1997). Dpp in turn, exerts a direct long-range organizing influence across the rest of the wing. Thus, formation of L3 and L4 veins are influenced by both Hh and Dpp signaling; while specification of the more distal veins, L2 and L5, depends only upon Dpp signaling, through the dose-sensitive regulation of target gene expression. These domains of the target gene expression establish the organization and position of wing veins by establishing boundaries of gene expression along which the veins form (reviewed in Crozatier et al., 2004). For example, the anterior boundary of the expression of *spalt-major* (*salm*) defines the position of the prospective L2 vein; the boundary of Optomotor-blind (Omb) and Brinker (Brk) contributes to positioning of the L5 veins (Cook et al., 2004). Mutations that specifically target the early role of Dpp result in vein loss, fusions of veins and loss of wing tissue (Segal and Gelbart, 1985; Spencer et al., 1982).

During pupal wing development, *dpp* expression in vein primordia is induced by epidermal growth factor receptor (EGFR) signaling and functions to maintain and refine the veins (de Celis, 1997; Yu et al., 1996). Mutations that disrupt the later function of

Dpp signalling result in wing vein abnormalities such as missing longitudinal and cross veins and occasionally ectopic veins (Segal and Gelbart, 1985).

3.1.6 Summary of the chapter

In this chapter, I describe a detailed analysis of a novel interaction between *nmo* and BMP signaling mediated by the *Drosophila* R-Smad Smad1 orthologue Mad. Through both phenotypic observations and genetic interaction studies in the wing, we have found that *nmo* acts as an antagonist of BMP signaling. These genetic interactions are supported by the finding that elevated Nemo can attenuate Dpp-target gene expression while loss of *nemo* results in elevated target gene expression. Biochemical studies establish that Nemo can bind to and phosphorylate both Mad and the co-Smad Medea and can prevent Mad's nuclear localization in cell culture. Nemo phosphorylates serine 25 in the MH1 domain of Mad and mutation of the single Nemo-phosphorylation site in Mad relieves the inhibition of nuclear translocation and causes ligand-independent nuclear translocation. This is the first example of inhibition of *Drosophila* BMP signaling by a MAPK and represents a novel mechanism of Smad inhibition.

3.2 Results

3.2.1 Co-localization of Nemo and receptor-activated Mad

During wing patterning *Drosophila* BMP signalling is carried out by two related BMPs, Decapentaplegic (Dpp) and Glass bottom boat (Gbb) (Padgett et al., 1987; Wharton et al., 1991). Dpp has been the best characterized and is found to act as a morphogen during the patterning of multiple tissues during embryonic and imaginal disc development (reviewed in Raftery and Sutherland, 1999). Dpp and Gbb activate the Punt receptor, which in turn phosphorylates Thickveins (Tkv), leading to the activation of the Smads. The Smad1 orthologue, Mothers against Dpp (Mad), is phosphorylated by activated Tkv and together with Medea (Med) translocates to the nucleus to regulate transcription of target genes (reviewed in Moustakas et al., 2001; Shi and Massague, 2003; ten Dijke and Hill, 2004). In the wing imaginal discs Dpp signaling regulates the expression of several genes, such as *optomoter blind (omb), spalt major (salm)* and *vestigial-quadrant enhancer* (vg^{Q}) (Burke and Basler, 1996; Grimm and Pflugfelder, 1996a; Kim et al., 1997; Lecuit et al., 1996; Lecuit and Cohen, 1998; Nellen et al., 1996). The Inhibitory-Smad homologue, *daughters against dpp* (*dad*), is also a Dpp target gene that acts in a negative feedback loop to inhibit Dpp signaling (Tsuneizumi et al., 1997).

Dpp signalling plays several distinct roles during larval and pupal wing development (Segal and Gelbart, 1985; Spencer et al., 1982). During larval disc development, Dpp participates in the initiation phase of vein specification as well as overall patterning of the wing. Dpp is expressed along the AP boundary of the disc in response to Hedgehog signaling (Tanimoto et al., 2000). Dpp protein distribution can be

monitored by using an anti-GFP antibody to detect a fusion protein of Dpp with GFP (Dpp-GFP) (Fig. 3.2.1A, B) (Teleman and Cohen, 2000). Localized phosphorylation and activation of Mad (pMad) results in characteristic patterns of reporter gene expression across the wing disc and can be monitored using an antibody that specifically recognizes pMad (Tanimoto et al., 2000). In the wing imaginal disc, pMad levels are highest in the cells flanking the AP boundary (Fig 3.2.1B, C). Expression is markedly lower in the Dpp-expressing cells themselves (Fig. 3.2.1B) (Tanimoto et al., 2000; Teleman and Cohen, 2000). A steep gradient drops off on either side of the central pMad region, thus pMad appears to be enriched in two stripes flanking the Dpp stripe (Fig 3.2.1C).

We have previously described the expression pattern of *nmo* during wing morphogenesis (Verheyen et al., 2001; Zeng and Verheyen, 2004). In addition to expression along the dorsal/ventral boundary, in late third instar wing discs *nmo* is expressed in two stripes flanking the AP boundary of the wing (Fig. 3.2.1D; Zeng and Verheyen, 2004). This pattern along the AP boundary is reminiscent of the pattern of phosphorylated Mad and corresponds to the site of the future longitudinal veins L3 and L4 (Tanimoto et al., 2000). Co-localization studies show that *nmo* and pMad are both expressed in overlapping domains flanking the AP boundary (Fig. 3.2.1D-F). During pupal wing development, *nmo* is expressed in intervein regions and enriched in the cells flanking the presumptive veins (Verheyen et al, 2001). This pattern of expression also overlaps with the expression of pMad and suggests a role for *nmo* during Dpp's role in vein patterning and refinement (Conley et al., 2000).

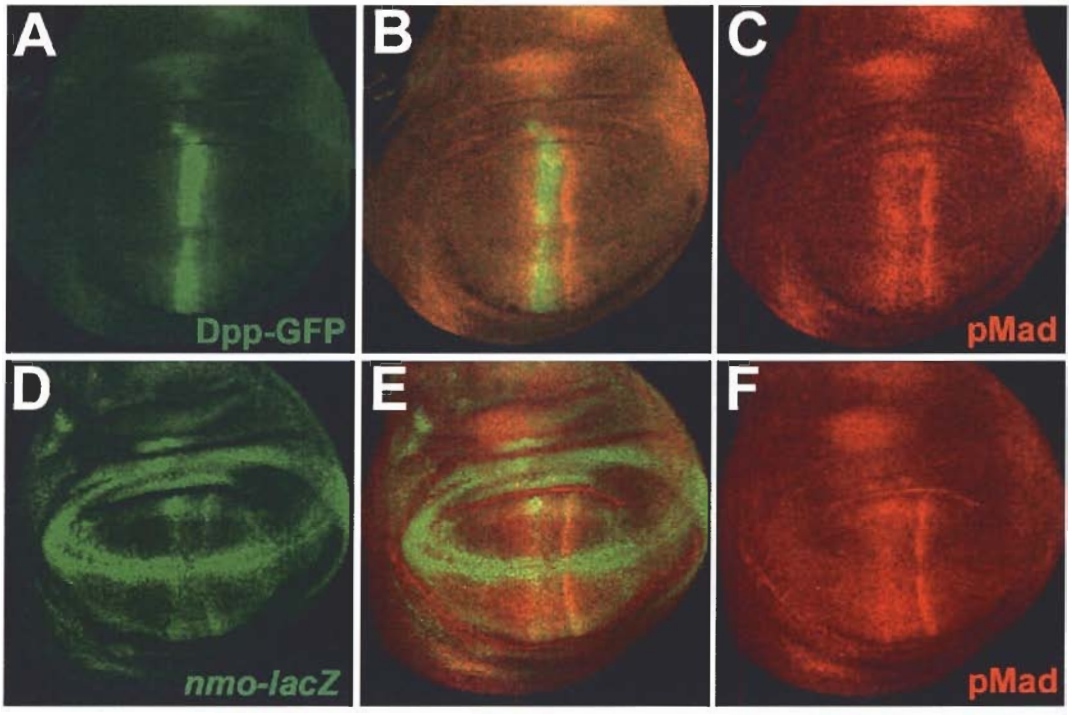

Figure 3.2.1 Nemo and pMad co-localize in L3 and L4 vein primordia

(A) Dpp distribution in late 3rd instar wing disc revealed using an anti-GFP antibody (green) in *dpp-GFP* flies. (B, C) pMad staining (red) is highest in the cells flanking the AP boundary; where the Dpp concentration is high, but is reduced in the Dpp-expressing cells themselves. (D, E) nmo^{lacZ} expression in late third instar stage wing discs (green) co-localizes in the L3 and L4 vein primordia flanking the AP boundary with highest levels of pMad staining (red in E, F).

3.2.2 *nmo* wing phenotypes suggest antagonism of Dpp signalling

The adult wing blade consists of two epithelial sheets of intervein cells intersected at regular intervals by an invariant pattern of longitudinal veins (numbered L2-L5) and crossveins, namely the anterior crossvein (ACV) and posterior crossvein (PCV) (Fig. 3.2.2A) (Bier, 2000a). During larval disc development, Dpp participates in the initiation phase of vein specification as well as overall patterning of the wing. Mutations that specifically target the early role of Dpp result in vein loss, fusions of veins and loss of wing tissue (Segal and Gelbart, 1985; Spencer et al., 1982). Later, during pupal wing development, *dpp* expression in vein primordia functions to maintain and refine the veins (de Celis, 1997; Yu et al., 1996).

The *nmo* loss of function wing phenotype is characterized by varying degrees of ectopic veins emanating from the posterior cross vein (PCV), posterior to L5 and between L2 and L3. A severe example, nmo^{DB24}, is shown in Fig. 3.2.2B. Such a phenotype suggests that normally *nmo* must be acting to inhibit vein formation. The *nmo* mutant phenotype is quite similar to those found in flies ectopically expressing components of BMP signaling, such as Dpp, Mad and Gbb (Haerry et al., 1998; Yu et al., 2000; Yu et al., 1996). Using the *vestigial-Gal4* (*vg-Gal4*) driver to express *UAS-mad* along the DV boundary causes activated signalling downstream of the receptor and gives rise to broader wing shape and ectopic veins along L2 and L5 and emanating from the PCV (Fig. 3.2.2C; also shown in (Tsuneizumi et al., 1997). Haerry et al. (1998) show a very similar phenotype when the *A9-Gal4* line is used to drive *UAS-gbb*.

Ectopic expression of Nemo using the Gal4-UAS misexpression system also

causes a number of different wing phenotypes (Brand and Perrimon, 1993; Mirkovic et al., 2002; Verheyen et al., 2001; Zeng and Verheyen, 2004). Using *69B-Gal4* results in varied loss of the PCV and a narrower wing blade (Fig. 3.2.2F; Verheyen et al., 2001). This phenotype is very similar to those found with loss-of-function mutations in *gbb* (Fig. 3.2.2D), *medea*, and in the *crossveinless* mutants, which are emerging as a class of agonists of BMP signalling (Conley et al., 2000; Hudson et al., 1998; Khalsa et al., 1998; Segal and Gelbart, 1985). Similarly, ectopic expression of the Dpp antagonist *sog* also leads to loss of PCV tissue (Yu et al., 1996; Fig. 3.2.2E). The observations that *nmo* mutants resemble phenotypes seen upon activation of BMP signalling, that ectopic *nmo* mimics loss of BMP signaling and that *nmo* is expressed in domains in which high levels of Dpp signalling are active suggest that Nemo may play an antagonistic role in BMP signaling during wing patterning.

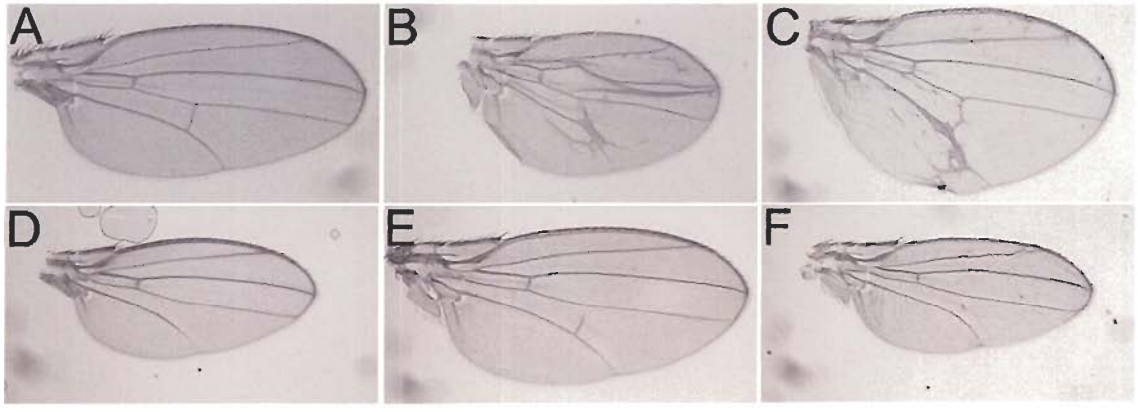

Figure 3.2.2 Modulation of *nmo* suggests an antagonism of BMP signaling

(A) A wild type adult wing. (B) A severe nmo^{DB24} loss of function wing phenotype. (C) Ectopic BMP signalling in a *UAS-mad/+; vg-Gal4/+* fly. (D) Reduced BMP signaling in gbb^{1}/gbb^{4} (E) Ectopic expression of the BMP antagonist Sog, *UAS-sog/+; 69B-Gal4/+*. (F) Ectopic Nemo in *UAS-nmo/+; 69B-Gal4/+* phenocopies reduced BMP signaling.

3.2.3 *nmo* is an antagonist of BMP signalling

To test the hypothesis that Nemo inhibits BMP signalling we first carried out genetic interaction studies. Several *Gal4* driver strains were used to express components of the BMP signalling pathway, and the ability of *nmo* to modulate the induced phenotypes was then examined.

Consistently, expression of *UAS-nmo* resulted in a dramatic reduction in the severity of phenotypes caused upon ectopic activation of Dpp signalling. Specifically, using *dpp-Gal4* to express a constitutively active Tkv receptor (*UAS-tkv^{QD}*) (Nellen et al., 1996) results in a 20.8% penetrant bifurcated wing blade phenotype (n= 53), which was completely suppressed by co-expression of *UAS-nmo* (Fig. 3.2.3A-C; n= 49). Although the bifurcation is suppressed, ectopic *nmo* is unable to fully restore the wing to wildtype morphology. The *vg>mad* phenotype is characterized by a broader wing shape and an abnormal wing vein phenotype (Fig. 3.2.2C and 3.2.3D). While vg>*nmo* caused no discernable phenotype (Fig. 3.2.3E), co-expression of *UAS-nmo* and *UAS-mad* leads to suppression of the phenotype induced by *UAS-mad* alone (Fig. 3.2.3F).

In addition to the suppression of activated Dpp signaling by ectopic Nemo, we observe an enhancement in the penetrance of the *dpp>tkv^{QD}* bifurcated wing phenotype from 20.8% to 86.3% in flies heterozygous for the *nmo^{P}* loss-of-function mutation *(dpp-Gal4, nmo^{P}/UAS-tkv^{QD}*; data not shown; n= 110), suggesting that reduction in the dosage of *nmo* can lead to elevated BMP signalling and induce a stronger phenotype. These genetic interactions all support the model that Nemo antagonizes Dpp signalling during wing development.

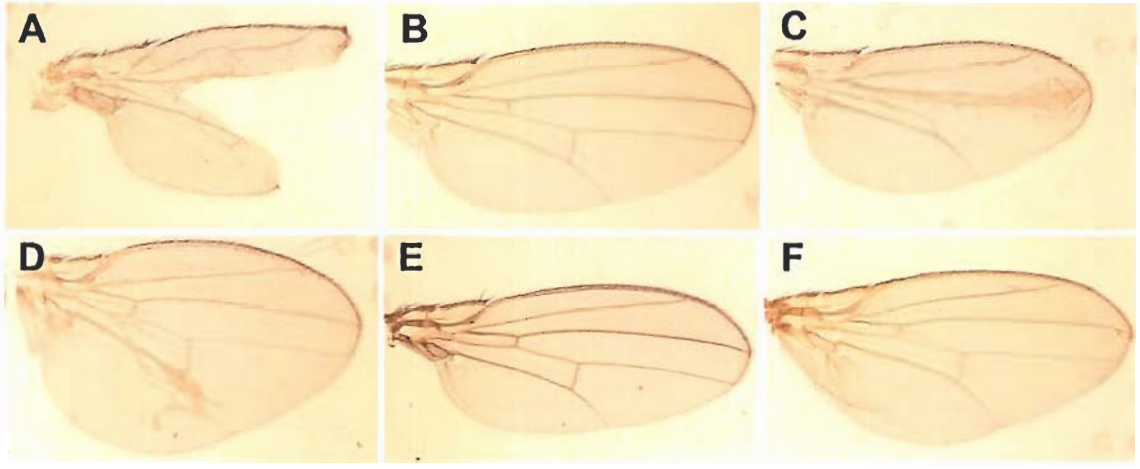

Figure 3.2.3 *nmo* antagonizes BMP signaling during wing development

(A) *dpp-Gal4> UAS-tkv*^{QD} results in a bifurcated wing blade. (B) *dpp-Gal4> UAS-nmo* has no visible wing defect. (C) Ectopic *nmo* is able to suppress the bifurcated phenotype in *UAS-nmo/+; dppGal4/UAS-tkv*^{QD} wings. (D) *vg-Gal4>UAS-mad.* (E) *vg-Gal4>UAS-nmo.* (F) *UAS-mad/+; vg-Gal4/UAS-nmo* rescues the broad wing blade and ectopic wing veins phenotype caused by ectopic *mad.*

3.2.4 Nemo can modulate Dpp-dependent gene expression in regions of high Dpp signaling in the wing disc

To further characterize the inhibitory effect of *nmo* on Dpp signaling, the expression of Dpp-target genes was monitored in 3rd instar larval wing discs bearing either *nmo* mutant clones or ectopic expression of *nmo*. Among the target genes in the wing, the *vestigial* quadrant (vg^{Q}) enhancer is expressed in four domains flanking the DV and AP boundaries (Fig. 3.2.4A). Mad has been shown to bind directly to the Dpp-responsive element within the vg^{Q} enhancer (Kim et al., 1997) and thus this gene serves well as a readout of Mad-mediated gene expression (Fig. 3.2.4A). *UAS-nmo* driven by the dorsally-expressed *apterous-Gal4* abolishes vg^{Q}-*lacZ* staining in the dorsal wing pouch (Fig. 3.2.4B). To further characterize this effect, vg^{Q} expression was monitored in wing discs containing *nmo* loss-of-function somatic clones (Fig. 3.2.4C-E; marked by absence of GFP). nmo^{DB24} clones in the central region of the wing where Dpp signaling is most active show elevated vg^{Q} expression (arrow in Fig. 3.2.4E), while clones outside of this region show no change in reporter gene expression (arrowhead in Fig. 3.2.4E). We speculate that Nemo is only acting in areas in which high levels of Dpp signalling occur and where enriched *nmo* expression is observed in wildtype (see Fig. 3.2.1D). In contrast, overexpression of Nemo with *ap-Gal4* causes elevated expression of Nemo throughout the dorsal wing surface where it can more broadly inhibit gene expression.

Consistent with this, *nmo* also suppresses the Dpp-dependent expression of *dad*. *dad* expression is induced by ectopic expression of *UAS-mad* (Tsuneizumi et al.,1997) Flip-out misexpression clones in which Mad is expressed at high levels in marked somatic wing disc clones show ectopic dad^{lacZ} expression (Fig. 3.2.4F-H). This

expression can be inhibited in double flip-out clones expressing both *UAS-mad* and *UAS-nmo* (Fig. 3.2.4I-K). Thus we observe the negative effect of Nemo on two Dpp-dependent target genes, suggesting it can act to block the transcriptional activation that is induced upon pathway activation.

Figure 3.2.4 *nmo* modulates Mad-dependent target gene expression

(A) vg^{Q}-*lacZ* expression in the wild type 3rd instar wing imaginal disc. (B) vg^{Q} expression is abolished in the dorsal wing pouch when *UAS-nmo* is expressed using the dorsal specific driver *ap-Gal4*. (C, D) nmo^{DB24} somatic clones (marked by the absence of GFP, green). (D, E) Expression of vg^{Q}-*lacZ* is increased in the clone abutting the AP boundary (arrow) but shows no detectable change in the clone further away from the levels of highest Dpp signaling, in which nmo expression is normally low (arrowhead). (F, G) Flip-out clones ectopically expressing *UAS-mad* (marked with GFP) (G, H) ectopic dad^{lacZ} expression in flip-out clones (anti-βGal antibody staining, red). (I, J) Double flip-out clones of *UAS-nmo* and *UAS-mad* show no Mad-dependent ectopic dad^{lacZ} expression (J, K).

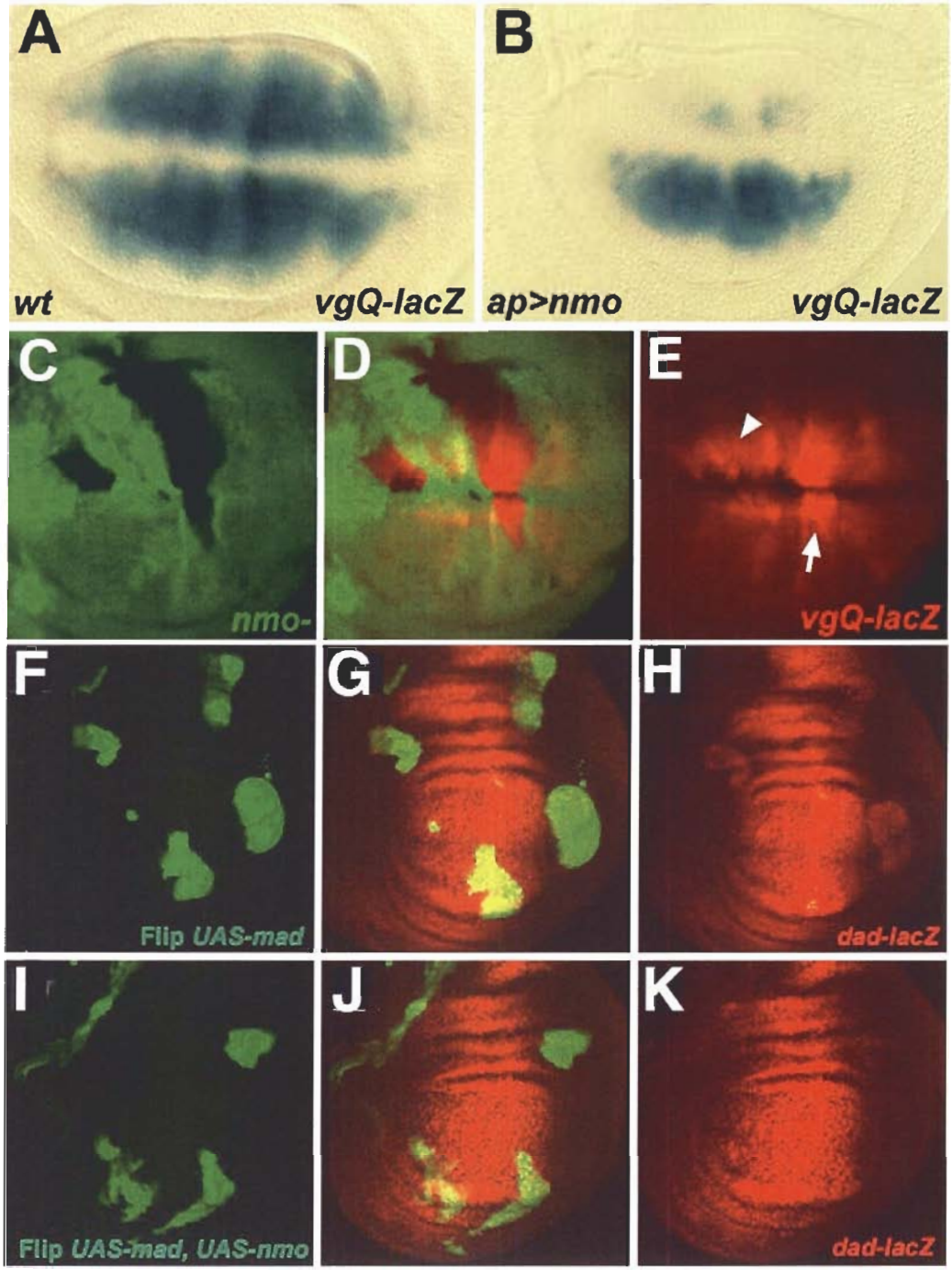
A
wt
vgQ-lacZ
B
ap>nmo
vgQ-lacZ
C
nmo-
D
E
vgQ-lacZ
F
Flip UAS-mad
G
H
dad-lacZ
I
Flip UAS-mad, UAS-nmo
J
K
dad-lacZ

3.2.5 Nemo binds to and phosphorylates Mad and Medea

Since Nemo was able to genetically inhibit Dpp, we sought to address the underlying biochemical mechanism for this suppression. NLKs have been shown to target a number of transcriptional regulators and affect their function both positively and negatively. Since Nemo can antagonize Mad-dependent target gene expression in vivo, binding studies were carried out with *Drosophila* Smads. HEK293 cells were transfected with T7-tagged Mad and Flag-tagged Nemo and immunoprecipitations were performed to determine whether the proteins interacted with each other. Reciprocal immunoprecipitations from cell lysates both resulted in the co-immunoprecipitation of Mad and Nemo (Fig. 3.2.5.1A).

I examined whether Nemo might also interact with Medea. As observed with Mad, Nemo and Medea were found to co-immunoprecipitation from cell lysates (Fig. 3.2.5.1B). These results demonstrate that Nemo can interact with both Mad and Medea and that it may affect their function through this interaction.

Next I addressed whether Nemo could phosphorylate either or both of these proteins. In vitro kinase assays were performed on cell lysates and Nemo was found to phosphorylate both Mad and Medea, as well as autophosphorylate (Fig. 3.2.5.1C, D). This was dependent on Nemo's kinase activity as a dominant negative Nemo (K69M) construct in which the Lysine residue in the ATP-binding domain was changed to Methionine did not show phosphorylation of Mad and Medea, nor did it show Nemo autophosphorylation (Fig. 3.2.5.1C, D).

To address the possibility that these interactions are conserved across species, I examined whether mammalian Nlk associates with Mad or Medea. Cells were transfected

with Flag-tagged Nlk and T7-tagged Mad and reciprocal immunoprecipitation with anti-Flag and anti-T7 antibodies were performed (Fig. 3.2.5.2A). Results indicated that Nlk, like its fly orthologs, binds Mad. Similarly, Nlk and Medea were also found to co-immunoprecipitation from transfected cell lysates (Fig. 3.2.5.2B).

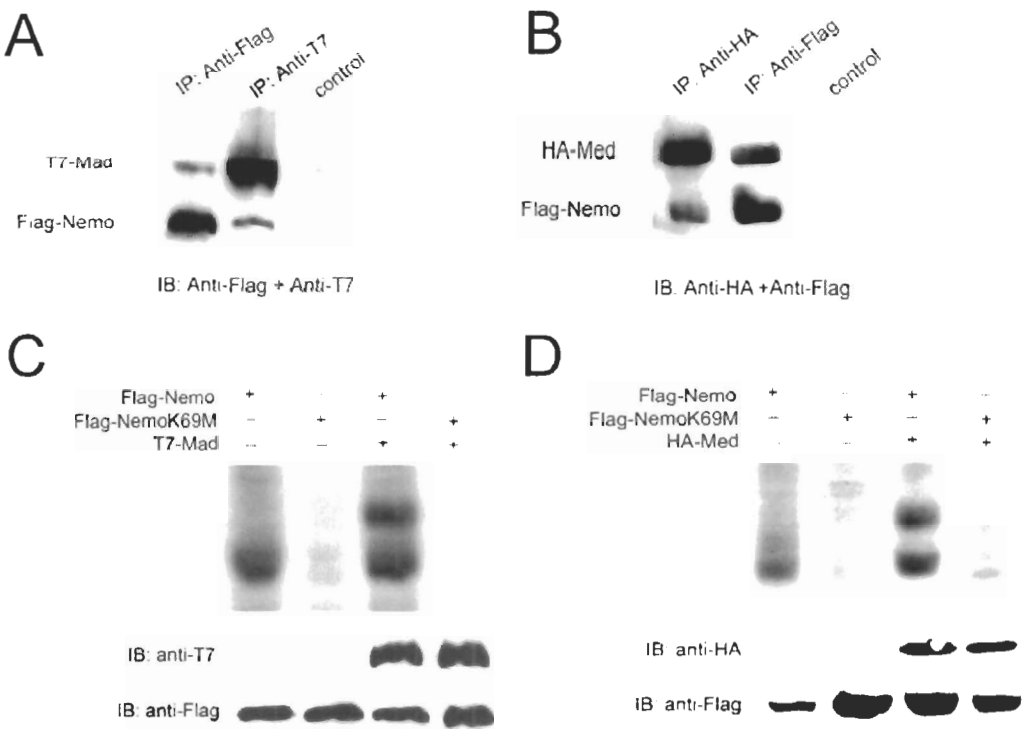

Figure 3.2.5.1 Nemo binds and phosphorylates both Mad and Medea.

(A) Binding of Nemo and Mad. pXJ-Flag-nemo and pCMV-T7-mad were co-transfected into HEK293 cells. Cell lysates were immunoprecipitated with anti-Flag, anti-T7 or IgG (control). Immunoblotting was performed with anti-Flag and anti-T7 antibodies. (B) Binding of Nemo and Medea. pXJ-Flag-Nemo and pCMV-HA-Med were co-transfected into HEK293 cells. Cell lysates were immunoprecipitated with anti-HA, anti-Flag or IgG (control). Immunoblotting was performed with anti-HA and anti-Flag antibodies. (C, D) Nemo phosphorylates Mad and Medea and autophosphorylates. HEK293 cells were transfected with expression vectors as indicated. Immunoprecipitated complexes with indicated antibodies were subjected to in vitro kinase assays and analyzed by autoradiography. The immunoprecipitates were also immunoblotted with indicated antibodies to confirm loading.

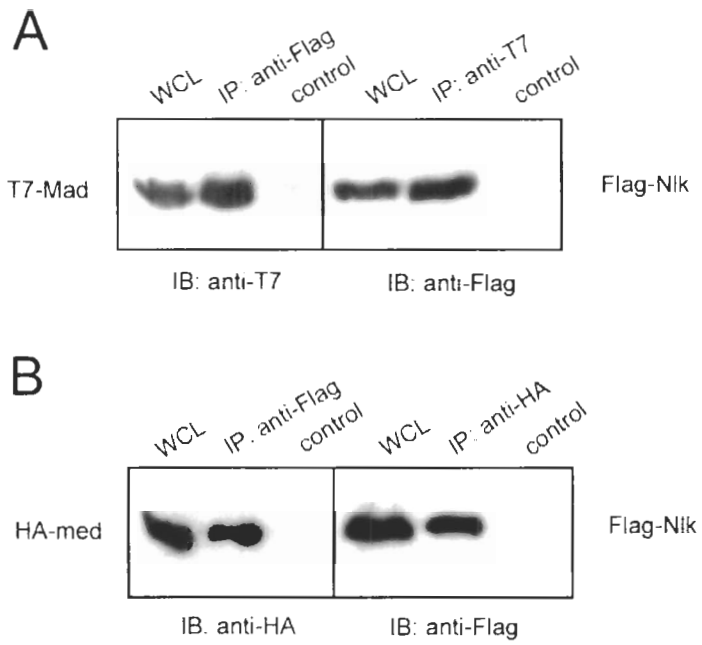

Figure 3.2.5.2 Nlk associates with Mad and Medea.

(A) Binding of Nlk and Mad. pCMV-Flag-nlk and pCMV-T7-mad were co-transfected into HEK293 cells. In the left panel, cell lysates were immunoprecipitated with anti-Flag or IgG (control). Immunoblotting was performed with anti-T7 antibody. In the left panel, cell lysates were immunoprecipitated with anti-T7 or IgG (control). Immunoblotting was performed with anti-Flag antibody. Whole cell lystate (WCL) was used as a positive control for Immunoblotting. (B) Binding of Nlk and Medea. pCMV-Flag-nlk and pCMV-HA-Med were co-transfected into HEK293 cells. In the left panel, cell lysates were immunoprecipitated with anti-Flag or IgG (control). Immunoblotting was performed with anti-HA antibody. In the left panel, cell lysates were immunoprecipitated with anti-HA or IgG (control). Immunoblotting was performed with anti-Flag antibody. Whole cell lystate (WCL) was used as a positive control for Immunoblotting.

3.2.6 Nemo targets Serine 25 in the MH1 domain of Mad

Since Nemo is a proline-directed serine/threonine kinase, we sought to identify Nemo target residues in Mad. Based on the precedent seen with Erk-mediated inhibition of Smads, we first targeted residues within the linker region of Mad. Site-directed mutagenesis was employed to alter serine 212 (S212) to alanine in the single consensus Erk phosphorylation site (PNSP) in the linker domain. In addition, two putative SP target sites (S202 and S226) in the linker and one in the carboxy terminus of the MH1 domain (S146) were mutated to alanine (Fig. 3.2.6A). Surprisingly, a construct expressing Mad in which these four sites were altered to serine residues (Mad-4SA) was still phosphorylated by Nemo (Fig. 3.2.6B).

BMP receptor activation leads to phosphorylation of three Serines (SSVS) at the C terminus of Mad (reviewed in ten Dijke and Hill, 2004). A Mad construct in which these sites were altered (Mad-AAVA; Fig. 3.2.6A) was still phosphorylated by Nemo (Fig. 3.2.6B), ruling out those residues as possible target sites.

To map the domain in which the target residue was located, a truncated Mad protein was generated in which the MH1 domain was deleted (Mad-ΔMH1; Fig. 3.2.6A). This protein was no longer phosphorylated by Nemo (Fig. 3.2.6B), indicating that the target site was contained within the deleted fragment. Within the deleted MH1 fragment there are two putative Nemo target sites, S25 and S146. Since the S146 residue had been altered in the Mad-4SA construct that was still phosphorylated by Nemo, we focused on S25 (Fig. 3.2.6A). Site directed mutagenesis of S25A was performed and in vitro kinase assays from transfected cells revealed that Nemo does not phosphorylate MadS25A (Fig. 3.2.6B). Thus we have determined that Nemo phosphorylates the single serine 25 residue

in the MH1 domain of Mad. This residue has not previously been shown to be targeted by any MAPK proteins and has not previously been implicated in regulation of Mad function.

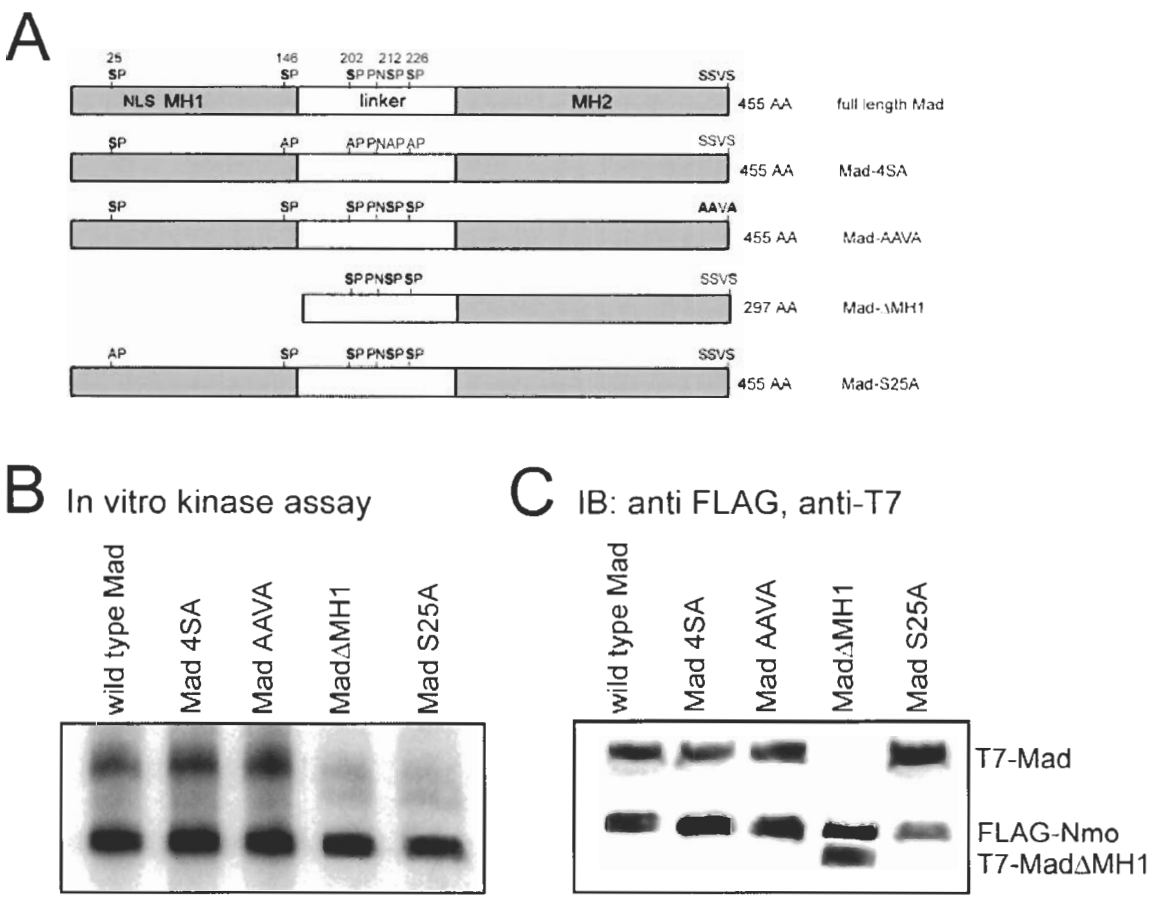

Figure 3.2.6 Nemo phosphorylates Serine 25 in the MH1 domain of Mad

(A) A schematic diagram of the full length Mad protein indicating the MH1, MH2 and linker domains, as well as the site of the nuclear localization sequence (NLS). Potential Nemo phosphorylation sites are indicated. Specific constructs were generated to identify residues that are phosphorylated by Nemo. (B) In vitro kinase assays performed with wildtype Mad, Mad 4SA, Mad AAVA, Mad-ΔMH1 and Mad S25A demonstrate that Nemo specifically targets Serine 25, and that Nemo autophosphorylates. (C) Immunoblot of cell extracts used in kinase assays showing relative expression of proteins.

3.2.7 Nemo blocks Tkv-dependent nuclear localization of Mad

Activation of BMP signaling leads to nuclear accumulation of receptor-phosphorylated Smads (reviewed in ten Dijke and Hill, 2004). Erk MAPK can inhibit this nuclear localization through its phosphorylation of Smads in the linker domain (reviewed in Massague, 2003). Since we have shown that Nemo can also phosphorylate Mad we examined whether this impacted the nuclear localization of Mad in transfected cells. Transfection of Cos7 cells with T7-Mad alone results in a uniform distribution of Mad (Fig. 3.2.7A and data not shown). Quantification shows that in 11.9% of transfected Cos7 cells (n= 388) Mad expression is nuclear. Co-transfection of an activated Tkv receptor (tkv^{QD}) leads to the dramatic nuclear accumulation of Mad (91.2% of cells; n= 457; Fig. 3.2.7B). This nuclear localization can be inhibited by co-transfection of wildtype Nemo with Mad and Tkv^{QD} (Fig. 3.2.7C). Quantification shows that Mad is nuclear in 40.1% (n= 424) of transfected cells. This effect is kinase dependent, as transfection with kinase dead Nemo (K69M) was unable to inhibit nuclear accumulation of Mad (Fig. 3.2.7D) as 87.1% of (n= 417) cells showed nuclear Mad.

3.2.8 Mutation of Mad-S25A results in receptor-independent nuclear localization

Examination of the subcellular localization of the Mad S25A protein in Cos7 and HeLa cells revealed a primarily nuclear localization of Mad, as compared to wildtype Mad which was primarily cytoplasmic (compare Fig. 3.2.7E to 3.2.7A). Significantly, the

nuclear localization was found to be constitutive and unaffected by either expression of activated receptor or the presence of Nemo (data not shown). This establishes that the phosphorylation of Mad by Nemo at Serine 25 is responsible for an inhibition of nuclear localization, which is abrogated when the residue is rendered immune to Nemo phosphorylation (Mad S25A).

Figure 3.2.7 Nemo-mediated phosphorylation inhibits the nuclear accumulation of Mad and Mad S25A shows receptor-independent nuclear localization

Cos7 cells were transfected with (A) T7-Mad; (B) T7-Mad and HA-Tkv^{QD} (constitutively active form); (C) T7-Mad, HA-Tkv^{QD} and Flag-Nemo; (D) T7-Mad, HA-TkvQD and Flag-NemoK69M (Kinase dead); (E) T7-Mad S25A. Immunostaining was preformed using anti-T7 and anti-HA antibodies to indicate the localization of T7-Mad (the left column) and expression of HA-Tkv^{QD} (the center column). DAPI staining was also performed prior to mounting (the right column). Expression of Nemo (C) can inhibit the Mad nuclear accumulation that occurs upon Tkv signaling (B). Expression of kinase dead Nemo does not affect Mad localization (D). (E) Mutation of the Nemo target site renders Mad S25A constitutively nuclear even in the absence of receptor activation.

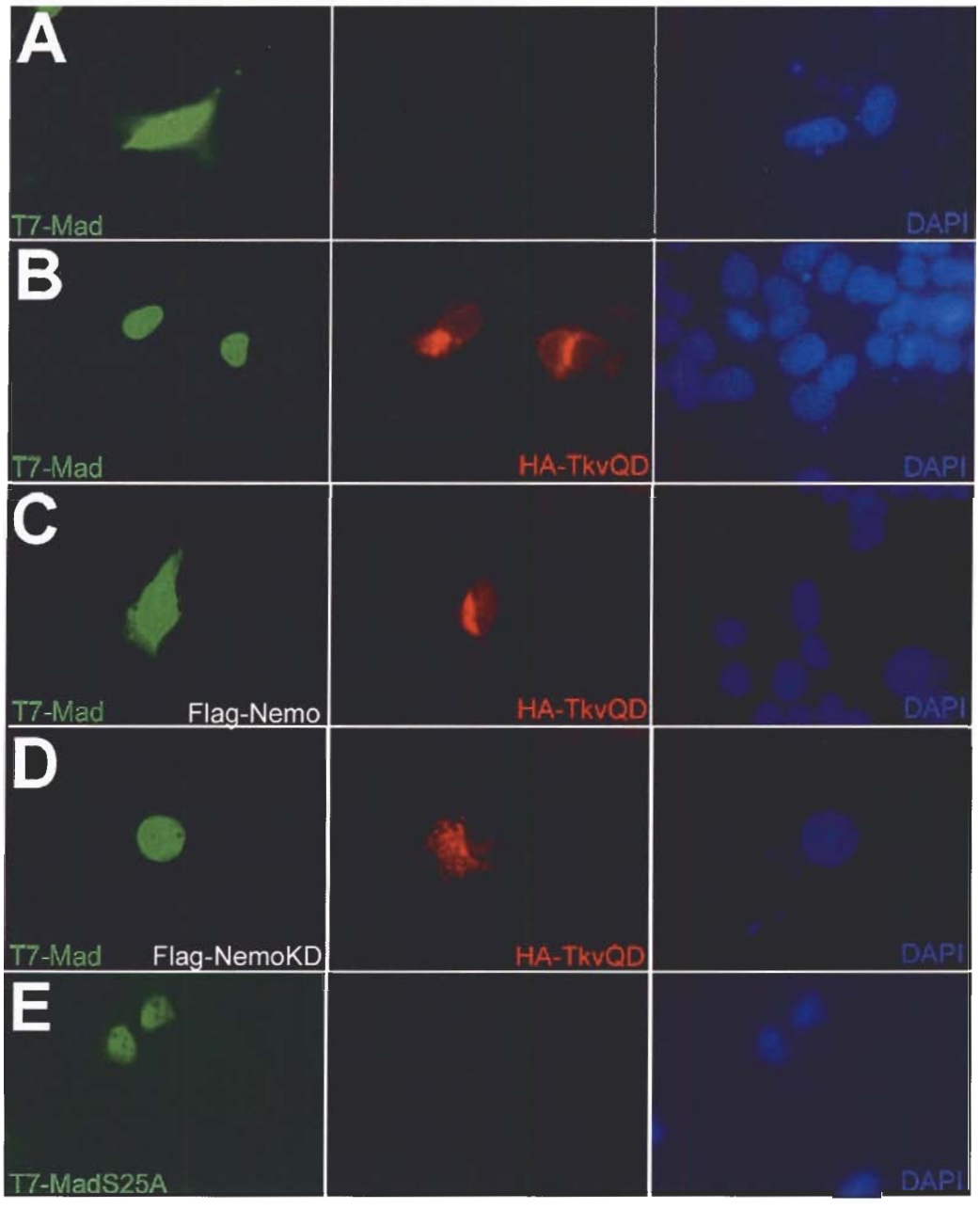
A
T7-Mad
DAPI
B
T7-Mad
HA-TkvQD
DAPI
C
T7-Mad
Flag-Nemo
HA-TkvQD
DAPI
D
T7-Mad
Flag-NemoKD
HA-TkvQD
DAPI
E
T7-MadS25A
DAPI

3.3 Discussion

3.3.1 Nemo antagonizes BMP signaling by inhibition of Mad

In this chapter, I demonstrate a novel regulatory role for the *Drosophila* NLK family member in a TGFβ superfamily signal transduction pathway. I provide the first evidence that Nemo is an antagonist of BMP signaling in *Drosophila* by examining its role in wing development through genetic analysis and examination of BMP-dependent gene expression. The genetic interaction studies show that phenotypes caused by ectopic activation of the Dpp pathway can be suppressed by ectopic *nmo* and enhanced by loss of *nmo*. Our data suggest that Nemo participates in the BMP pathway by modulating Mad activity. This is seen in the inhibition of Mad-dependent gene expression by Nemo and in the elevated expression of Mad target genes observed in *nmo* mutant clones. Nemo can bind to and phosphorylate both Mad and Medea and the phosphorylation of Mad has direct consequences on nuclear localization of Mad in cell culture. I have mapped the single Nemo target residue to Serine 25 within the MH1 domain of Mad and find that it is distinct from sites previously implicated in the regulation of Mad activity and nuclear localization.

3.3.2 Regulation of Mad nuclear localization by phosphorylation

The vertebrate Mad ortholog Smad1 normally shuttles between the cytoplasm and nucleus in the absence of signal, but upon receptor activation become phosphorylated, binds the Co-Smad and accumulates exclusively in the nucleus (Xiao et al., 2001). Such

nucleocytoplasmic shuffling is observed with R-Smads participating in both BMP and TGFβ signaling (reviewed in ten Dijke and Hill, 2004).

I show that Nemo can inhibit BMP signalling by antagonizing the nuclear localization of Mad in a kinase-dependent manner. Such a mechanism has been attributed previously to crosstalk between Erk MAPK signalling and TGFβ and BMP signalling (reviewed in Massague, 2003). Our research presents Nemo as the first MAPK attenuating *Drosophila* BMP pathway activity through phosphorylation of Mad. We have also found that murine NLK can bind to Mad and Medea, raising the intriguing speculation that this mechanism is conserved across species.

A number of studies using mammalian cell culture have revealed that MAPK can repress TGFβ superfamily signaling by targeting Smads (Aubin et al., 2004; Grimm and Gurdon, 2002; Kretzschmar et al., 1997; Kretzschmar et al., 1999; Pera et al., 2003). The BMP-specific Smad1 is a target of cross regulation by EGF signaling through the Erk MAPK pathway. Erk phosphorylates Smad1 in the linker domain between the DNA-binding and the transcriptional activation domains. This phosphorylation inhibits both the nuclear accumulation and transcriptional activity of Smad1 in cell culture and the in vivo role of Smad1 in neural induction and tissue homeostasis (Aubin et al., 2004; Kretzschmar et al., 1997; Pera et al., 2003). Ras-stimulated Erk also phosphorylates two R-Smads involved in TGFβ Activin signaling, namely Smad2 and Smad3, and prevents their nuclear accumulation (Kretzschmar et al., 1999). The phosphorylation sites within these Smads all differ, thus providing a mechanism for preferentially selective inhibition of one subtype (reviewed in Massague, 2003). Thus the distinct Nemo phosphorylation site in the MH1 domain represents an additional level of regulation of these proteins.

3.3.3 Targeting of the Mad MH1 domain by Nemo kinase

The phosphorylation of Serine 25 in the MH1 domain of Mad represents a novel point of regulation of Smads. This protein domain is involved in the nuclear localization, DNA binding and association with transcriptional regulators (Kretzschmar and Massagué, 1998). Within the MH1 domain, the most amino terminal sequence of Mad orthologues predicts a flexible region, then a short alpha-helix followed by a linker region and a longer second alpha-helix (Chai et al., 2003). The second helix contains the predicted nuclear localization sequence (NLS) (Xiao et al., 2001). Serine 25 is located just N terminal to the first alpha helix. The added negative charge following phosphorylation by Nemo could cause the two alpha helical regions to influence each other and potentially neutralize the positively charged NLS and prevent nuclear localization of Mad. Such a model is also supported by the finding that mutation of serine to alanine renders Mad constitutively nuclear and resistant to inhibition by Nemo. Interestingly, Kretzschmar et al. (1997) observed a similar constitutively nuclear localization when they mutated the Erk phosphorylation sites in Smad1. This suggests that both Nemo and Erk MAPK are involved in the inhibition of BMP signaling and that their distinct sites of action all function to block nuclear accumulation of Smads. Thus the cellular factors that induce either NLK or Erk activity can oppose the functions of BMP signaling.

3.3.4 Nemo's in vivo inhibition of Dpp signaling during wing patterning

In addition to the biochemical and cell culture evidence that Nemo targets the MH1 domain of Mad to inhibit its nuclear localization, I present in vivo evidence that Nemo antagonizes Mad-dependent BMP signaling during wing development. The co-localization of *nmo* expression with elevated pMad, combined with phenotypic observations suggested that *nmo* acts as an antagonist of BMP signaling during wing patterning. Genetic interaction studies confirmed such an antagonistic role since elevated Nemo could suppress the mutant phenotypes induced by elevated BMP signaling and reductions in *nmo* enhanced the penetrance of activated BMP phenotypes. In addition, modulation of *nmo* levels can influence the expression of Mad-dependent target genes. Specifically, elevated Nemo can attenuate the expression of two Dpp-targets, vg^{Q} and *dad,* while *nmo* somatic clones show elevated target gene expression. Thus the phenotypic analyses support and extend the biochemical model of Nemo's inhibition of Mad and BMP signaling.

3.3.5 NLKs integrate multiple signaling pathways during development

We have previously demonstrated that Nemo can antagonize *Drosophila* Wg signaling during wing development (Zeng and Verheyen, 2004). In this study I demonstrate that Nemo also acts to attenuate BMP signalling by targeting the action of Mad. In both of these signaling pathways the net outcome is the inhibition by Nemo of pathway-dependent target gene expression. These results demonstrate that Nemo and by extension the Nemo-like kinases play important roles in refining signaling pathways during development.

An intriguing but still incomplete picture is emerging regarding the regulation of both NLK expression and activity and it represents a potential point of crosstalk between signalling pathways. We have shown that *nmo* is transcriptionally regulated by Wg signaling (Zeng and Verheyen, 2004). Others have found that NLK kinase activity is stimulated by Tak1 after Wnt induction (Ishitani et al., 2003a; Smit et al., 2004; Kanei-Ishii et al., 2003) and that Tak1 can be activated by BMP signaling (Yamaguchi et al., 1995). Activated NLKs can inhibit TCF/LEF proteins and modulate Wnt-dependent gene expression (Ishitani et al., 2003b; Ishitani et al., 1999; Zeng and Verheyen, 2004). In this study I have found that *Drosophila* NLK is playing an important role in modulating BMP signaling and Mad-dependent gene expression. These findings represent an additional point of cross regulation and refinement between signaling molecules.

Chapter 4

Dpp represses Wg signaling by inhibiting the association of Arm and dTCF

4.1 Introduction

4.1.1 Crosstalk between Wnt and TGFβ signaling in vertebrates

Wnt and TGFβ are two distinct families of secreted ligands which employ different signaling components to exert their biological effect (see introductions in **2.1.1** and **3.1.1**). Both pathways play essential roles in cell fate specification during development and also contribute to cancer formation and progression. Crosstalk between TGFβ and Wnt signaling pathways has been studied, mainly describing the cooperation of the two pathways in controlling gene expression.

In vertebrates, cross regulation of the two pathways were reported in various organisms and tissues. Gastrin, a gastrointestinal hormone and growth factor, has been previously designated as a downstream target of the canonical Wnt pathway and a promoter of gastrointestinal cancer (Koh et al., 2000; Pradeep et al., 2004). The mouse gastrin promoter, possessing both TCF and Smad binding sites, was shown to be synergistically regulated by β-catenin/ TCF and Smad3/4 (Lei et al., 2004). Studies have identified the proto-oncogene *c-myc* as a target gene for an activated TCF4/β-catenin complex (Barker et al., 2000). Hu and Rosenblum (2005) recently provided evidence that a complex consisting of TCF4/β-catenin and Smad1 (transmitting the BMP signal) synergistically controls the c-*myc* promoter in dysplastic mice kidney tissue (Hu and Rosenblum, 2005). While in a different context, Chen *et al.* (2002) showed that Smad3/4 (mediating the TGFβ signal) represses the expression of human *c-myc* (Chen et al., 2002).

In *Xenopus* organizer formation, evidence suggests synergistic crosstalk between Wnt and activin/Vg1 signaling pathways. LEF1/TCF and Smad4 can interact directly in inducing the expression of the Wnt/β-catenin target gene *Xtwn* during gastrulation (Nishita et al., 2000). Labbe *et al.* (2000) showed that this activation results from a physical interaction between Smad3 and the HMG box domain of LEF1 (Labbe et al., 2000). Noticeably, the promoter sequences of *gastrin*, *c-myc* and *Xtwn* all contain adjacent Wnt and TGFβ responsive elements, TCF and Smad binding sites respectively.

4.1.2 Crosstalk between Wg and Dpp signaling in flies

In *Drosophila*, accumulating evidence has shown that signaling inputs from Dpp and Wg exert cooperative or antagonistic effects to define target gene expression. In

embryonic midgut visceral mesoderm formation, Dpp and Wg act independently but synergistically on the visceral mesoderm enhancer of the *Ultrabithorax* (*Ubx*) gene, which also possesses adjacent Wg- and Dpp-responsive elements to enhance *Ubx* expression (Riese et al., 1997). In contrast, *labial* (*lab*) expression in the midgut endoderm is activated by Dpp and repressed by Wg (Hoppler and Bienz, 1995).

The development of the leg imaginal disc has provided an excellent example of the antagonistic and cooperative functions of these two factors. *dpp* and *wg* are expressed adjacently on the anterior side of the anterior-posterior compartment boundary of the disc; *wg* is expressed ventrally, whereas *dpp* is expressed at high levels dorsally. Both Wg and Dpp inhibit the expression of each other and antagonistically function in specifying the DV boundary of the leg disc compartments (Jiang and Struhl, 1996; Johnston and Schubiger, 1996; Theisen et al., 1996). The convergence of both signals is required to induce *Distal-less* (*Dll*) and *aristaless* (*al*) (Campbell et al., 1993; Cohen et al., 1993); and repress *homothorax* (*hth*) and *teashirt* (*tsh*) in the center of the disc (Abu-Shaar and Mann, 1998; Wu and Cohen, 1999; Wu and Cohen, 2000). On the other hand, the expression of a ventral marker, H15, is activated by Wg and repressed by Dpp. Thus, the antagonistic effects of these two factors restrict H15 expression ventrally (Brook and Cohen, 1996).

In the *Drosophila* wing disc development, the Wg signalling pathway organizes the DV axis, while the Dpp signaling pathway is required to pattern the AP axis. Interactions between *wg* expressing cells and *dpp* expressing cells in part specify the patterning along the proximal-distal (PD) axis (Diaz-Benjumea et al., 1994). In the

earliest event in wing specification, Teashirt (Tsh) and Homothorax (Hth), are initially co-expressed throughout the entire wing disc, but are later repressed by Wg and Dpp signaling in distal cells, permitting the subsequent elaboration of distal fates. (Wu and Cohen, 2002; Yu et al., 1998). Later in development, Wg and Dpp synergistically induce vg^{Q} enhancer and *omb* expression (Grimm and Pflugfelder, 1996b; Klein and Arias, 1999). Examples of the cross regulation of Wnt and TGFβ signaling are emerging; yet the molecular mechanisms are still poorly understood.

4.1.3 Summary of the chapter

In this chapter, I report a novel model of crosstalk between *Drosophila* Wg and Dpp signaling, in which ectopic Mad and Arm compete for association with dTCF to influence Wg dependent gene expression during wing development. Clonal analyses in the larval wing disc revealed that expression of Wg target genes is repressed by ectopic Dpp signaling. Overexpression of Mad in cell culture is able to suppress Wg-responsive reporter activation. dTCF physically interacts with Mad in co-immunoprecipitation. In addition, Arm and Mad compete for binding of dTCF in cell culture. Consistent with such a model, ectopic expression of dTCF in vivo is able to suppress the inhibitory effect of Mad. Thus, our results suggest a novel mechanism by which Dpp represses Wg target genes by influencing the binding of Arm and dTCF. dTCF, consistent with its architectural role in regulating the assembly of enhancer complexes, coordinates inputs from Wg and Dpp signaling during wing development.

4.2 Results

4.2.1 Ectopic Dpp signaling repress *nmo* expression

We have previously shown that *nemo* (*nmo*) is a transcriptional target of Wg signaling and plays inhibitory roles in both Wg and Dpp signaling pathways (Zeng and Verheyen, 2004; Chapter 2 and 3). During larval wing disc development, *nmo* is enriched in two rows of cells flanking the DV boundary as well as in the ring domain surrounding the wing pouch. In addition, *nmo* is also expressed in L3, L4 and L5 wing vien premodia (Zeng and Verheyen, 2004). While characterizing *nmo* expression pattern, we observed that expression in two thin stripes flanking the DV boundary of the wing disc is weaker where the AP boundary intersects the DV boundary starting from mid-third instar stage (Fig. 2.2.1C). This finding prompted us to look for an antagonistic signal that silences *nmo* expression in the AP boundary and Dpp signaling was an ideal candidate. *dpp-Gal4* was used to overexpress *UAS-dpp-GFP* in its endogenous domain, and Dpp protein distribution was monitored by anti-GFP antibody staining (Fig. 4.2.1A, B). *nmo-lacZ* expression in these wing discs is detected by anti-β-galactosidase staining (Fig. 4.2.1B, C). The co-localization suggests that ectopic Dpp signaling correlates to reduced *nmo* expression at the DV boundary.

To examine the possible regulation of *nmo* expression by Dpp signaling, I examined flies ectopically expressing a constitutively active Thickveins (Tkv^{QD}) receptor (Nellen et al., 1996). The *Dpp-Gal4* driver was used to express *UAS-*Tkv^{QD} in the cells of the AP boundary (Fig. 4.2.1D, E). A specific inhibition of *nmo* in the cells of the DV boundary that are bisected by the AP boundary is observed (Fig. 4.2.1E, F), a

cleft occurs which bisects the disc (arrowhead in Fig. 4.2.1M) and manifests itself in adult wings as a severe notch at the AP boundary (Fig. 3.2.3A). The expression of *nmo* in these discs is also inhibited specifically in the cells that intersect both axes (Fig. 4.2.1E, F, M).

To further define this regulation, I generated somatic clones in which UAS transgenes were ectopically expressed using the flip-out technique. Flip-out clones ectopically expressing either *UAS-Tkv*^{QD} (Fig. 4.2.1G, H) or *UAS-Mad* (Fig. 4.2.1J,K) suppress *nmo* expression in a cell autonomous manner (Fig. 4.2.1H, I, K, L). There is apparently no effect from Dpp on the expression of *nmo* in the presumptive vein primordia (arrowheads in Fig 4.2.1C, I).

I also tried to examine the effect of loss of Dpp signaling. However clones of *mad*$^{1-2}$ and *tkv*^{1} mutant were not able to survive to the 3rd instar larval stage due to proliferation defects (Fig 4.2.1O, P).

Figure 4.2.1 *nmo* expression is suppressed by ectopic DPP signaling

(A-C) *nmo-lacZ* expression is suppressed by *dpp-Gal4>UAS-dpp, GFP* in the late 3rd instar wing disc. Dpp distribution is revealed using an anti-GFP antibody (green). *nmo* expression is detected by anti-β-galactosidase staining (red). Noticeably, *nmo* expression in the L3 primordium is not suppressed, arrowhead in (C). (D-F) *nmo-lacZ* expression is suppressed by *dpp-Gal4>UAS-tkv^{QD}, UAS-GFP*. *dpp-Gal4* expression domain is exhibited by GFP (green) (G-I) *nmo-lacZ* expression is suppressed in a clone etopically expressing *UAS-tkv^{QD}*. (J-L) *nmo-lacZ* expression is suppressed in a clone etopically expressing *UAS-mad*. (M) *nmo* expression is detected by X-gal staining in *dpp-Gal4>UAS-tkv^{QD}* wing disc. A cleft occurs that bisects the disc (arrowhead) due to ectopic active Tkv. (O) *mad $^{1-2}$* clones and (P) *tkv^{1}* clones were not able to survive to the 3rd instar larval stage due to proliferation defects, evidenced by seeing the twinspot, but not the mutant clone.

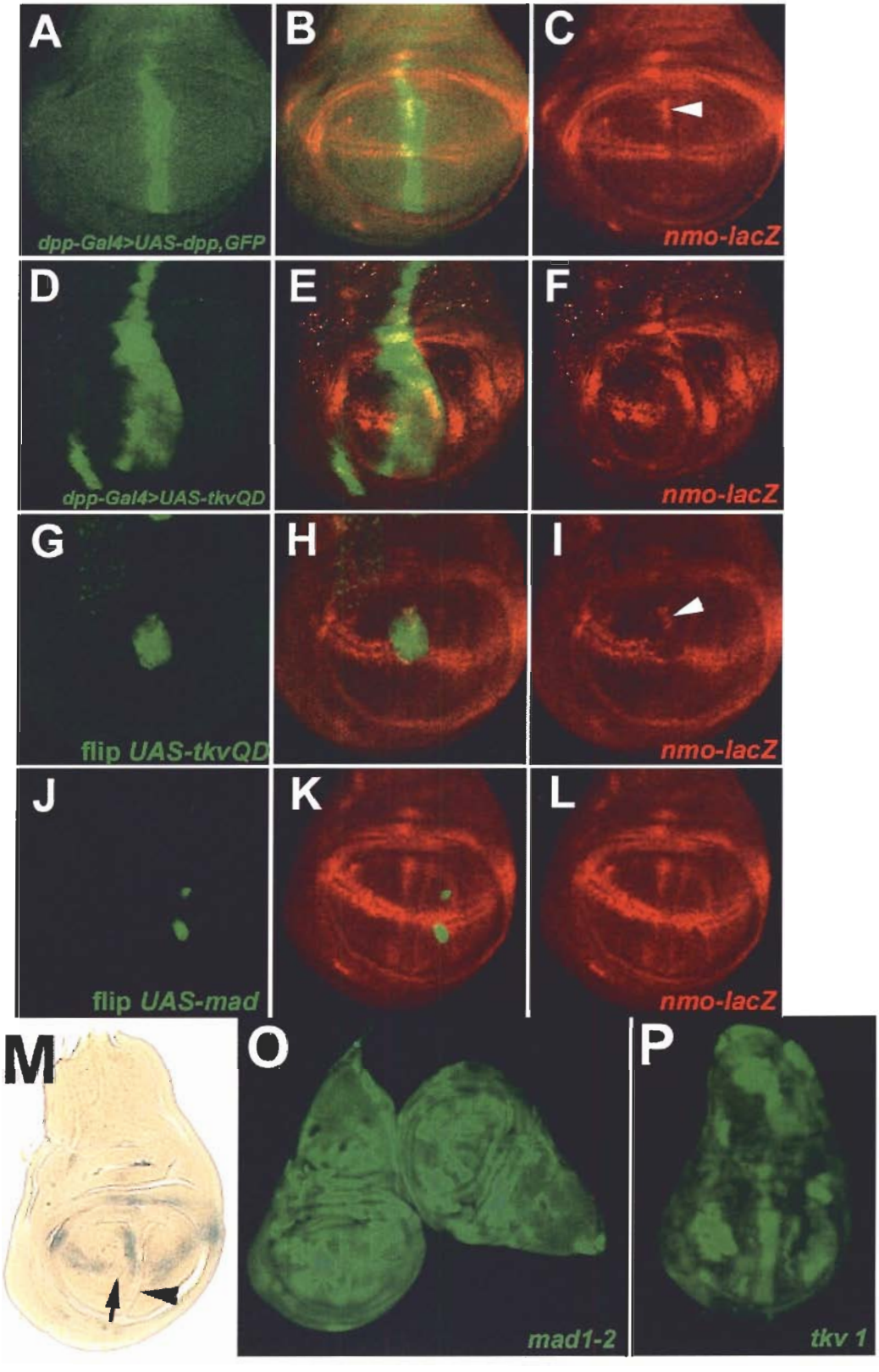
A
dpp-Gal4>UAS-dpp,GFP
B
C
nmo-lacZ
D
dpp-Gal4>UAS-tkvQD
E
F
nmo-lacZ
G
flip UAS-tkvQD
H
I
nmo-lacZ
J
flip UAS-mad
K
L
nmo-lacZ
M
O
mad1-2
P
tkv 1

4.2.2 Dpp's suppression of *nmo* is not due to changes in *wg* expression

Previous research has established that *nmo* is a target gene of Wg signaling (chapter 2; Zeng and Verheyen, 2004). Since Wg and Dpp mutually inhibit the expression of each other in the development of leg discs, I addressed whether Dpp affects *wg* expression to suppress *nmo* in the wing. Double staining of *nmo-lacZ* and anti-Wg was performed on *dpp-Gal4>UAS-Tkv*^{QD} wing discs (Fig. 4.2.2 A-C). No reduction of Wg staining is seen in comparison to the suppression of *nmo-lacZ* staining caused by ectopic Dpp signaling (compare arrows in Fig. 4.2.2A and C). The ectopic region of Wg staining along the AP boundary (arrowhead in Fig. 4.2.2C) is most probably due to the morphological change of the wing disc caused by the formation of the cleft mentioned above (Fig. 4.2.1F, M), although the exact cause is unknown. Ectopic *nmo* induced by the ectopic Wg along the cleft is also seen clearly in Fig. 4.2.1F and M.

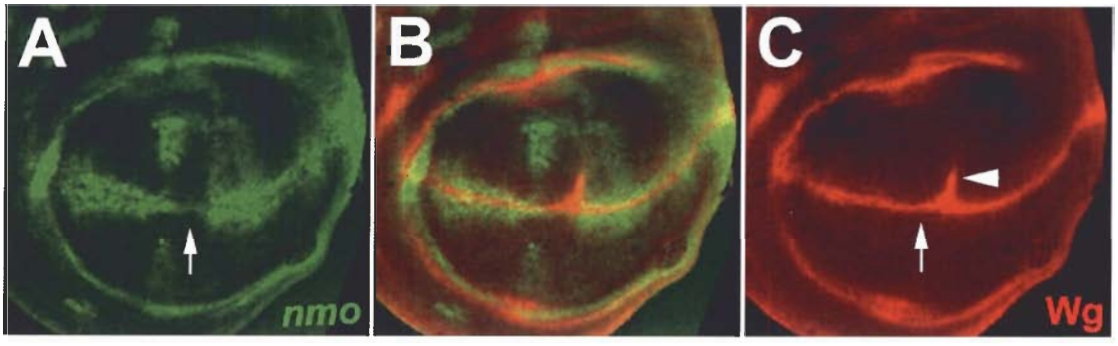

Figure 4.2.2 *wg* expression is not suppressed by ectopic DPP signaling

Double staining of *nmo-lacZ* and anti-Wg was performed on *dpp-Gal4>UAS-Tkv*^{QD} wing discs. (A) *nmo* expression detected by anti- β-galactosidase staining (green) is suppressed by ectopic active Tkv (arrow); While Wg expression in the same area is not reduced (arrow in C). Ectopic Wg staining is also detected along the AP boundary, presumably caused by morphological change in the *dpp-Gal4>UAS-Tkv*^{QD} wing disc (arrowhead in C).

4.2.3 Ectopic Dpp signaling suppress other Wg-dependent gene expression

It is equally possible that *nmo* transcription could be independently regulated by both signaling pathways or could involve a more general inhibition of Wg-dependent gene expression by Dpp signaling. To address the latter possibility, I examined whether the expression of other Wg target genes were similarly inhibited after modulation of Dpp signaling. During wing development, in addition to *nmo*, Wg targets include *Dll*, *achaete* (*ac*) and *senseless* (*sens*). In *dpp-Gal4>UAS-Tkv*^{QD} wing discs, the expression of *Dll* and *ac* are also specifically inhibited (Fig 4.2.3A-F). In addition, flip-out clones ectopically expressing *UAS-Tkv*^{QD} autonomously suppress *sens* expression (Fig. 4.2.3G-I) and clones ectopically expressing *UAS-Mad* inhibit *Dll* expression (Fig. 4.2.2J-L). Thus I have found four Wg target genes whose expression is inhibited by excess Dpp signaling. This may reflect a general inhibition of Wg-dependent gene expression by Dpp and suggests a previously unidentified crosstalk between the two pathways in the wing.

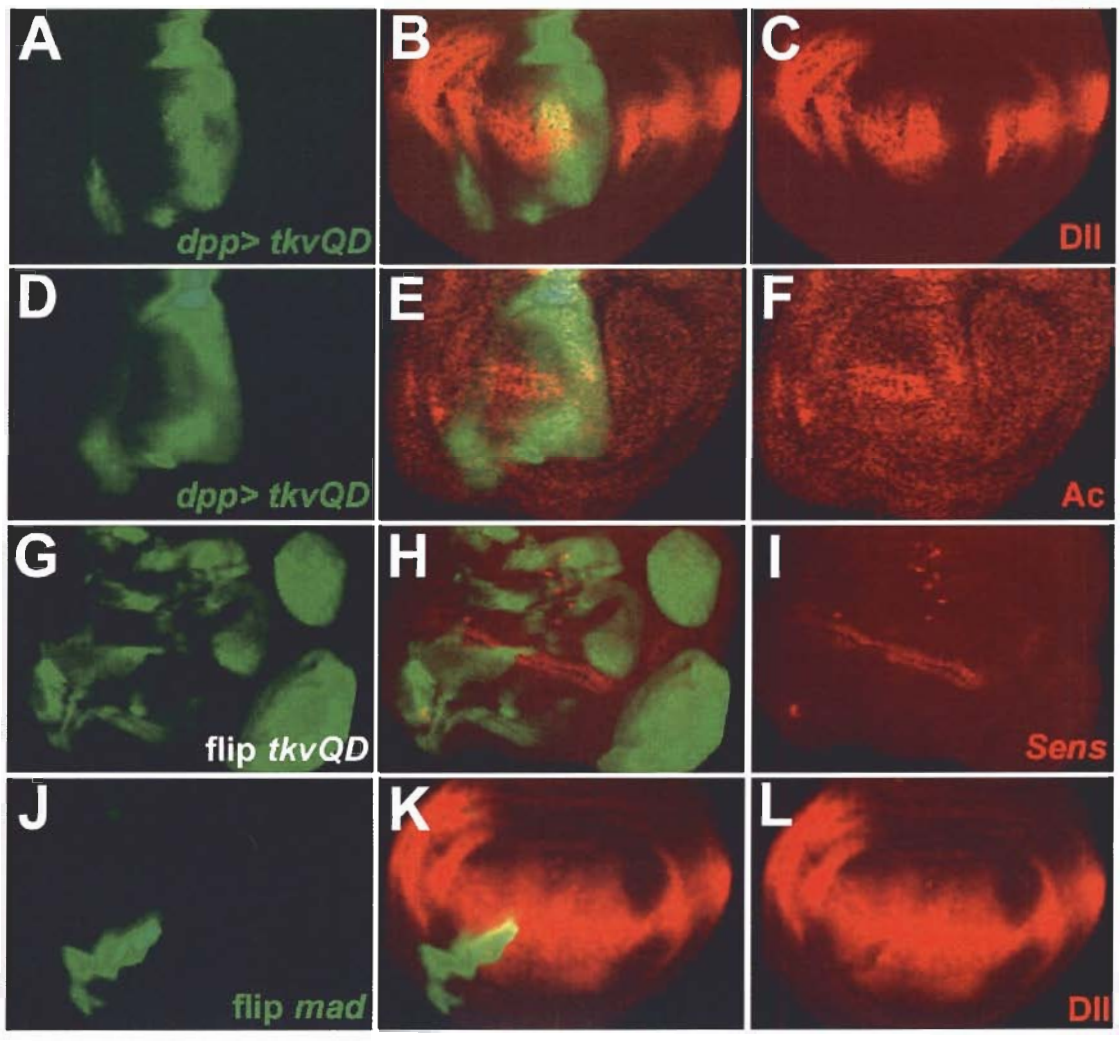

Figure 4.2.3 The expression of Wg target genes is suppressed by ectopic Dpp signaling (A-C) *Dll* expression is suppressed by *dpp-Gal4>UAS-tkv^{QD}, UAS-GFP*. *dpp-Gal4* expression domain is indicated with GFP (green). Similarly, *Ac* expression is suppressed in *dpp>UAS-tkv^{QD}, UAS-GFP* (D-F). (G-I) *sens* expression is suppressed in clones ectopically expressing *UAS-tkv^{QD}*. (J-L) *Dll* expression is suppressed in clone ectopically expressing *UAS-mad*.

4.2.4 Ectopic Dpp signaling exhibits loss of wing margin phenotype

The inhibitory effect of Dpp on Wg target gene expression can be observed as a *wg* loss of function-like phenotype in adult wings. Wings from *vg-Gal4>UAS-med* and *omb-Gal4>UAS-mad* flies exhibit loss of the wing margin, a typical phenotype seen with loss of *wg* signaling (Couso et al., 1994) (Fig. 4.2.4B, C). Consistently, misexpression of the *Drosophila* inhibitory Smad, Dad, results in ectopic wing margin bristles on the wing blade, a phenotype associated with ectopic Wg signal (Fig. 4.2.4 D). These findings reflect that relative levels of BMP signaling can influence Wg signaling both positively and negatively.

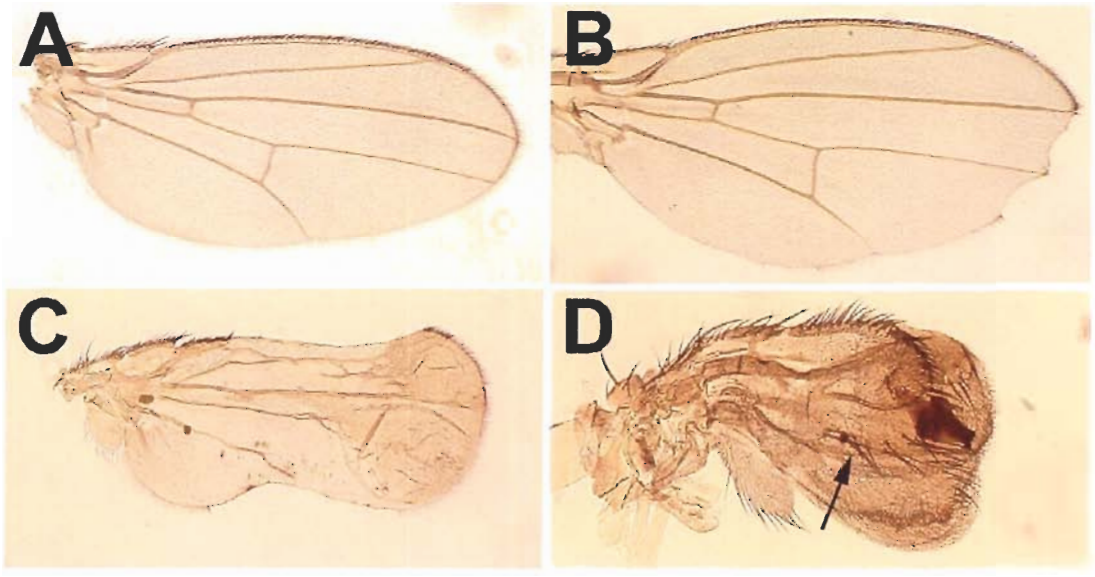

Figure 4.2.4 Loss of wing margin phenotype caused by ectopic Dpp signaling

(A) A wildtype adult wing. *vg-Gal4>UAS-med* (B) and *omb-Gal4>UAS-mad* (C) exhibits loss of *wg* phenotype.(D) *vg-Gal4>UAS-dad* has ectopic wing margin bristles on the wing (arrows), 2X higher magnification than A-C.

4.2.5 Mad interacts with dTCF

In mammalian cell culture studies, it has been previously shown that vertebrate TCF/LEF proteins can bind to certain Smad proteins and modulate the expression of specific target genes. These interactions are generally positive and synergistic, involving the regulation of promoters with binding sites for both proteins. To explore the possible mechanism of the observed Wg and Dpp cross regulation, biochemical studies were performed with *Drosophila* dTCF and Mad. HEK293 cells were transfected with T7-tagged Mad and Myc-tagged dTCF and immunoprecipitations were performed to determine whether the proteins interacted with each other. Reciprocal immunoprecipitations from cell lysates both resulted in the co-immunoprecipitation of dTCF and Mad (Fig. 4.2.5A), indicating the two proteins can form a complex.

Transactivation of Wg target genes requires the association of the classical coactivator Arm and dTCF. I also examined whether Mad interacts with Arm. HEK293 cells were transfected with T7-Mad and HA-Arm. Neither reciprocal immunoprecipitations from cell lysates detect their association (Fig. 4.2.5B). These results demonstrate that Mad can interact with dTCF but not Arm.

To further characterize the association of Mad and dTCF, truncation constructs of both were made as indicated in Fig. 4.2.5.E. I first examined which domain of Mad interacts with dTCF (Fig. 4.2.5C). Co-immunoprecipitations were performed with anti-Myc to precipitate truncated Mad protein bound to dTCF. Immunoblotting with anti-Myc, and anti-T7 indicated that dTCF can precipitate full length Mad as well as Mad ΔMH1, but not Mad ΔMH2 and Mad Linker domain. These results suggested that dTCF binds the MH2 domain of Mad. I next examined which domain of dTCF associates with

Mad, using anti-Myc to precipitate Mad bound to truncations of dTCF (Fig. 4.2.5D). The results suggest that Mad interacts with dTCF ΔC1 (partial deletion of the C terminus) and dTCF ΔC, but not with dTCF ΔHMG (Fig. 4.2.5D, E). Therefore, Mad associates with the HMG domain of dTCF.

Figure 4.2.5 Mad binds dTCF but not Arm

(A) Binding of Mad and dTCF. pCMV-T7-mad and pCMV-Myc-dTCF were co-transfected into HEK293 cells. Cell lysates were immunoprecipitated with anti-Myc, anti-T7 or IgG (control). Immunoblotting was performed with anti-Myc and anti-T7 antibodies. (B) Mad and Arm do not associate directly. pCMV-T7-mad and pCMV-HA-Arm were co-transfected into HEK293 cells. Cell lysates were immunoprecipitated with anti-HA, anti-T7 or IgG (control). Immunoblotting was performed with anti-HA and anti-T7antibodies. (C) dTCF binds the MH2 domain of Mad. HEK293 cells are transfected with Myc-dTCF and T7-Mad (lane 1, 2), T7-Mad ΔMH1 (lane 3, 4), T7-Mad ΔMH2 (lane 5, 6) or T7-Mad Linker domain (lane 7, 8). Cell lysates were immunoprecipitated with anti-Myc or IgG (control). Immunoblotting was performed with anti-Myc and anti-T7 antibodies. (D) Mad interacts with the HMG domain of dTCF. HEK293 cells are transfected with T7-Mad and dTCF ΔC1 (partial deletion of the C terminus) (lane 1, 2), or dTCF ΔC (lane 3, 4), or dTCF ΔHMG (lane 5, 6). Cell lysates were immunoprecipitated with anti-Myc or IgG (control). Immunoblotting was performed with anti-Myc and anti-T7 antibodies. (E) Schematic map of the truncation constructs of dTCF and Mad.

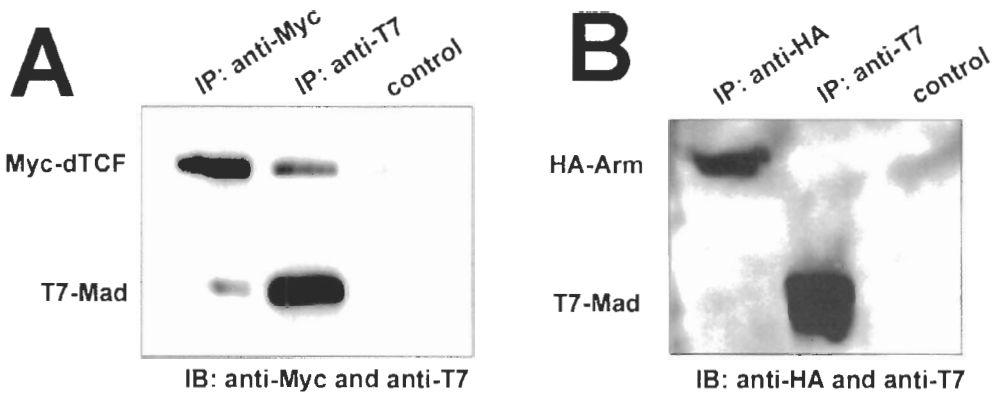
A
IP: anti-Myc
IP: anti-T7
control
Myc-dTCF
T7-Mad
IB: anti-Myc and anti-T7
B
IP: anti-HA
IP: anti-T7
control
HA-Arm
T7-Mad
IB: anti-HA and anti-T7

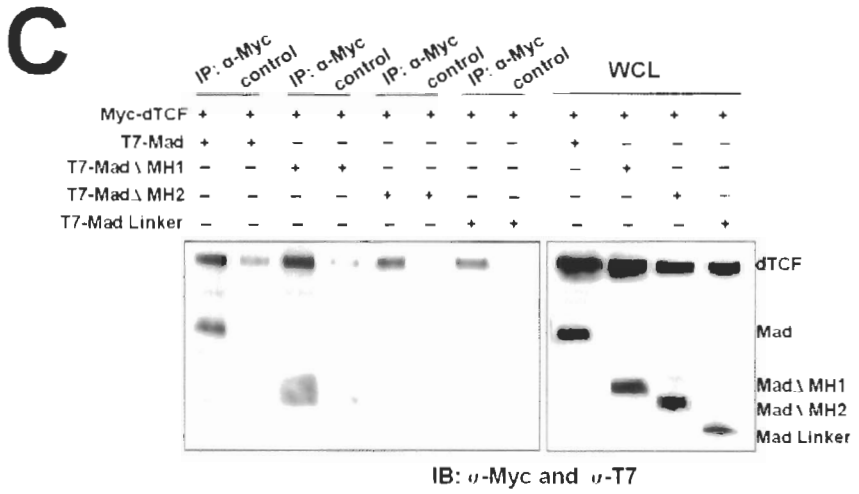
C
IP: α-Myc
control
WCL
Myc-dTCF
T7-Mad
T7-Mad \ MH1
T7-Mad Δ MH2
T7-Mad Linker
dTCF
Mad
Mad Δ MH1
Mad \ MH2
Mad Linker
IB: α-Myc and α-T7

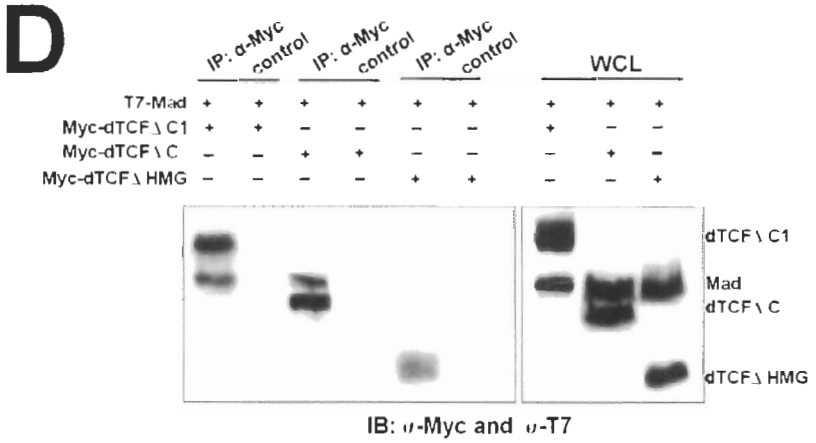
D
IP: α-Myc
control
WCL
T7-Mad
Myc-dTCF \ C1
Myc-dTCF \ C
Myc-dTCF Δ HMG
dTCF \ C1
Mad
dTCF \ C
dTCF Δ HMG
IB: α-Myc and α-T7


E
Mad
dTCF
dTCF
Mad
MH1
Linker
MH2
N
HMG
C

4.2.6 Mad and Arm compete for the binding of dTCF

Arm is known as a classical co-activator of dTCF. To address whether the binding of Mad and dTCF affects the Arm/dTCF interaction, these factors were placed in the same context. HEK293 cells were transfected with T7-Mad, and Myc-dTCF and increasing amounts of HA-Arm as indicated in Fig. 4.2.6A. Immunoprecipitations were performed with anti-Myc to precipitate proteins bound to dTCF, followed by immunoblotting with anti-Myc, anti-HA and anti-T7. Notably, dTCF can precipitate both Mad and Arm when the HA-Arm amount is relatively low as indicated in fig. 4.2.6A (lane 2 and 3). Elevated amounts of Arm predominantly bound dTCF and are able to inhibit the association of Mad and dTCF (Fig. 4.2.6A lane 4).

I next examined whether increasing amounts of Mad can reciprocally influence the binding of Arm and dTCF. HEK293 cells were transfected with Myc-dTCF, HA-Arm and graded amount of T7-Mad as indicated in Fig. 4.2.6B. Similarly, a Myc-dTCF immunoprecipitate can pull down both Arm and Mad when the amount of Mad is relatively low as indicated in Fig. 4.2.6B (lane 2 and 3). Greater amounts of Mad can also compete out the association of Arm and dTCF (Fig. 4.2.6B lane 4). However, the apparent affinity of dTCF for Arm is much stronger than that for Mad. Therefore, in order to see the competition between Mad and Arm, Arm levels were kept low, while the concentration of Mad was increased.

The observation that dTCF can precipitate both Mad and Arm, raises the question of whether these proteins form a complex of three or two different complexes exist. Therefore, cell lysates containing Myc-dTCF, HA-Arm and T7-Mad were immunoprecipitated with anti-T7 or reciprocally with anti-HA to determine whether Mad

can interact with Arm through a bridge of dTCF (Fig. 4.2.6C, D). Immunoprecipitation with anti-T7 to precipitate Mad did not pull down Arm (Fig. 4.2.6C). Similarly, Immunoprecipitation of Arm could not pull down Mad, even in the presence of dTCF (Fig. 4.2.6D). Both results suggested that Arm, dTCF and Mad do not form a complex of three. Precipitates seen in Fig. 4.2.6A, B (lane 2, 3) most likely represent complexes of dTCF/Arm and dTCF/Mad.

To examine whether the binding of Mad and dTCF is functionally relevant to suppression of Wg signaling, I carried out the TOPFLASH assay based on a luciferase reporter linked to TCF binding sites (pTOPFLASH) (Korinek et al., 1997). This quantitative assay is highly specific to TCF-mediated transcription, and serves as a direct readout of the function of exogenous gene on TCF-mediated Wnt signaling. Arm and dTCF association showed very high TOPFLASH values (Fig. 4.2.6E). These values are reduced substantially after co-transfection with increasing amount of Mad. Co-transfection of Mad and constructively active Tkv (Tkv^{QD}) further suppressed the luciferase activities (data not shown). The control values of FOPFLASH (containing mutant TCF sites) are low and unchanged in all reactions. In this assay, dTCF and Arm were kept at low doses as indicated in figure 4.2.6C.

Taken together, I conclude that Mad and Arm compete for the binding of dTCF and these interactions are dose-sensitive; and that the binding between Mad and dTCF can play a role in the level of dTCF-mediated transcriptional activity. In light of the biochemical results, I speculate that the inhibitory effect of Dpp signaling on Wg target gene expression is through occupying dTCF by excess Mad, thus preventing its association with Arm.

Figure 4.2.6 Mad and Arm compete for the binding with dTCF

(A) Certain concentrations of Arm can inhibit the Mad/dTCF complex. 1.5μg of T7-mad, 1.5μg of Myc-dTCF and graded amount of HA-Arm were co-transfected into HEK293 cells as indicated in the figure. Cell lysates were immunoprecipitated with anti-Myc. Immunoblotting was performed with anti-HA, anti-Myc and anti-T7 antibodies. Whole cell lysates were also blotted to examine the proper expression of various components in the lysates. Notably, in lane 2 and 3, dTCF can precipitate both Arm and Mad when the HA-Arm amount is relatively low as indicated in the figure. Elevated amounts of Arm were able to compete off the association of Mad and dTCF in lane 4. (B) High dose of Mad can inhibit Arm/dTCF complex fomation. 500ng of HA-Arm, 800ng of Myc-dTCF and graded amounts of T7-Mad were co-transfected into HEK293 cells as indicated in the figure. Cell lysates were immunoprecipitated with anti-Myc. Immunoblotting was performed with anti-HA, anti-Myc and anti-T7 antibodies. Similarly, in lane 2 and 3, dTCF can precipitate both Arm and Mad when T7-Mad amount was relatively low as indicated. Elevated amounts of Mad were able to titrate off the complex of Arm and dTCF in lane 4. (C, D) Transfected cell lysates containing Myc-dTCF, HA-Arm and T7-Mad were immunoprecipitated with anti-T7 (C) or reciprocally with anti-HA (D), followed by immunoblotting with anti-T7 and anti-HA. (E) TOPFLASH assays in HEK293 cells. TOPFLASH values are given on the right in black columns. These values are from the average of three independent transfection experiments. Vectors used for each experiment are as indicated in the figure. pCMV empty vector was used to top up every transfection reaction to equalize the amount of DNA. Control FOPFLASH values are given on the left in white columns.

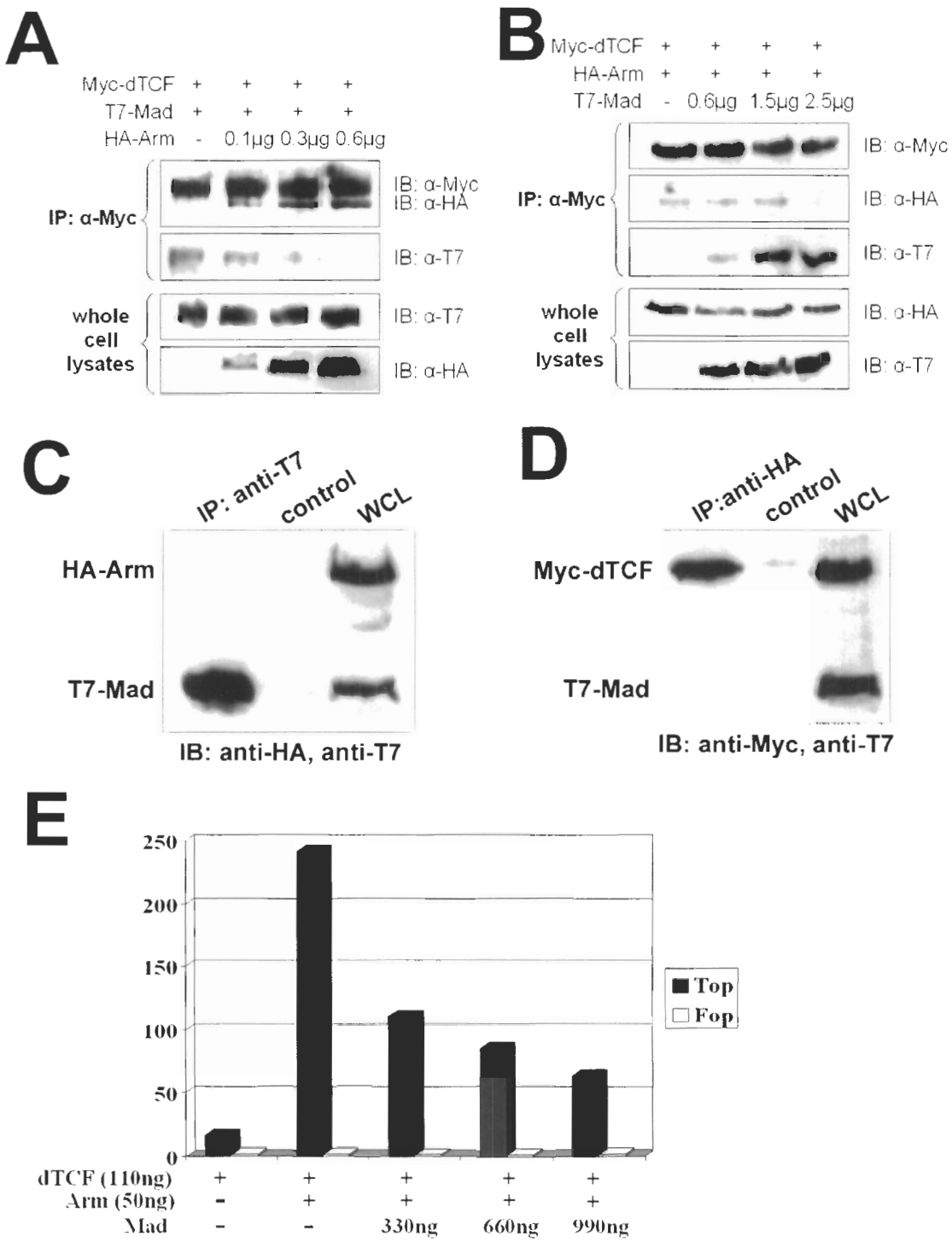
A
Myc-dTCF + + + +
T7-Mad + + + +
HA-Arm - 0.1μg 0.3μg 0.6μg
IP: α-Myc
IB: α-Myc
IB: α-HA
IB: α-T7
whole cell lysates
IB: α-T7
IB: α-HA
B
Myc-dTCF + + + +
HA-Arm + + + +
T7-Mad - 0.6μg 1.5μg 2.5μg
IP: α-Myc
IB: α-Myc
IB: α-HA
IB: α-T7
whole cell lysates
IB: α-HA
IB: α-T7
C
IP: anti-T7
control
WCL
HA-Arm
T7-Mad
IB: anti-HA, anti-T7
D
IP:anti-HA
control
WCL
Myc-dTCF
T7-Mad
IB: anti-Myc, anti-T7
E
250
200
150
100
50
0
Top
Fop
dTCF (110ng) + + + + +
Arm (50ng) - + + + +
Mad - - 330ng 660ng 990ng

4.2.7 Ectopic Dpp signaling affects the stability of Arm

If the TOPFLASH assay provides a direct readout of the function of exogenous gene on TCF-mediated Wnt signaling in cells, Arm protein stabilization is a direct consequence of Wg pathway activation in flies. Arm stabilization requires two necessary steps: inhibition of GSK3 degradation complex by Wg signal and Arm binding to its nuclear anchor, dTCF. Arm is not available for export when it is in a complex with dTCF, therefore making it resistant to degradation (Behrens et al., 1996; Tolwinski and Wieschaus, 2001). One way to examine whether ectopic Dpp signaling occupies dTCF and inhibits its binding to Arm, is to monitor the Arm protein stabilization. To address whether Dpp signaling influences Arm destabilization, *UAS-dpp-GFP* was overexpressed in its endogenous domain driven by *dpp-Gal4*, and Dpp protein distribution was monitored by anti-GFP antibody staining (Fig. 4.2.7A, B). Arm stabilization was detected by anti-Arm antibody staining (Fig. 4.2.7B, C). Co-localization analysis suggests that Arm protein levels are lower along the AP boundary where Dpp is overexpressed (arrow in Fig. 4.2.7 C). In addition, Arm protein levels are more intense in the region where the DV and AP boundaries intersect and this region shows no Dpp-GFP staining.

To further characterize this correlation, anti-Arm staining was performed on discs bearing flip-out clones ectopically expressing Tkv^{QD} (Fig. 4.2.7 D-F). Indeed, ectopic expression of Tkv^{QD} can lead to cell-autonomous reduction in Arm protein levels (arrow in Fig. 4.2.7 F). These results suggest that ectopic Dpp signaling negatively influences the stability of Arm.

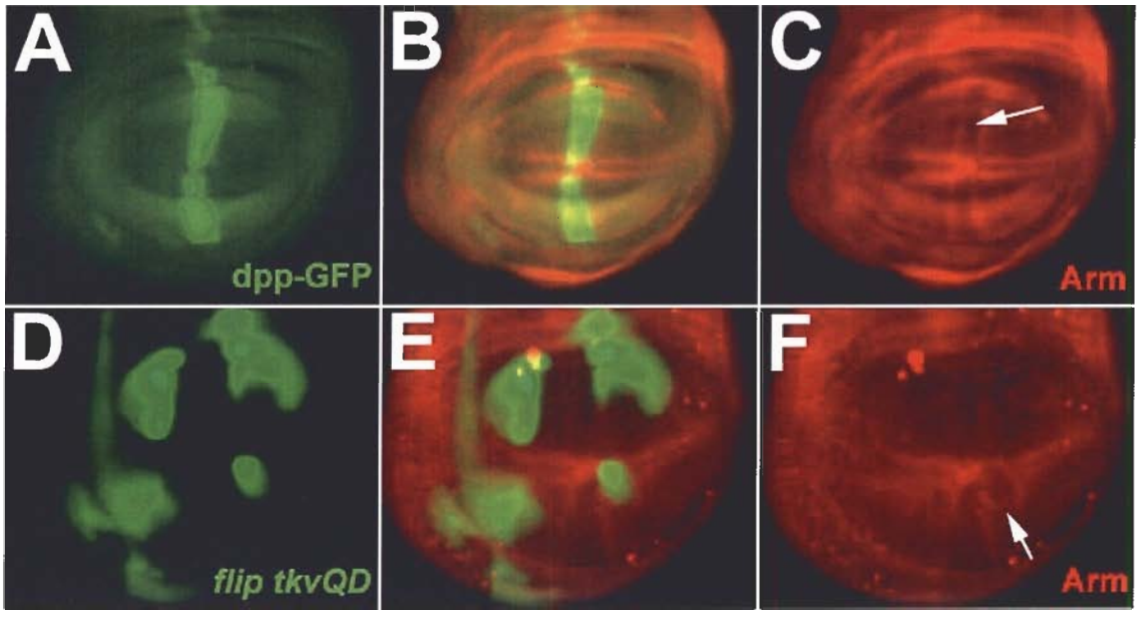

Figure 4.2.7 Dpp signaling negatively influences stability of Arm

(A-C) Co-localization of Arm and Dpp in *dpp-Gal4>UAS-dpp, GFP* flies. It shows that Arm protein levels are lower along the AP boundary where Dpp is overexpressed. In addition, Arm protein levels are more intense in the intersection of the DV and AP boundaries where shows less Dpp-GFP staining. Dpp distribution is revealed using an anti-GFP antibody (green). Arm stability is detected by anti-Arm staining (red). (D-F) Arm stability is cell-autonomously suppressed in clones ectopically expressing *UAS-tkv^{QD}*.

4.2.8 Overexpression of dTCF suppresses the inhibition of Wg-target gene expression caused by ectopic Mad

Biochemical analyses suggest that Arm and Mad compete for the association with dTCF, therefore, ectopic Mad occupies dTCF and inhibites the formation of Arm/dTCF complexes. To examine the hypothesis in vivo, the expression of Wg target genes was monitored in 3rd instar larval wing discs bearing clones ectopically expressing Mad as well as dTCF. Previous research has demonstrated that TCF/LEF family members rather than directly activate transcription, primarily serve an architectural function and accommodate the binding of co-activators or suppressors (reviewed in van Noort and Clevers, 2002). Thus, overexpression of dTCF alone has no effect on Wg target gene expression (data not shown).

As described above (Fig. 4.2.3J-L), *Dll* expression is suppressed in clones ectopically expressing Mad (Fig. 4.2.8A-C). Simultaneous overexpression of dTCF in these clones suppresses the inhibitory effect caused by ectopic Mad (Fig 4.2.8D-F). Similarly, *sens* expression is suppressed in flip-out *mad* clone (Fig. 4.2.8G-I). Overexpression of dTCF in this genetic background also suppresses the inhibition of *sens* (Fig. 4.2.8K-L).

salm is a target gene of Dpp signaling during wing development. Overexpression of Mad induces ectopic Salm with or without dTCF (Fig 4.2.8M-R). These results suggest that co-expression of dTCF did not affect the function of Mad in Dpp signaling, whereas it buffers the inhibitory influence of Mad on Wg signaling. It is consistent with the idea that excess Mad occupies dTCF and antagonizes the formation of Arm and dTCF complex.

Figure 4.2.8 Overexpression of dTCF suppresses the inhibitory effect caused by ectopic Mad

(A-C) *Dll* expression is suppressed in clones ectopically expressing *mad*. This suppression is rescued in clones expressing *mad* as well as *dTcf* (D-F). (G-I) *sens* expression is suppressed in clone ectopically expressing *mad*. Overexpression of dTCF similarly rescues this effect (J-L). Overexpression of Mad induces ectopic expression of Dpp target gene *salm* (M-O). Overexpression of both Mad and Arm did not suppress the ectopic induction of *salm* (P-R).

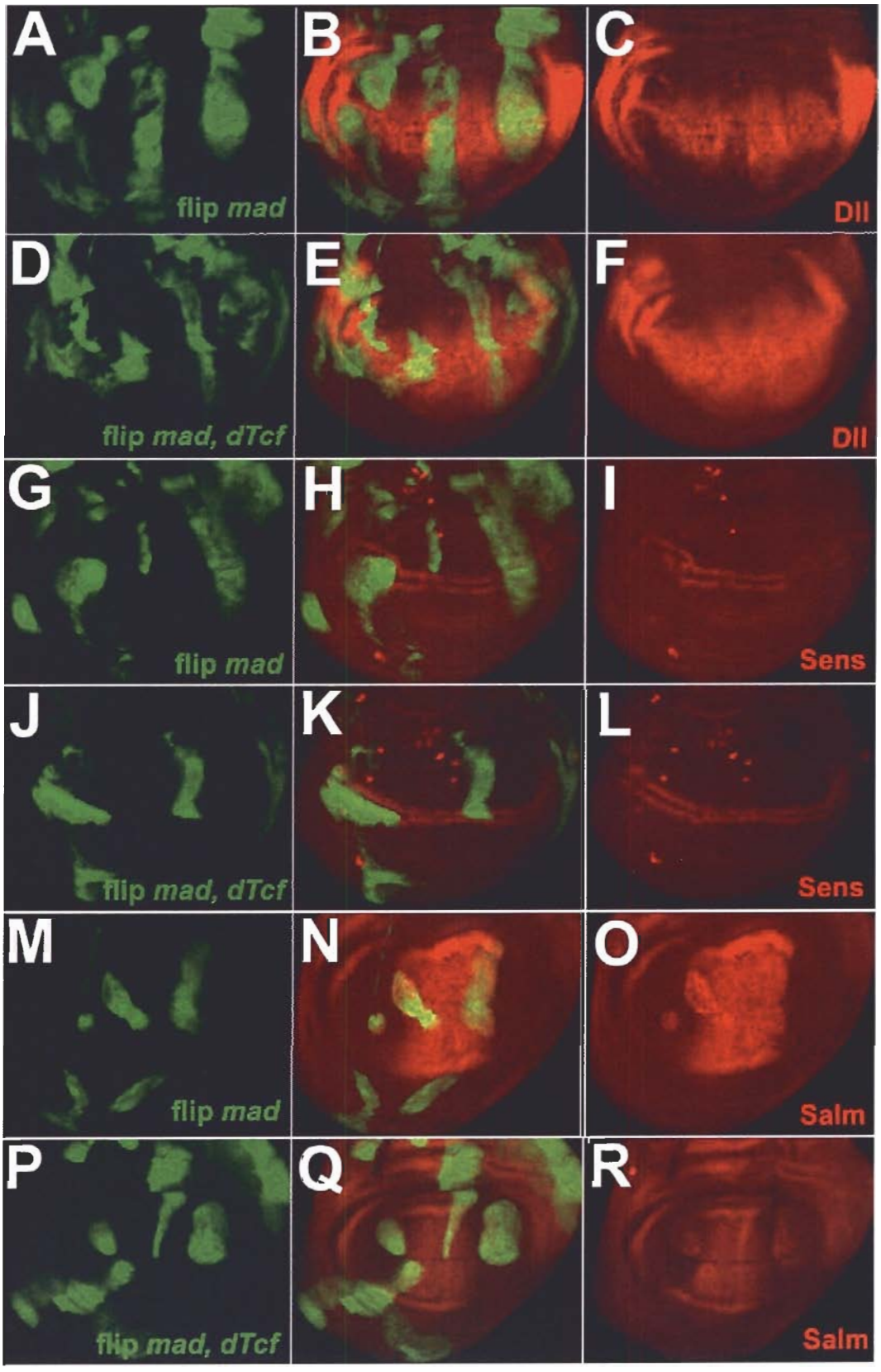
A
flip mad
B
C
Dll
D
flip mad, dTcf
E
F
Dll
G
flip mad
H
I
Sens
J
flip mad, dTcf
K
L
Sens
M
flip mad
N
O
Salm
P
flip mad, dTcf
Q
R
Salm

4.3 Discussion

4.3.1 *nmo* expression in primordial wing veins

In chapter 1, the expression pattern of *nmo* in the third instar discs was described as two thin stripes flanking the DV boundary and a ring encircling the future wing pouch. This expression pattern is reminiscent of Wg protein distribution and is consistent with the idea that *nmo* is a target gene of Wg signaling. However *nmo* staining is also seen in the primordia of longitudinal wing veins 3, 4 and 5, beginning in the late third instar stage. It raises the question of whether it is the Wg signal that activates *nmo* expression in the wing vein primordia. In this chapter, a general inhibition of Wg target gene expression by ectopic Dpp signaling in larval wing disc development was described. I propose that ectopic Mad inhibits the association of Arm and dTCF, hence antagonizes Wg signaling. Interestingly, *nmo* expression in the wing vein primordia was not suppressed by ectopic Dpp signaling. It becomes more likely that it is not Wg which initiates *nmo* expression in this domain. I speculate that activation of *nmo* expression in the primordial veins is regulated by signaling which functions in the provein in the late larval stage, such as N and EGFR signaling pathways.

4.3.2 Nemo is not a feedback inhibitor of Dpp signaling

In chapter 3, I presented evidence that Nemo participates in Dpp signaling and plays an inhibitory role. In the current chapter, evidence suggests that *nmo* expression is negatively regulated by Dpp signaling. However, Nemo is not a feedback inhibitor of

Dpp signaling because these two interactions occur in different domains of the wing (Fig. 4.3.1). Along the DV boundary, Wg signaling activates *nmo* gene expression; Nemo in turn antagonizes Wg signaling by targeting the Arm and dTCF complex. Excess Mad resulting from activation of Dpp signaling inhibits the association of Arm and dTCF, hence suppressing the expression of Wg target genes, including *nmo* expression along the DV boundary. In contrast, a different mechanism occurs at the AP boundary. It is still unknown which signaling pathway initiates *nmo* expression in the vein primordia and the signaling pathways in the provein such as N and EGFR are likely candidates. Along the AP boundary, Nemo attenuates Dpp signaling by targeting Mad and most likely inhibiting its nuclear accumulation. Thus, the observations that suppression of *nmo* by Dpp signaling and Nemo antagonizing Dpp signaling, are in distinct developmental contexts and therefore Nemo is not a feedback inhibitor of Dpp signaling.

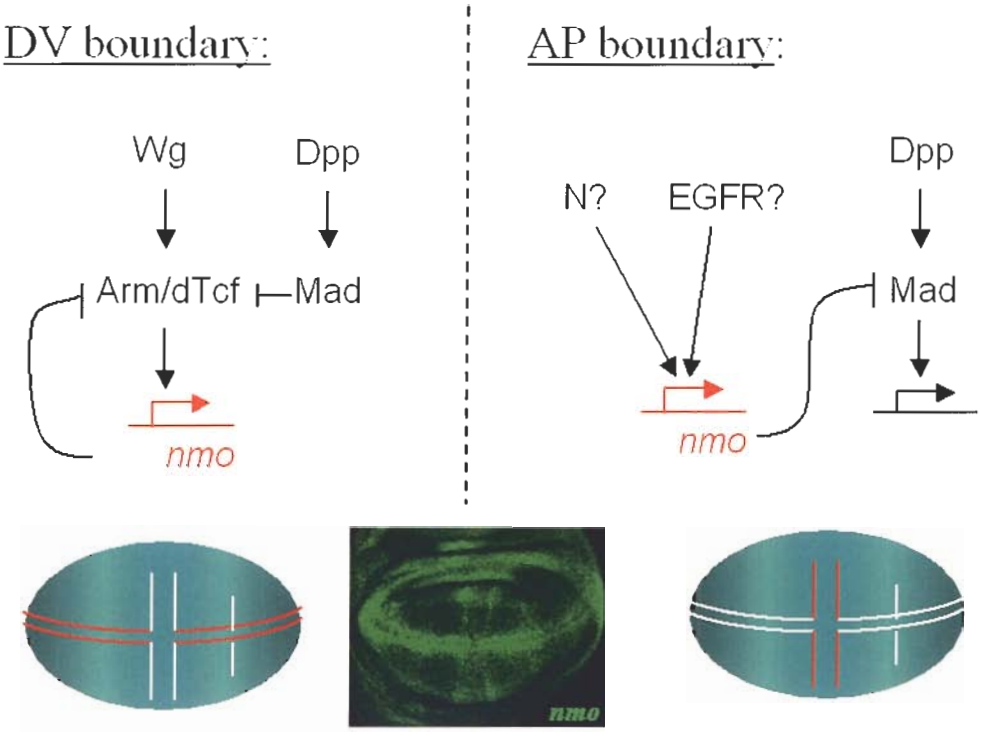

Figure 4.3.1 Nemo is not a feedback inhibitor of Dpp signaling

nmo expression is highlighted in red in the DV and AP boundary of third instar wing imaginal disc.

At the DV boundary, Wg signaling activates nmo gene expression; Nemo in turn antagonizes Wg signaling transduction. Excess Mad resulting from Dpp signaling activation inhibits the Arm/dTCF complex formation; hence suppressing Wg dependent gene expression, including *nmo* expression along the DV boundary.

At the AP boundary, *nmo* expression in the vein primordia is probably initiated by N or EGFR. Nemo attenuates Dpp signaling by inhibiting nuclear translocalization of Mad.

4.3.3 Mad and Arm compete for binding to dTCF

In mammalian studies, accumulating evidence suggests that TGFβ/Smad interacts with Wnt/TCF and cross regulate the expression of specific target genes. Those genes which have been studied, all possess both Wnt and TGFβ responsive elements. Many interaction studies to date are performed by using overexpression assays in cell culture, and only a handful of experiments have demonstrated the presence of such interactions in vivo, for example, in dysplastic mice tissues. However this in vivo criterion is the most challenging and important piece of evidence to demonstrate the biological relevance of the findings.

In the current study, I provide evidence that Wg-dependent gene expression is repressed by ectopic Dpp signaling during wing development. In light of a series of observations in cell culture: association of Mad with dTCF; suppression of wg-responsive reporter activity by overexpressed Mad; the association of Mad and dTCF titrates off the binding of Arm and dTCF and vice versa, I propose that Mad and Arm compete for binding to dTCF, hence ectopic Mad inhibits Wg signaling. The observation that stabilization of Arm was inhibited by ectopic Dpp signaling supports such a view. Arm would lose its nuclear anchor, dTCF, in the presence of excess Mad, and is therefore exported to the cytoplasm and is vulnerable to degradation by the GSK3 complex. The hypothesis was further examined in vivo, in which overexpression of dTCF rescues the suppression of wg-dependent gene expression caused by overexpression of Mad.

To my knowledge, all the previous research which describes effects of Smads and TCF/LEF on gene expression involve reporters with binding sites for both. This is the

first example of Wnt and TGFβ crosstalk which highlights a more general mechanism of interplay of TCF and other transcriptional factors or co-factors.

4.3.4 Competing influences of different signaling in wing development

In a bigger picture, the cross regulation in which ectopic Dpp signal suppresses the activities of Wg signaling is important to maintaining a delicate balance of signaling networks, and is critical for the correct patterning of the developing wing. In *Drosophila* wing imaginal disc development, N activates the expression of *wg* (reviewed in Irvine and Vogt, 1997). Diffusion of Wg refines expression of target genes along the DV axis, and both N and Wg signaling are required to organize the differentiation of wing margin structures (Couso et al., 1994; de Celis et al., 1996). *dpp* expression in the AP axis is initiated by Hedgehog (Hh) signaling. Hh and Dpp signaling are required for patterning along the AP axis (reviewed in Lawrence and Struhl, 1996).

The competing influences of N, Wg, Hh and Dpp in establishing gene expression domains are essential. Glise et al. (2002) provided evidence that the expression of Hh target genes, including *dpp*, are repressed by N and Wg signaling along the DV boundary and failure of this repression leads to the loss of wing margin (Glise et al., 2002). The current study adds an additional layer of complexity to the functional hierarchy of these signaling cascades, in which ectopic Dpp inhibits the activity of Wg signaling. It may suggest a feedback loop in which Wg signaling suppresses *dpp* gene expression; Dpp signaling inhibits the activities of Wg signaling and restricts the suppression of *dpp*

expression (Fig. 4.3.2). The existence of such a feedback circuit would help to refine the regulatory network and ensure the proper development of the wing.

Staining of Wg and Dpp in different stages of larval wing discs suggests the balance between Wg and Dpp signaling is dynamic throughout larval development. In the early to mid 3rd instar larval stage, Dpp-GFP staining continually bisects A and P compartments and Wg staining encircles the wing pouch and crosses the DV boundary (Fig.4.3.3A-C). Wg staining remains the same until the late 3rd instar larval stage, except the outer ring domain becomes more clear (Fig.4.3.3F). However Dpp-GFP staining appears broken in the notum and the intersection where the AP intersects with DV axes (Fig.4.3.3D). It is intriguing to speculate that the antagonistic balance between Wg and Dpp signaling would vary throughout development. During early larval development, Dpp and Wg exert their global patterning function in organizing the AP and DV axes. In this stage, Wg signaling suppresses the expression of *dpp*, and Dpp signaling manages to inhibit this suppression. Therefore a balance is maintained and *dpp* is expressed throughout the AP boundary (Fig.4.3.3A). Later in the late 3rd instar larval stage, Wg functions in wing margin organization, which requires repression of the expression of Hh target genes including *dpp* through an unknown mechanism (Glise et al., 2002). In this stage, Dpp has completed setting up the position of the wing veins by establishing boundaries of target gene expression. Presumably, Dpp is no longer required at the DV boundary, and concurrently its expression is excluded from the DV boundary by Wg and N signaling (Fig.4.3.3D).

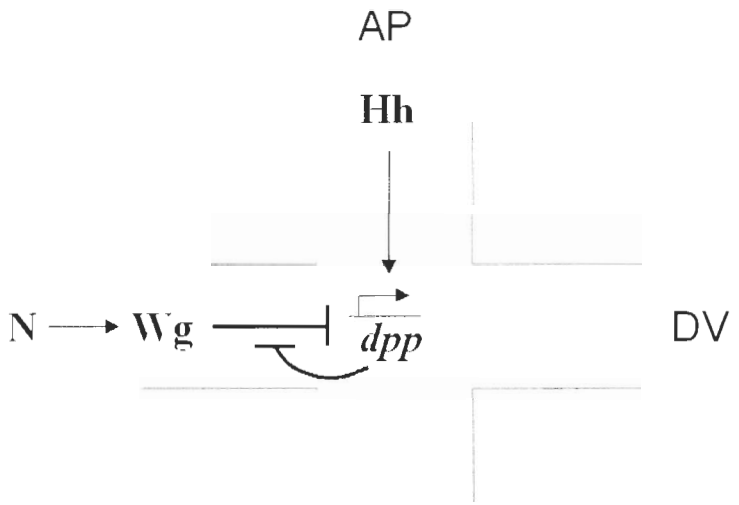

Figure 4.3.2 A model of the feedback loop of Wg and Dpp signaling

Hedgehog (Hh) signaling initiates *dpp* gene expression in the AP axis. Wg expression in the DV axis is induced by N signaling. Wg signaling functions to suppress *dpp* expression along the DV axis, while Dpp signaling inhibits the activities of Wg signaling and restricts the suppression of *dpp* expression.

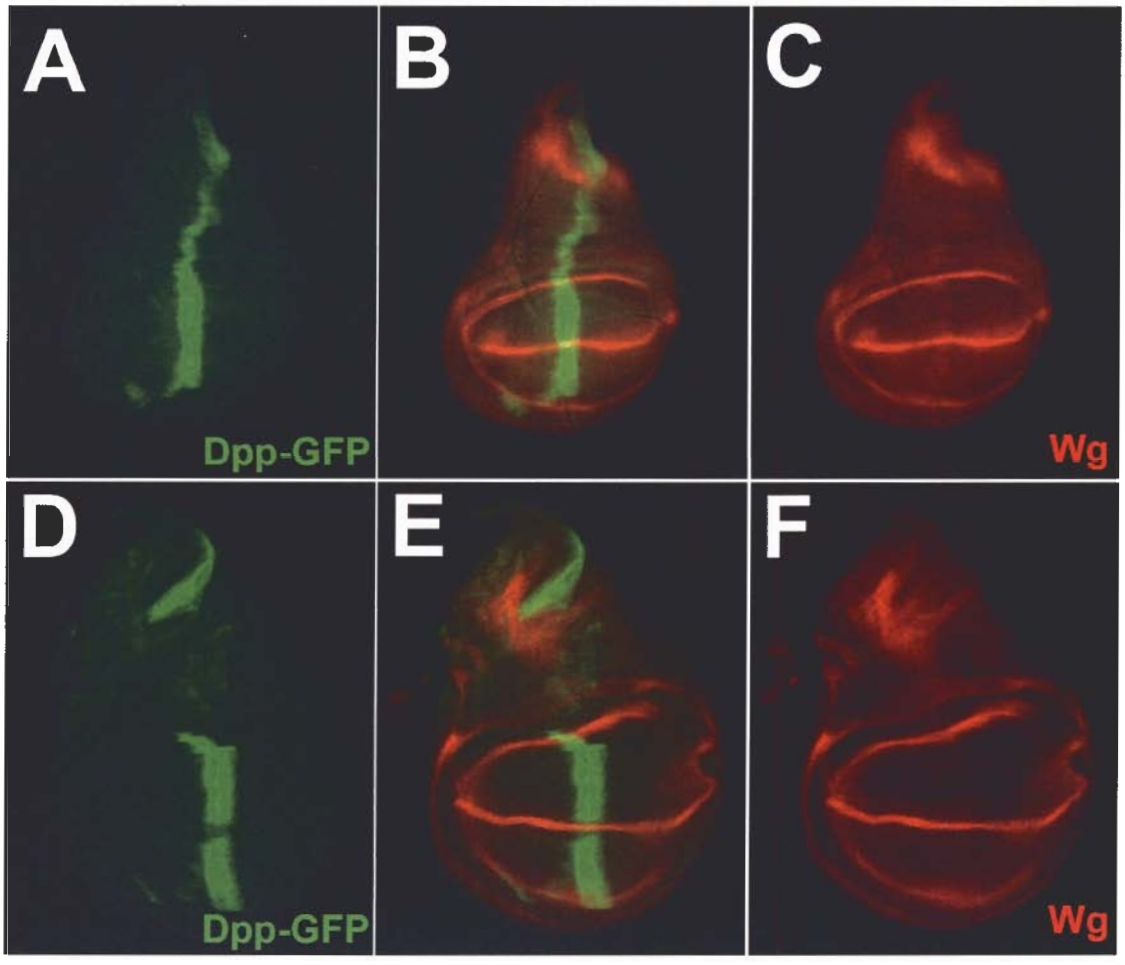

Figure 4.3.3 Wg and Dpp expression domain in the developing wing disc

(A-C) Dpp-GFP and Wg staining in the early-mid 3rd instar wing disc. Dpp is distributed continuously along the AP axis. (D-F) Dpp-GFP and Wg staining in the late 3rd instar wing disc. Dpp staining appears broken in the intersection of AP and DV boundaries.

Wnt and TGFβ signaling play critical roles in many developmental events. However, convergence of these two signaling pathways may represent a simple and logical way to provide a greater diversity of cellular responses during development and tissue stasis. Wnt and TGFβ pathways also contribute to cancer formation and progression. Whereas Wnt signaling is clearly pro-oncogenic, TGFβ signaling is cell- and context-dependent, manifesting both inhibitory and proliferative effects. Studying the crosstalk between the two pathways will provide a better understanding of their roles in tumorigenesis.

Chapter 5

Materials and Methods

5.1 Fly Stocks

The following fly strains were used: w^{1118} were used as "wild-type" strains. nmo^{DB24} (Zeng and Verheyen, 2004); nmo^{adk1} and *UAS-nmo*$^{C5-1e}$ (Verheyen et al., 2001); nmo^{P} (also referred to as *nmo-lacZ*, Choi and Benzer, 1994; Zeng and Verheyen, 2004); dsh^{v26}; dpp^{s11}; gbb^{1}; gbb^{4}; $zw3^{m11}$; mad^{1-2}; *sd-Gal4*($sd^{SG29.1}$); *sd-Gal4* (expressed along the DV boundary); *omb-Gal4* (expressed along the DV boundary); *vg-Gal4* (expressed along the DV boundary); *71B-Gal4* (ubiquitously expressed in the wing disc); *69B-Gal4* (ubiquitously expressed in the wing disc); *ap-Gal4* (expressed in the dorsal wing disc compartment); *dpp-Gal4* (expressed along the AP boundary); *ptc-Gal4* (expressed along the AP boundary); *vg-Gal4* (expressed along the DV boundary); *UAS-Daxin*$^{A2-4}$ (Willert et al., 1999); *UAS-fluΔ arm* and *AyGal4.25-UAS-GFP.S65T* (Ito et al., 1997; Zecca et al., 1996); *Dll-lacZ*, *Ubi-GFP FRT* 79D; *dpp-lacZ* (Morimura et al., 1996); *UAS-lacZ*; *UAS-*

DFz2N (Zhang and Carthew, 1998); *UAS-mad, UAS-med, UAS-dTCF, UAS-tkv*^{QD} (Nellen et al., 1996); *UAS-tkv; UAS-dpp-GFP* (Teleman and Cohen, 2000); *UAS-dad* and *P{lacW}dad*^{1E4} *(*designated *dad-lacZ)* (Tsuneizumi et al., 1997); *vg*^{Q}*-lacZ and UAS-GFP.*

5.2 Clonal analysis

nmo somatic clones were induced using the FLP/FRT method (Xu and Rubin, 1993). To induce *nmo* loss-of-function clones, embryos from the appropriate crosses were collected for 24 hours, aged for 24 hours and heat shocked at 38°C for 90 minutes at 48 hours of development. Flip-out ectopic expression clones were generated as described in Zeng and Verheyen (2004). Cells marked with GFP are those in which the UAS transgenes are expressed. For each genotype at least 30 clones were induced and examined.

The genotypes examined were:

For Wg and Arm staining in *nmo* clones:

y hs-Flp122; *nmo FRT 79D/Ubi-GFP FRT79D*

For β-galactosidase staining of *Dll-lacZ* in *nmoDB24* clones:

y hs-Flp122; Dll-lacZ/+; nmoDB24 FRT 79D/Ubi-GFP FRT79D

For β-gal staining of *nmo-lacZ* in *dsh* clones:

dsh^{v26}*, FRT18A/GFP,FRT 18A; hsFLP38/+; nmo-lacZ/+*

For β-gal staining of *nmo-lacZ* in ectopic active Arm clones:

AyGal4.25-UAS-GFP.S65T/ UAS-flu Δarm; nmo-lacZ/ hs-Flp

For Wg staining in ectopic Nemo clones:

AyGal4.25-UAS-GFP.S65T, UAS-nmoC5–1e/+; hs-Flp/+

For *nmo-lacZ* staining in ectopic Daxin clones:

hs-Flp/+; AyGal4.25-UAS-GFP.S65/+; nmo-lacZ/ UAS-Daxin

For β-gal staining of *nmo-lacZ* in mad^{1-2} clones:

mad^{1-2}, FRT101A/GFP,FRT 101A; hsFLP38/+; nmo-lacZ/+

For β-gal staining of *nmo-lacZ* in *tkv* clones:

f, hs-Flp/+; tkv^{12}, FRT42/GFP,FRT 42; nmo-lacZ/+

For β-gal staining of *dad-lacZ* in ectopic Mad clones:

f, hs-Flp/UAS-mad; AyGal4.25-UASGFP.S65T; dad-lacZ/+

For β-gal staining of *dad-lacZ* in ectopic Mad and Nemo clones:

f, hs-Flp/UAS-mad; UASnmo/AyGal4.25-UAS-GFP.S65T; dad-lacZ/+

For β-gal staining of *nmo-lacZ* staining in ectopic active Tkv clones:

hs-Flp/+; AyGal4.25-UAS-GFP.S65/+; nmo-lacZ/ UAS-tkv^{QD}

For β-gal staining of *nmo-lacZ* in ectopic Mad clones:

UAS-mad/+; AyGal4.25-UAS-GFP.S65/+; nmo-lacZ/ hs-Flp

For Senseless and Arm staining in ectopic active Tkv clones:

AyGal4.25-UAS-GFP.S65/+; hs-Flp/ UAS-tkv^{QD}

For Dll and Senseless staining in ectopic Mad clones:

UAS-mad/+; AyGal4.25-UAS-GFP.S65/+; hs-Flp/+

For Dll staining in ectopic Dad clones:

AyGal4.25-UAS-GFP.S65/+; hs-Flp/ UAS-dad

For Salm staining in ectopic Mad clones:

UAS-mad/+; AyGal4.25-UAS-GFP.S65/+; hs-Flp/+

For Dll, Sens and Salm staining in ectopic Mad and dTcf clones:

UAS-mad/+; AyGal4.25-UAS-GFP.S65/+; hs-Flp/ UAS-dTcf

5.3 Mounted wing analysis

Adult wings were dissected and rinsed in 100% EtOH followed by mounting in Aquatex (EM Science) and examined by microcopy.

5.4 X-Gal staining

Reagents:

X-Gal staining buffer: 10mM NaH_2PO_4: H_2O/ NaH_2PO_4: $2H_2O$ (pH 7.2), 150mM NaCl, 1.0mM MgCl2;6H2O, 3.1mM $K_4[Fe^{II}(CN)^6]$, 3.1mM $K_3[Fe^{III}(CN)^6]$ and 0.3% Triton X-100

X-Gal stock: 8% X-Gal in DMSO

10X PBS: (Phosphate Buffered Saline) Dissolve 80g of NaCl, 2.0g of KCl, 14.4g of Na_2HPO_4, and 2.4g of KH_2PO_4 in 800ml distilled H_2O; adjust pH to 7.4 with HCl; adjust volume to 1L with additional distilled H_2O and sterilize by autoclaving.

PBT: PBS, 0.1% Triton

3rd instar larvae were dissected in PBS, fixed in 1% glutaraldehyde in PBS for 5 minutes, wash for three times in PBT for each time 5 minutes. Tissues were then incubated in 1:50 X-Gal stock in X-Gal staining buffer for the appropriate time until the desired staining appears. Follow staining, tissues were then washed twice in PBT for 5 minute and mounted in 75% glycerol.

5.5 Immunostaining of imaginal discs

Antibody staining was carried out using standard protocols. The antibodies used were: mouse anti-Wg (1:100) and anti-Armadillo (1:200) concentrated supernatants from the Developmental Studies Hybridoma Bank; mouse anti β-galactosidase (1:500) from Promega; rabbit anti β-galactosidase (1:2000) from Cappel. rabbit anti-pMad (1:10,000), rabbit anti Salm (1:600); rat anti Dll (1:500); mouse anti AC (1:50) ; rabbit anti GFP (1:500) and guinea pig anti Sens (1:1500).

Secondary antibodies used were: donkey anti-mouse FITC (Jackson Immunolabs), donkey anti-mouse AlexaFluor 594 (Molecular Probes), donkey anti-rabbit CY3 and FITC (Jackson Immunolabs), donkey anti- guinea pig CY3 (Vector Labortory). All secondary antibodies were used at 1:200 dilutions.

5.6 Expression constructs

The following plasmids were generated using standard molecular biology techniques.

pEGFP-nemo was generated by amplifying the ORF of nmo (II) cDNA with primers engineered with a 5' EcoR I site and a 3' Kpn I site. PCR products and pEGFP empty vector were digested with EcoR I and Kpn I, and isolated using the Quick Gel Extraction Kit (Qiagen) following the manufacturer's instruction. Ligation was preformed according to standard molecular biology techniques. A reaction contained 1 unit of T4 DNA ligase (Gibco BRL), 1mM of dATP, 50mM Tris-HCl (PH 7.6), 10 mM MgCl2, 1mM dithiothreitol and 5% (w/v) polyethylene glycol–8000. Ligation was allowed to proceed overnight at 4°C. Transformation and digestion were preformed according to standard molecular biology techniques to select the clones harbouring the desired plasmid.

The primers used for subcloning were

GFP-NMO-R1: TATGAATTCTATGAGCGTTTCG

GFP-NMO-KPN1: TGGTACCTCATTTTGCCGTCAT

pXJ-Flag-nemo, pXJ-Flag-nemo^{K69M}, pCMV-HA-arm and pCMV-Myc-dTcf were kindly provided by D.C. Bessette (Bessette and Verheyen, unpublished data)

pGex-arm was kindly provided by L. Waltzer (Waltzer, 1998)

pCMV-T7-mad was kindly provided by D. Watton (Hyman et al., 2003).

pCMV-HA-medea was kindly provided by L.A. Raftery (Wisotzkey et al., 1998).

pCDNA-HA-tkv^{QD} was kindly provided by T. Imamura (Inoue et al., 1998),

pCMV-Flag-nlk was kindly provided by T. Ishitani (Ishitani, 1999).

5.7 Generation of the dTcf and mad deletion constructs

The open reading frame of dTcf is 2256 bp. The dTcf ΔC1 construct was made by excision of an Ava I – kpn I fragment (993 bp) from the 3' coding region of the pCMV-Myc-dTcf plasmid (Fig. 5.1). pCMV-Myc-dTcf contains one Ava I site located 1563 bp away from the start codon; one kpn I site is in the 3' multiple cloning site. dTcf ΔC1 constructs were obtained by Ava I –kpn digestion, Klenow treatment to create blunt ends, gel purification of the vector plus 5' sequences, and re-ligation resulting in fusion of Myc with the remainder of the dTcf coding region, deleting the partial C terminus.

The dTcf ΔC construct was made by excision of an Ava I – kpn I fragment (1076 bp) from the 3' coding region of the pCMV-Myc-dTcf plasmid (Fig. 5.1). pCMV-Myc-dTcf contains one Bsg I site located 1182 bp away from the start codon; one kpn I site is in the 3' multiple cloning site. dTcf ΔC constructs were obtained by Bsg I –kpn digestion, Klenow treatment to create blunt ends, gel purification of the vector plus 5' sequences, and re-ligation resulting in fusion of Myc with the remainder of the dTcf coding region, deleting the C terminus.

The dTcf ΔHMG construct was made by excision of an EcoR V-kpn I fragment (1526 bp) from the 3' coding region of the pCMV-Myc-dTcf plasmid (Fig. 5.1). pCMV-Myc-dTcf contains one EcoR V site 730 bp away from the start condon. dTcf Δ HMG constructs were obtained by EcoR V- kpn I digestion, Klenow treatment to create blunt ends, gel purification of the vector plus 5' sequences, and re-ligation resulting in fusion of Myc with the remainder of the dTcf coding region, deleting the HMG conserved domain and the C terminus.

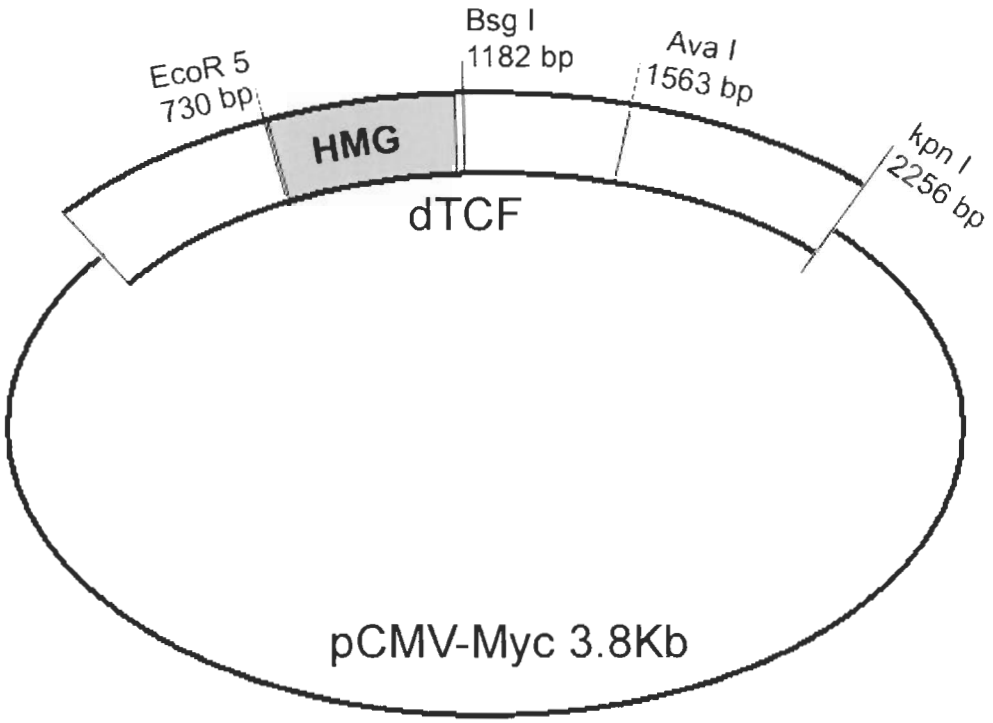

Figure 5.1 pCMV-Myc-dTcf plasmid map with restriction sites

pCMV-Myc-dTcf ΔC1 construct was made by excision of an Ava I – kpn I fragment; pCMV-Myc-dTcf ΔC construct was made by excision of an Bsg I – kpn I fragment; pCMV-Myc-dTcf ΔHMG construct was made by excision of an EcoR V-kpn I fragment.

The open reading frame of mad is 1360 bp. The Mad ΔMH1 construct was made by excision of an EcoR I fragment (890 bp) from the 5' coding region of the pCMV-T7-mad plasmid (Fig. 5.2). pCMV-T7-mad contains two EcoR I sites: one is located in the 5' multiple cloning site, the other one is in the boundary of the MH1 domain and the linker domain, 470 bp distance from the starting ATG. Mad ΔMH1 was obtained by EcoR I digestion, gel purification of the vector plus 3' sequences and re-ligation resulting in an in-frame fusion of T7 with the remainder of the Mad coding region, deleting the MH1 domain.

To create Mad ΔMH1 and linker constructs, BamH I sites was engineered in both of the original plasmid and the ΔMH1 plasmid located at the boundary of Linker and MH2 domains. GGAGCC was mutated to GGATCC at 768 bp position by Site directed mutagenesis. pCMV-T7-Mad ΔMH2 construct was made by excision of a BamH I fragment from pCMV-T7-Mad plasmid; pCMV-T7-Mad linker construct was made by excision of a BamH I fragment from pCMV-T7- Mad ΔMH1 plasmid (Fig. 5.2). The vector plus 5' sequences were gel purified and re-ligated, resulting in an in-frame fusion of T7 with the remainder of the Mad coding region, deleting the MH2 domain.

The primers used to engineer BamH I site are listed below and the nucleotide changes are marked by underscore.

E257BamH5: CAGGTTAGCTATTCGGATCCCGCCTTCTGGGCG

E257BamH3: CGCCCAGAAGGCGGGATCCGAATAGCTAACCTG

The dTcf and Mad deletion constructs were generated in collaboration with M. Rahmana.

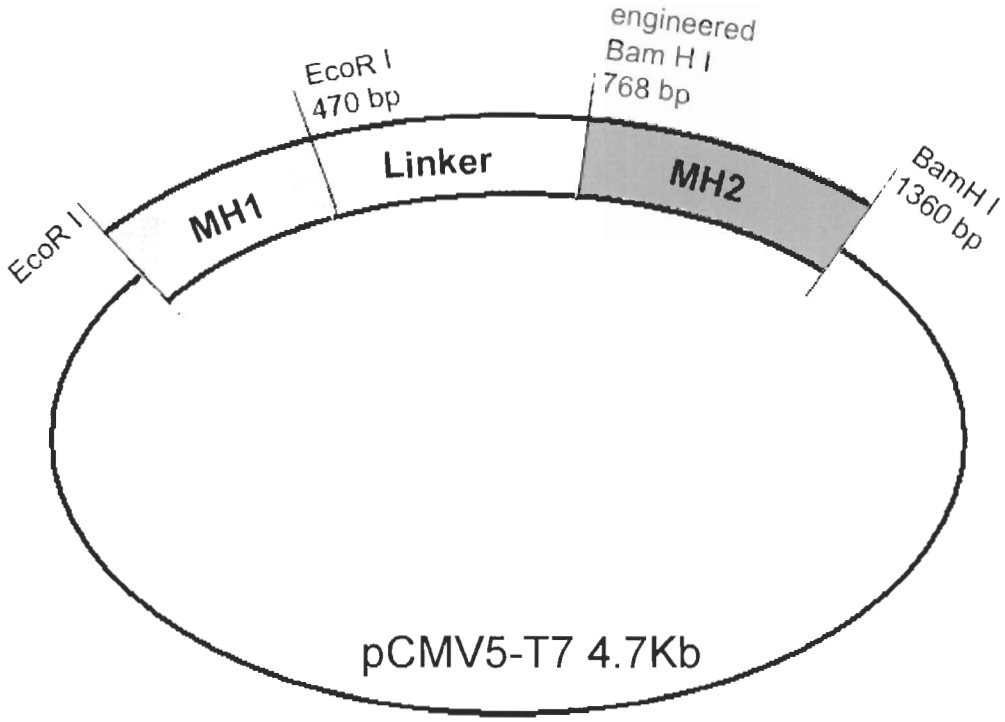

Figure 5.2 pCMV5-T7-mad plasmid map with restriction sites

pCMV-T7-Mad ΔMH1 construct was made by excision of an EcoR I fragment from the original pCMV-T7-Mad plasmid. BamH I sites were engineered in both of the original plasmid and the ΔMH1 plasmid located at the boundary of Linker and MH2 domains. pCMV-T7-Mad ΔMH2 construct was made by excision of a BamH I fragment from pCMV-T7-Mad plasmid; pCMV-T7-Mad linker construct was made by excision of a BamH I fragment from pCMV-T7- Mad ΔMH1 plasmid.

5.8 Site directed mutagenesis of Mad

Mutagenesis was performed on the pCMV-T7-mad plasmid, using the QuickChange site-directed mutagenesis kit, according to the manufacturer's instructions (Stratagene). Both forward and reverse PCR primers were designed to harbour several nucleotide changes, with the rest of the sequence corresponding to the template. A high fidelity PfuTurbo DNA polymerase and a reduced number of cycles were used to minimize errors during PCR amplification. The *DpnI* endonuclease, which is specific for methylated and hemimethylated DNA, was then used to digest the parental DNA template and to select for mutation containing synthesized DNA. Almost all DNA from *E.coli* strains is *dam* methylated and therefore susceptible to *DpnI* digestion. The mutation-containing DNA was then transformed into *E.coli* XL1-Blue.

The primers used for the mutagenesis are listed below and the nucleotide changes are marked by underscore.

Mad S25A:

TTCTCCTTCACAGCGCCGGCGGTGAAGAAG

CTTCTTCACCGCCGGCGCTGTGAAGGAGAA

Mad S146A:

TATCACTATAAGCGCGTGGAGGCGCCGGTGCTCCCGCCAGTACTC

GAGTACTGGCGGGAGCACCGGCGCCTCCACGCGCTTATAGTGATA

Mad S202A and S212A:

AACACATCGGTGGGCGCGCCGAGTTCCGTCAACTCCAATCCCAATGCGCCGT

AC

GTACGGCGCATTGGGATTGGAGTTGACGGAACTCGGCGCGCCCACCGATGTG

TT

Mad S226A:

ACACCGCCACCCGCCTACGCGCCCTCGGAGGATGGCAAC

GTTGCCATCCTCCGAGGGCGCGTAGGCGGGTGGCGGTGT

These constructs were generated in collaboration with M. Rahnama. The change in sequence was verified by sequencing. Sequencing was carried out at the University of British Columbia Center for Molecular Medicine and Therapeutics (CMMT) or University of Calgary University Core DNA services. The modified cDNA was then used for cell culture studies.

5.9 Protein isolation from bacterial lysates

Reagents:

LB: 5g bactotryptone, 5g NaCl, 2.5g bacto-yeast extract in 500mL of water. Autoclaved.

LB agar: LB + 7.5g agar. Autoclaved. Cooled to 55°C and ampicillin added to 50μg/mL. Poured into petri-dishes.

LB + ampicillin: LB. Autoclaved. Cooled to 55°C and ampicillin added to 50μg/mL.

GST buffer: 50mM Tris pH 7.5 (as per Sambrook et al. (1989)), 150mM NaCl, 0.5mM $MgCl_2$, 0.1% Triton-X.

Lysis buffer: GST buffer, 5mM DTT, Complete Protease Inhibitor with no EDTA from Roche Pharmaceuticals per 50mL buffer

Elution buffer: 20mM glutathione, 100mM Tris-HCl pH 8.0 and 120mM NaCl

A single bacterial colony of BL21 containing pGEX (2 mod) or pGEX-Arm was inoculated into 100mL of LB + ampicillin and cultured at 37°C overnight (O/N). The O/N culture was added to 1L of LB + ampillicin and grown at 37°C until the $O.D._{600}$ reached 0.600. The culture was induced with 0.8mM isopropyl β–D-1-thiogalactopyranosida (IPTG) at 37°C for three hours, and then spun at 9000rpm for 20 minutes in 250mL or 500mL centrifuge bottles. The supernatant was discarded and the cell pellet was stored at -70°C. The next day, pellet was thawed, resuspended in 10mL of lysis buffer by drawing up and down with a 10mL. The suspension was sonicated at level 20 for three times, each time for 30 seconds. The debris was spun down and the supernatant was transferred to a clean tube and supplemented with 1mL of 80% glycerol. Aliquots of 1mL each were flash frozen and stored at -70°C.

Equal amount of GST and GST-Arm were incubated with 40μL of 50% slurry of Glutathione Sepharose 4 Fast Flow beads (Amersham Pharmacia Biotech) in PBS containing fresh Complete Protease Inhibitors for one hour at 4°C. The tube was then spun at maximum speed for 2 minutes and the supernatant was discarded. Beads were washed 3X with 500μL of GST buffer, inverting a few times, pelleting down and removing the supernatant.

To serve as substrates for kinase assay, GST fusion proteins were eluted from beads. 1/3 volume of elution buffer was used per volume of beads, incubating at room temperature

for 20 minutes, pelleting down. Supernatant was transferred to a clean tube. Repeat for two times and keep each eluted fraction separate.

5.10 In vitro binding assays

Reagents:

SDS sample buffer: 0.01% mercaptoethanol, 2% SDS, 0.01% bromophenol blue, 6% glycerol, 25mM Tris pH 6.8.

Coomassie

Destain buffer: 50% MeOH, 40% dH_2O and 10% Acetic Acid

In vitro translated ^{35}S labelled Nemo (II) was conducted using the pXJFLAG-nemo plasmid and the TNT Quick Coupled Transcription/Translation kit available from Promega. Manufacturer's instructions were followed.

400μL of wash buffer with protease inhibitors was added to the GST or GST-Arm bound beads along with desired amounts of *in vitro* transcribed translated reaction. Reaction was mixed on a Nutator at 4°C for 1 hour. The protein-loaded beads were washed four times with GST buffer.

The washed beads were resuspended in 10uL of SDS sample buffer and boiled for 5 minutes. Beads were pelleted down and the supernatant loaded on a 10% SDS-PAGE gel and electrophoresed using Bio-Rad Mini-Protein gel system III following standard techniques. The SDS-PAGE gel was stained with Coomassie for 15 minutes and

destained. The gel was then dried down onto Whatmann 3M filter paper and subjected to autoradiography.

5.11 Co-immunoprecipitation

Reagents:

Lysis buffer stock: 10% Glycerol, 1% Triton, 50mM Tris Ph 7.5, 5mM EDTA, 150mM NaCl.

Lysis buffer: Lysis buffer stock, fresh complete protease inhibitors (Roche, 1 tablet is dissolved in 2ml dH2O, use 40ul per 1 ml lysis buffer), 100 mM β-glycerol phosphate, 1 mM sodium vanadate and 5 mM NaF.

HEK293 cells were cultured in Dulbecco's modified Eagle's medium (DMEM) (GIBCO) supplemented with 10% fetal bovine serum (GIBCO) at 37°C. Cells at 70~80% confluency were subjected to transient transfection by using the Polyfect transfection reagent (Qiagen) following the manufacturer's instruction. A total of 8ug DNA consisting of various expression vectors, pXJ-Flag-nemo, pCMV-HA –Arm, pCMV-Myc-dTcf, pCMV-T7-mad or pCMV-HA-medea were used in 10cm^2 dishes. 24-48 hours after transfection, cells were washed in 5 mL PBS and lysed in 1mL lysis buffer at room temperature for 10 minutes. Lysates were collected in 1.5 mL Eppendorf tubes and subjected to sonication at level 7 for two times, each time for 10 seconds. Lysates were centrifuged for 2 minutes at 14,000rpm and 4°C. Supernatants were transferred to clean Eppendorf tubes and stored at –20°C.

Mouse anti- Flag (Sigma), mouse anti-T7 (Novagen) mouse anti-Myc (Sigma) or mouse anti-HA (Sigma) were added in desired amount of lysates in 1:1000 dilution. Protein-antibody complex is formed by nutating O/N at 4°C. For each reaction, 30uL of 50% slurry of protein G-sepharose beads (Sigma) were used for immunoprecipitation for one hour at 4°C. The immunocomplexes were wash three times with lysis buffer and boiled in 5 ul SDS sample buffer, subjected to SDS-PAGE and western analysis.

5.12 Western blot Analysis

Reagents:

Protein sample buffer: 0.01% mercaptoethanol, 2% SDS, 0.01% bromophenol blue, 6% glycerol, 25mM Tris pH 6.8.

Running buffer: 2.5mM Tris pH 8.3, 19.2mM glycine, 0.01%SDS.

Transfer buffer: 2.5mM Tris pH 8.3, 19.2mM glycine, 0.01%SDS, 20% methanol.

10X TBS: 12.1g Tris Base, 87.7g NaCl, 950ml ddH2O, adjusting pH to 8.0 with concentrated HCl, bringing final volume to 1L

TBST: 50mM Tris-HCl pH 7.5, 150mM NaCl, 0.1% Tween20

Blocking buffer: 5% Western Blocking Reagent (Roche) in 1X TBS

Protein samples were separated on 10% or 12% SDS-PAGE gels using the BioRad Mini-Protean II Electrophoresis Cell and transferred to nitrocellulose membrane

using the BioRad Trans-Blot Semi Dry following manufacturer's instructions. Protein samples were loaded with SDS sample buffer and electrophoresis carried out in running buffer. The Trans-Blot was run at 18V for 25 minutes using the transfer buffer to transfer the proteins from the gel to the nitrocellulose membrane (Perkin Elmer Life Sciences).

The membrane was blocked with 1X blocking buffer for 1 hour, then incubated in appropriate primary antibody at room temperature for 1 hour, followed by three 15 minute washes with TBST. The membrane was then incubated with desired secondary antibody for 1 hour, followed by three 15 minute washes with TBST. Western blot is visualized by Enhanced Chemiluminescence (ECL) Western Blotting system (Amersham).

Concentrations of primary antibodies as follows: mouse anti- Flag (1:1000) (Sigma), mouse anti-T7 (Novagen), mouse anti-Myc (1:2000) (Sigma) or mouse anti-HA (1:1000) (Sigma). Secondary antibody used is Goat anti mouse HRP light chain specific (1:5000, Jackson Immunolabs).

5.13 in vitro Kinase assay

Reagent:

Kinase assay buffer: 25 mM HEPES, pH 7.2, 25 mM magnesium chloride, 50 mM β-glycerol phosphate, 2 mM dithiothreitol, 0.5 mM sodium vanadate and 0.1mM ribo-ATP

Aliquots of cell lysates were incubated with protein G-sepharose beads to preclear by rotating at 4°C for 1~2 hours, and then incubated with appropriate antibodies coupled to protein G-sepharose beads at 4°C for overnight. Beads with associated kinase (Flag-Nemo or Flag-Nemo K69M) and/or substrates (Myc-dTCF, HA-Arm, T7-Mad or HA-Med) were washed three times with lysis buffer and once with kinase assay buffer. Kinase reactions were initiated by the addition of 20 uL of kinase assay buffer containing 10 μCi of [γ-^{32}P] ATP at room temperature and stopped after 20 min by the addition of 5 uL SDS-sample buffer. Samples were boiled in SDS sample buffer and subjected to SDS-PAGE and transferred to nitrocellulose membrane (Perkin Elmer Life Sciences) according to standard protocols, and visualized by autoradiography.

5.14 Immunostaining of cultured cells

COS-7 or Hela cells were seeded in 6-well plates with glass coverslips 24 hrs prior to transfection. Cells at 50~70% confluency were transiently transfected with various combinations of vectors, pCMV-T7-mad, pCDNA-HA-tkv^{QD}, pXJ-Flag-nemo, pXJ-Flag-nemo^{K69M}, pCMV-T7-madΔMH1 or pCMV-T7-madS25A. 24 hrs after transfection, cells on the coverslips were fixed with 4% paraformaldehye in PBS for 10 minutes at room temperature. After two washes with PBS, immunostaining was performed using mouse anti-T7 (1:2000, Novagen) and rabbit anti-HA (1:1000, Sigma) antibody, followed by two washes with PBS. Secondary antibodies used were: donkey anti-mouse FITC (1:200) and donkey anti-rabbit CY3 (1:200, Jackson Immunolabs).

After two washes with PBS, coverslips were mounted cell-side down with Prolong Gold antifade reagent with DAPI (Molecular Probes) and dried O/N.

5.15 Luciferase assay

HEK293 cells were cultured in 6 well plates and transiently transfected by using Polyfect method as described above (**5.11**).

This TCF-mediated transcription activity can be measured with a luciferase reporter (TOPFLASH) that contains multiple TCF binding sites or a control reporter FOPFLASH containing mutated TCF binding sites (Korinek, 1997), pRL-CMV (based on renilla) served as an internal reference for luciferase. Transfections contained 1ug of TOPFLASH or FOPFLASH reporter, 0.1ug of pRL-CMV, 1.5ug of pCMV-Myc-dTCF, 0.4ug of pCMV-HA-Arm, 4ug of pCMV-T7-mad or mad truncation constructs. PCMV empty vector is used to add to a total of 7 ug per well.

Luciferase assays were performed with the Dual Luciferase Reporter assay system (Promega). Manufacturer's instructions were followed. Samples are measured in Luminometer D20/20 (Turner Design). Firefly (TOPFLASH or FOPFLASH) luciferase activity was corrected by Renilla luciferase activity. For the relative luciferase values shown in Fig. 4.2.6E, luciferase: renilla ratios were calculated for samples from three independent transfection experiments.

References

Aberle, H., Bauer, A., Stappert, J., Kispert, A. and Kemler, R. (1997). beta-catenin is a target for the ubiquitin-proteasome pathway. *Embo J* **16**, 3797-804.

Abu-Shaar, M. and Mann, R. S. (1998). Generation of multiple antagonistic domains along the proximodistal axis during *Drosophila* leg development. *Development* **125**, 3821-30.

Anderson, K. V. and Ingham, P. W. (2003). The transformation of the model organism: a decade of developmental genetics. *Nat Genet* **33**, 285-93.

Arora, K., Dai, H., Kazuko, S. G., Jamal, J., O'Connor, M. B., Letsou, A. and Warrior, R. (1995). The *Drosophila* schnurri gene acts in the Dpp/TGF beta signaling pathway and encodes a transcription factor homologous to the human MBP family. *Cell* **81**, 781-90.

Arora, K., Levine, M. S. and O'Connor, M. B. (1994). The screw gene encodes a ubiquitously expressed member of the TGF-beta family required for specification of dorsal cell fates in the Drosophila embryo. *Genes Dev* **8**, 2588-601.

Attisano, L. and Wrana, J. L. (2002). Signal transduction by the TGF-beta superfamily. *Science* **296**, 1646-7.

Aubin, J., Davy, A. and Soriano, P. (2004). In vivo convergence of BMP and MAPK signaling pathways: impact of differential Smad1 phosphorylation on development and homeostasis. *Genes Dev* **18**, 1482-94.

Bajpai, R., Makhijani, K., Rao, P. R. and Shashidhara, L. S. (2004). Drosophila Twins regulates Armadillo levels in response to Wg/Wnt signal. *Development* **131**, 1007-16.

Baker, N. E. (1988). Transcription of the segment-polarity gene wingless in the imaginal discs of Drosophila, and the phenotype of a pupal-lethal wg mutation. *Development* **102**, 489-97.

Barker, N., Morin, P. J. and Clevers, H. (2000). The Yin-Yang of TCF/beta-catenin signaling. *Adv Cancer Res* **77**, 1-24.

Barth, A. I., Pollack, A. L., Altschuler, Y., Mostov, K. E. and Nelson, W. J. (1997). NH2-terminal deletion of beta-catenin results in stable colocalization of mutant beta-catenin with adenomatous polyposis coli protein and altered MDCK cell adhesion. *J Cell Biol* **136**, 693-706.

Behrens, J. (2000). Cross-regulation of the Wnt signalling pathway: a role of MAP kinases. *J Cell Sci* **113**, 911-9.

Behrens, J., von Kries, J. P., Kuhl, M., Bruhn, L., Wedlich, D., Grosschedl, R. and Birchmeier, W. (1996). Functional interaction of beta-catenin with the transcription factor LEF-1. *Nature* **382**, 638-42.

Bejsovec, A. and Martinez, A. A. (1991). Roles of wingless in patterning the larval epidermis of Drosophila. *Development* **113**, 471-85.

Bier, E. (2000). Drawing lines in the Drosophila wing: initiation of wing vein development. *Curr Opin Genet Dev* **10**, 393-8.

Brabant, M. C., Fristrom, D., Bunch, T. A. and Brower, D. L. (1996). Distinct spatial and temporal functions for PS integrins during Drosophila wing morphogenesis. *Development* **122**, 3307-17.

Brand, A. and Perrimon, N. (1993). Targetted gene expression as a means of altering cell fates and generating dominant phenotypes. *Development* **118**, 401-415.

Brook, W. J. and Cohen, S. M. (1996). Antagonistic interactions between wingless and decapentaplegic responsible for dorsal-ventral pattern in the Drosophila Leg. *Science* **273**, 1373-7.

Brott, B., Pinsky, B. and Reikson, R. (1998). Nlk is a murine protein kinase related to Erk/MAP kinases and localized in the nucleus. *Proc. Natl. Acad. Sci. USA* **95**, 963-968.

Brown, K. E. and Freeman, M. (2003). Egfr signalling defines a protective function for ommatidial orientation in the Drosophila eye. *Development* **130**, 5401-12.

Brummel, T., Abdollah, S., Haerry, T. E., Shimell, M. J., Merriam, J., Raftery, L., Wrana, J. L. and O'Connor, M. B. (1999). The Drosophila activin receptor baboon signals through dSmad2 and controls cell proliferation but not patterning during larval development. *Genes Dev* **13**, 98-111.

Brunner, E., Peter, O., Schweizer, L. and Basler, K. (1997). pangolin encodes a Lef-1 homologue that acts downstream of Armadillo to transduce the Wingless signal in Drosophila. *Nature* **385**, 829-33.

Burke, R. and Basler, K. (1996). Dpp receptors are autonomously required for cell proliferation in the entire developing Drosophila wing. *Development* **122**, 2261-9.

Cadigan, K. M. and Nusse, R. (1997). Wnt signaling: a common theme in animal development. *Genes Dev* **11**, 3286-305.

Cadigan, K. M., Fish, M. P., Rulifson, E. J. and Nusse, R. (1998). Wingless repression of Drosophila frizzled 2 expression shapes the Wingless morphogen gradient in the wing. *Cell* **93**, 767-77.

Campbell, G. and Tomlinson, A. (1999). Transducing the Dpp morphogen gradient in the wing of Drosophila: regulation of Dpp targets by brinker. *Cell* **96**, 553-62.

Campbell, G., Weaver, T. and Tomlinson, A. (1993). Axis specification in the developing Drosophila appendage: the role of wingless, decapentaplegic, and the homeobox gene aristaless. *Cell* **74**, 1113-23.

Chai, J., Wu, J. W., Yan, N., Massague, J., Pavletich, N. P. and Shi, Y. (2003). Features of a Smad3 MH1-DNA complex. Roles of water and zinc in DNA binding. *J Biol Chem* **278**, 20327-31.

Chen, C. R., Kang, Y., Siegel, P. M. and Massague, J. (2002). E2F4/5 and p107 as Smad cofactors linking the TGFbeta receptor to c-myc repression. *Cell* **110**, 19-32.

Chen, X., Rubock, M. J. and Whitman, M. (1996). A transcriptional partner for MAD proteins in TGF-beta signalling. *Nature* **383**, 691-6.

Chen, Y., Riese, M. J., Killinger, M. A. and Hoffmann, F. M. (1998). A genetic screen for modifiers of Drosophila decapentaplegic signaling identifies mutations in punt, Mothers against dpp and the BMP-7 homologue, 60A. *Development* **125**, 1759-68.

Choi, K. W. and Benzer, S. (1994). Rotation of photoreceptor clusters in the developing *Drosophila* eye requires the *nemo* gene. *Cell* **78**, 125-136.

Christian, J. L. and Nakayama, T. (1999). Can't get no SMADisfaction: Smad proteins as positive and negative regulators of TGF-beta family signals. *Bioessays* **21**, 382-90.

Cohen, B., Simcox, A. A. and Cohen, S. M. (1993). Allocation of the thoracic imaginal primordia in the Drosophila embryo. *Development* **117**, 597-608.

Conley, C., Silburn, R., Singer, M., Ralston, A., Rohwer-Nutter, D., Olson, D., Gelbart, W. and Blair, S. (2000). Crossveinless 2 contains cysteine-rich domains and is required for high levels of BMP-like activity during the formation of the cross veins in Drosophila. *Development* **127**, 3947-3959.

Cook, O., Biehs, B. and Bier, E. (2004). brinker and optomotor-blind act coordinately to initiate development of the L5 wing vein primordium in Drosophila. *Development* **131**, 2113-24.

Couso, J. P. and Arias, A. M. (1994). Notch is required for *wingless* signaling in the epidemis of Drosophila. *Cell* **79**, pp. 259-272.

Couso, J. P., Bishop, S. A. and Martinez-Arias, A. (1994). The wingless signalling pathway and the patterning of the wing margin in *Drosophila*. *Development* **120**, pp. 621-636.

Crozatier, M., Glise, B. and Vincent, A. (2004). Patterns in evolution: veins of the Drosophila wing. *Trends Genet* **20**, 498-505.

Das, P., Maduzia, L. L., Wang, H., Finelli, A. L., Cho, S. H., Smith, M. M. and Padgett, R. W. (1998). The Drosophila gene Medea demonstrates the requirement for different classes of Smads in dpp signaling. *Development* **125**, 1519-28.

de Celis, J. F. (1997). Expression and function of decapentaplegic and thick veins during the differentiation of the veins in the Drosophila wing. *Development* **124**, 1007-18.

de Celis, J. F., Garcia-Bellido, A. and Bray, S. J. (1996). Activation and function of *Notch* at the dorsal-ventral boundary of the wing imaginal disc. *Development* **122**, pp. 359-369.

Diaz-Benjumea, F. and Cohen, S. (1995). Serrate signals through Notch to establish a Wingless-dependent organizer at the dorsal/ventral compartment boundary of the Drosophila wing. *Development* **121**, 4215-4225.

Diaz-Benjumea, F. J., Cohen, B. and Cohen, S. M. (1994). Cell interaction between compartments establishes the proximal-distal axis of Drosophila legs. *Nature* **372**, 175-9.

Doctor, J. S., Jackson, P. D., Rashka, K. E., Visalli, M. and Hoffmann, F. M. (1992). Sequence, biochemical characterization, and developmental expression of a new member of the TGF-beta superfamily in Drosophila melanogaster. *Dev Biol* **151**, 491-505.

Ebisawa, T., Fukuchi, M., Murakami, G., Chiba, T., Tanaka, K., Imamura, T. and Miyazono, K. (2001). Smurf1 interacts with transforming growth factor-beta type I receptor through Smad7 and induces receptor degradation. *J Biol Chem* **276**, 12477-80.

Eklof Spink, K., Fridman, S. G. and Weis, W. I. (2001). Molecular mechanisms of beta-catenin recognition by adenomatous polyposis coli revealed by the structure of an APC-beta-catenin complex. *Embo J* **20**, 6203-12.

Francois, V., Solloway, M., O'Neill, J. W., Emery, J. and Bier, E. (1994). Dorsal-ventral patterning of the Drosophila embryo depends on a putative negative growth factor encoded by the short gastrulation gene. *Genes Dev* **8**, 2602-16.

Freeman, M. (2000). Feedback control of intercellular signalling in development. *Nature* **408**, 313-9.

Fristrom, D., Wilcox, M. and Fristrom, J. (1993). The distribution of PS integrins, laminin A and F-actin during key stages in Drosophila wing development. *Development* **117**, 509-23.

Gerlitz, O. and Basler, K. (2002). Wingful, an extracellular feedback inhibitor of Wingless. *Genes Dev* **16**, 1055-9.

Glise, B., Jones, D. L. and Ingham, P. W. (2002). Notch and Wingless modulate the response of cells to Hedgehog signalling in the Drosophila wing. *Dev Biol* **248**, 93-106.

Golan, T., Yaniv, A., Bafico, A., Liu, G. and Gazit, A. (2004). The human Frizzled 6 (HFz6) acts as a negative regulator of the canonical Wnt. beta-catenin signaling cascade. *J Biol Chem* **279**, 14879-88. Epub 2004 Jan 27.

Graham, T. A., Ferkey, D. M., Mao, F., Kimelman, D. and Xu, W. (2001). Tcf4 can specifically recognize beta-catenin using alternative conformations. *Nat Struct Biol* **8**, 1048-52.

Graham, T. A., Weaver, C., Mao, F., Kimelman, D. and Xu, W. (2000). Crystal structure of a beta-catenin/Tcf complex. *Cell* **103**, 885-96.

Grieder, N. C., Nellen, D., Burke, R., Basler, K. and Affolter, M. (1995). Schnurri is required for Drosophila Dpp signaling and encodes a zinc finger protein similar to the mammalian transcription factor PRDII-BF1. *Cell* **81**, 791-800.

Grimm, O. H. and Gurdon, J. B. (2002). Nuclear exclusion of Smad2 is a mechanism leading to loss of competence. *Nat Cell Biol* **4**, 519-22.

Grimm, S. and Pflugfelder, G. O. (1996). Control of the gene optomotor-blind in Drosophila wing development by *decapentaplegic* and *wingless*. *Science* **271**, pp. 1601-1604.

Haerry, T. E., Khalsa, O., O'Connor, M. B. and Wharton, K. A. (1998). Synergistic signaling by two BMP ligands through the SAX and TKV receptors controls wing growth and patterning in Drosophila. *Development* **125**, 3977-87.

Hamada, F., Tomoyasu, Y., Takatsu, Y., Nakamura, M., Nagai, S., Suzuki, A., Fujita, F., Shibuya, H., Toyoshima, K., Ueno, N. et al. (1999). Negative regulation of Wingless signaling by D-axin, a Drosophila homolog of axin. *Science* **283**, 1739-42.

Harada, H., Yoshida, S., Nobe, Y., Ezura, Y., Atake, T., Koguchi, T. and Emi, M. (2002). Genomic structure of the human NLK (nemo-like kinase) gene and analysis of its promoter region. *Gene* **285**, 175-82.

Hata, A., Lo, R. S., Wotton, D., Lagna, G. and Massague, J. (1997). Mutations increasing autoinhibition inactivate tumour suppressors Smad2 and Smad4. *Nature* **388**, 82-7.

Henderson, B. R. and Fagotto, F. (2002). The ins and outs of APC and beta-catenin nuclear transport. *EMBO Rep* **3**, 834-9.

Hoffmans, R. and Basler, K. (2004). Identification and in vivo role of the Armadillo-Legless interaction. *Development* **131**, 4393-400.

Hooper, J. E. (1994). Distinct pathways for autocrine and paracrine Wingless signalling in Drosophila embryos. *Nature* **372**, 461-4.

Hoppler, S. and Bienz, M. (1995). Two different thresholds of wingless signalling with distinct developmental consequences in the Drosophila midgut. *Embo J* **14**, 5016-26.

Hu, M. C. and Rosenblum, N. D. (2005). Smad1, beta-catenin and Tcf4 associate in a molecular complex with the Myc promoter in dysplastic renal tissue and cooperate to control Myc transcription. *Development* **132**, 215-25.

Huber, A. H. and Weis, W. I. (2001). The structure of the beta-catenin/E-cadherin complex and the molecular basis of diverse ligand recognition by beta-catenin. *Cell* **105**, 391-402.

Huber, O., Korn, R., McLaughlin, J., Ohsugi, M., Herrmann, B. G. and Kemler, R. (1996). Nuclear localization of beta-catenin by interaction with transcription factor LEF-1. *Mech Dev* **59**, 3-10.

Hudson, J. B., Podos, S. D., Keith, K., Simpson, S. L. and Ferguson, E. L. (1998). The Drosophila Medea gene is required downstream of dpp and encodes a functional homolog of human Smad4. *Development* **125**, 1407-20.

Hulsken, J., Birchmeier, W. and Behrens, J. (1994). E-cadherin and APC compete for the interaction with beta-catenin and the cytoskeleton. *J Cell Biol* **127**, 2061-9.

Hyodo-Miura, J., Urushiyama, S., Nagai, S., Nishita, M., Ueno, N. and Shibuya, H. (2002). Involvement of NLK and Sox11 in neural induction in Xenopus development. *Genes to Cells* 7, 487-496.

Inoue, H., Imamura, T., Ishidou, Y., Takase, M., Udagawa, Y., Oka, Y., Tsuneizumi, K., Tabata, T., Miyazono, K. and Kawabata, M. (1998). Interplay of signal mediators of decapentaplegic (Dpp): molecular characterization of mothers against dpp, Medea, and daughters against dpp. *Mol Biol Cell* **9**, 2145-56.

Irvine, K. D. and Vogt, T. F. (1997). Dorsal-ventral signaling in limb development. *Curr Opin Cell Biol* **9**, 867-76.

Ishitani, T., Kishida, S., Hyodo-Miura, J., Ueno, N., Yasuda, J., Waterman, M., Shibuya, H., Moon, R. T., Ninomiya-Tsuji, J. and Matsumoto, K. (2003a). The TAK1-NLK mitogen-activated protein kinase cascade functions in the Wnt-5a/Ca(2+) pathway to antagonize Wnt/beta-catenin signaling. *Mol Cell Biol* **23**, 131-9.

Ishitani, T., Ninomiya-Tsuji, J. and Matsumoto, K. (2003b). Regulation of lymphoid enhancer factor 1/T-cell factor by mitogen-activated protein kinase-related Nemo-like kinase-dependent phosphorylation in Wnt/beta-catenin signaling. *Mol Cell Biol* **23**, 1379-89.

Ishitani, T., Ninomiya-Tsuji, J., Nagai, S., Nishita, M., Meneghini, M., Barker, N., Waterman, M., Bowerman, B., Clevers, H., Shibuya, H. et al. (1999). The TAK1-NLK-MAPK-related pathway antagonizes signalling between beta- catenin and transcription factor TCF [In Process Citation]. *Nature* **399**, 798-802.

Ito, K., Awano, W., Suzuki, K., Hiromi, Y. and Yamamoto, D. (1997). The Drosophila mushroom body is a quadruple structure of clonal units each of which contains a virtually identical set of neurones and glial cells. *Development* **124**, 761-71.

Jazwinska, A., Kirov, N., Wieschaus, E., Roth, S. and Rushlow, C. (1999). The Drosophila gene brinker reveals a novel mechanism of Dpp target gene regulation. *Cell* **96**, 563-73.

Jho, E. H., Zhang, T., Domon, C., Joo, C. K., Freund, J. N. and Costantini, F. (2002). Wnt/beta-catenin/Tcf signaling induces the transcription of Axin2, a negative regulator of the signaling pathway. *Mol Cell Biol* **22**, 1172-83.

Jiang, J. and Struhl, G. (1996). Complementary and mutually exclusive activities of decapentaplegic and wingless organize axial patterning during Drosophila leg development. *Cell* **86**, 401-9.

Johnston, L. A. and Schubiger, G. (1996). Ectopic expression of wingless in imaginal discs interferes with decapentaplegic expression and alters cell determination. *Development* **122**, 3519-29.

Kanei-Ishii, C., Ninomiya-Tsuji, J., Tanikawa, J., Nomura, T., Ishitani, T., Kishida, S., Kokura, K., Kurahashi, T., Ichikawa-Iwata, E., Kim, Y. et al. (2004). Wnt-1 signal induces phosphorylation and degradation of c-Myb protein via TAK1, HIPK2, and NLK. *Genes Dev* **18**, 816-29.

Kawabata, M., Inoue, H., Hanyu, A., Imamura, T. and Miyazono, K. (1998). Smad proteins exist as monomers in vivo and undergo homo- and hetero-oligomerization upon activation by serine/threonine kinase receptors. *Embo J* **17**, 4056-65.

Kehrer-Sawatzki, H., Moschgath, E., Maier, C., Legius, E., Elgar, G. and Krone, W. (2000). Characterization of the Fugu rubripes NLK and FN5 genes flanking the NF1 (Neurofibromatosis type 1) gene in the 5' direction and mapping of the human counterparts. *Gene* **251**, 63-71.

Khalsa, O., Yoon, J. W., Torres-Schumann, S. and Wharton, K. A. (1998). TGF-beta/BMP superfamily members, Gbb-60A and Dpp, cooperate to provide pattern information and establish cell identity in the Drosophila wing. *Development* **125**, 2723-34.

Kim, J., Johnson, K., Chen, H. J., Carroll, S. and Laughon, A. (1997). Drosophila Mad binds to DNA and directly mediates activation of vestigial by Decapentaplegic. *Nature* **388**, 304-8.

Klein, T. (2001). Wing disc development in the fly: the early stages. *Curr Opin Genet Dev* **11**, 470-5.

Klein, T. and Arias, A. M. (1999). The vestigial gene product provides a molecular context for the interpretation of signals during the development of the wing in Drosophila. *Development* **126**, 913-25.

Koh, T. J., Bulitta, C. J., Fleming, J. V., Dockray, G. J., Varro, A. and Wang, T. C. (2000). Gastrin is a target of the beta-catenin/TCF-4 growth-signaling pathway in a model of intestinal polyposis. *J Clin Invest* **106**, 533-9.

Korinek, V., Barker, N., Moerer, P., van Donselaar, E., Huls, G., Peters, P. J. and Clevers, H. (1998). Depletion of epithelial stem-cell compartments in the small intestine of mice lacking Tcf-4. *Nat Genet* **19**, 379-83.

Korinek, V., Barker, N., Morin, P. J., van Wichen, D., de Weger, R., Kinzler, K. W., Vogelstein, B. and Clevers, H. (1997). Constitutive transcriptional activation by a beta-catenin-Tcf complex in APC-/- colon carcinoma. *Science* **275**, 1784-7.

Kramps, T., Peter, O., Brunner, E., Nellen, D., Froesch, B., Chatterjee, S., Murone, M., Zullig, S. and Basler, K. (2002). Wnt/wingless signaling requires BCL9/legless-

mediated recruitment of pygopus to the nuclear beta-catenin-TCF complex. *Cell* **109**, 47-60.

Kretzschmar, M., Doody, J. and Massague, J. (1997). Opposing BMP and EGF signalling pathways converge on the TGF-beta family mediator Smad1. *Nature* **389**, 618-22.

Kretzschmar, M., Doody, J., Timokhina, I. and Massague, J. (1999). A mechanism of repression of TGFbeta/ Smad signaling by oncogenic Ras. *Genes Dev* **13**, 804-16.

Labbe, E., Letamendia, A. and Attisano, L. (2000). Association of Smads with lymphoid enhancer binding factor 1/T cell-specific factor mediates cooperative signaling by the transforming growth factor-beta and wnt pathways. *Proc Natl Acad Sci U S A* **97**, 8358-63.

Lawrence, P. A. and Struhl, G. (1996). Morphogens, compartments, and pattern: lessons from drosophila? *Cell* **85**, 951-61.

Lecuit, T. and Cohen, S. M. (1998). Dpp receptor levels contribute to shaping the Dpp morphogen gradient in the Drosophila wing imaginal disc. *Development* **125**, 4901-7.

Lecuit, T., Brook, W. J., Ng, M., Calleja, M., Sun, H. and Cohen, S. M. (1996). Two distinct mechanisms for long-range patterning by Decapentaplegic in the Drosophila wing. *Nature* **381**, 387-93.

Lei, S., Dubeykovskiy, A., Chakladar, A., Wojtukiewicz, L. and Wang, T. C. (2004). The murine gastrin promoter is synergistically activated by transforming growth factor-beta/Smad and Wnt signaling pathways. *J Biol Chem* **279**, 42492-502.

Lin, R., Thompson, S. and Priess, J. R. (1995). pop-1 encodes an HMG box protein required for the specification of a mesoderm precursor in early C. elegans embryos. *Cell* **83**, 599-609.

Liu, F., Pouponnot, C. and Massague, J. (1997). Dual role of the Smad4/DPC4 tumor suppressor in TGFbeta-inducible transcriptional complexes. *Genes Dev* **11**, 3157-67.

Logan, C. Y. and Nusse, R. (2004). The Wnt signaling pathway in development and disease. *Annu Rev Cell Dev Biol* **20**, 781-810.

Macias-Silva, M., Abdollah, S., Hoodless, P. A., Pirone, R., Attisano, L. and Wrana, J. L. (1996). MADR2 is a substrate of the TGFbeta receptor and its phosphorylation is required for nuclear accumulation and signaling. *Cell* **87**, 1215-24.

Marques, G., Musacchio, M., Shimell, M. J., Wunnenberg-Stapleton, K., Cho, K. W. and O'Connor, M. B. (1997). Production of a DPP activity gradient in the early Drosophila embryo through the opposing actions of the SOG and TLD proteins. *Cell* **91**, 417-26.

Martinez Arias, A. (2003). Wnts as morphogens? The view from the wing of Drosophila. *Nat Rev Mol Cell Biol* **4**, 321-5.

Martinez Arias, A., Brown, A. M. and Brennan, K. (1999). Wnt signalling: pathway or network? *Curr Opin Genet Dev* **9**, 447-54.

Massague, J. (1998). TGF-beta signal transduction. *Annu Rev Biochem* **67**, 753-91.

Massague, J. (2003). Integration of Smad and MAPK pathways: a link and a linker revisited. *Genes Dev* **17**, 2993-7.

Massague, J. and Chen, Y. G. (2000). Controlling TGF-beta signaling. *Genes Dev* **14**, 627-44.

Meneghini, M. D., Ishitani, T., Carter, J. C., Hisamoto, N., Ninomiya-Tsuji, J., Thorpe, C. J., Hamill, D. R., Matsumoto, K. and Bowerman, B. (1999). MAP kinase and Wnt pathways converge to downregulate an HMG-domain repressor in Caenorhabditis elegans [In Process Citation]. *Nature* **399**, 793-7.

Minami, M., Kinoshita, N., Kamoshida, Y., Tanimoto, H. and Tabata, T. (1999). brinker is a target of Dpp in Drosophila that negatively regulates Dpp- dependent genes. *Nature* **398**, 242-6.

Mirkovic, I., Charish, K., Gorski, S. M., McKnight, K. and Verheyen, E. M. (2002). Drosophila nemo is an essential gene involved in the regulation of programmed cell death. *Mechanisms of Development* **119**, 9-20.

Mohit, P., Bajpai, R. and Shashidhara, L. S. (2003). Regulation of Wingless and Vestigial expression in wing and haltere discs of Drosophila. *Development* **130**, 1537-47.

Molenaar, M., van de Wetering, M., Oosterwegel, M., Peterson-Maduro, J., Godsave, S., Korinek, V., Roose, J., Destree, O. and Clevers, H. (1996). XTcf-3 transcription factor mediates beta-catenin-induced axis formation in Xenopus embryos. *Cell* **86**, 391-9.

Morata, G. and Lawrence, P. A. (1977). The development of wingless, a homeotic mutation of Drosophila. *Dev Biol* **56**, 227-40.

Morimura, S., Maves, L., Chen, Y. and Hoffmann, F. M. (1996). decapentaplegic overexpression affects Drosophila wing and leg imaginal disc development and wingless expression. *Dev Biol* **177**, 136-51.

Moustakas, A., Souchelnytskyi, S. and Heldin, C. H. (2001). Smad regulation in TGF-beta signal transduction. *J Cell Sci* **114**, 4359-69.

Mullor, J. L., Calleja, M., Capdevila, J. and Guerrero, I. (1997). Hedgehog activity, independent of decapentaplegic, participates in wing disc patterning. *Development* **124**, 1227-37.

Munemitsu, S., Albert, I., Rubinfeld, B. and Polakis, P. (1996). Deletion of an amino-terminal sequence beta-catenin in vivo and promotes hyperphosporylation of the adenomatous polyposis coli tumor suppressor protein. *Mol Cell Biol* **16**, 4088-94.

Nellen, D., Burke, R., Struhl, G. and Basler, K. (1996). Direct and long-range action of a DPP morphogen gradient. *Cell* **85**, 357-68.

Neumann, C. J. and Cohen, S. M. (1996). A hierarchy of cross-regulation involving Notch, wingless, vestigial and cut organizes the dorsal/ventral axis of the Drosophila wing. *Development* **122**, 3477-85.

Neumann, C. J. and Cohen, S. M. (1997). Long-range action of Wingless organizes the dorsal-ventral axis of the Drosophila wing. *Development* **124**, 871-80.

Ng, M., Diaz-Benjumea, F. J., Vincent, J. P., Wu, J. and Cohen, S. M. (1996). Specification of the wing by localized expression of wingless protein. *Nature* **381**, 316-8.

Ninomiya-Tsuji, J., Kishimoto, K., Hiyama, A., Inoue, J., Cao, Z. and Matsumoto, K. (1999). The kinase TAK1 can activate the NIK-1 kappaB as well as the MAP kinase cascade in the IL-1 signalling pathway. *Nature* **398**, 252-6.

Nishita, M., Hashimoto, M. K., Ogata, S., Laurent, M. N., Ueno, N., Shibuya, H. and Cho, K. W. (2000). Interaction between Wnt and TGF-beta signalling pathways during formation of Spemann's organizer. *Nature* **403**, 781-5.

Nusse, R. and Varmus, H. E. (1982). Many tumors induced by the mouse mammary tumor virus contain a provirus integrated in the same region of the host genome. *Cell* **31**, 99-109.

Ohkawara, B., Shirakabe, K., Hyodo-Miura, J., Matsuo, R., Ueno, N., Matsumoto, K. and Shibuya, H. (2004). Role of the TAK1-NLK-STAT3 pathway in TGF-beta-mediated mesoderm induction. *Genes Dev* **18**, 381-6.

Omer, C. A., Miller, P. J., Diehl, R. E. and Kral, A. M. (1999). Identification of Tcf4 residues involved in high-affinity beta-catenin binding. *Biochem Biophys Res Commun* **256**, 584-90.

Orsulic, S. and Peifer, M. (1996). An in vivo structure-function study of armadillo, the beta-catenin homologue, reveals both separate and overlapping regions of the protein required for cell adhesion and for wingless signaling. *J Cell Biol* **134**, 1283-300.

Padgett, R. W., St Johnston, R. D. and Gelbart, W. M. (1987). A transcript from a Drosophila pattern gene predicts a protein homologous to the transforming growth factor-beta family. *Nature* **325**, 81-4.

Peifer, M., Rauskolb, C., Williams, M., Riggleman, B. and Wieschaus, E. (1991). The segment polarity gene armadillo interacts with the wingless signaling pathway in both embryonic and adult pattern formation. *Development* **111**, 1029-43.

Pera, E. M., Ikeda, A., Eivers, E. and De Robertis, E. M. (2003). Integration of IGF, FGF, and anti-BMP signals via Smad1 phosphorylation in neural induction. *Genes Dev* **17**, 3023-8.

Perrimon, N. and McMahon, A. P. (1999). Negative feedback mechanisms and their roles during pattern formation. *Cell* **97**, 13-6.

Phillips, R. G. and Whittle, J. R. (1993). wingless expression mediates determination of peripheral nervous system elements in late stages of Drosophila wing disc development. *Development* **118**, 427-38.

Phillips, R. G., Warner, N. L. and Whittle, J. R. (1999). Wingless signaling leads to an asymmetric response to decapentaplegic-dependent signaling during sense organ patterning on the notum of Drosophila melanogaster. *Dev Biol* **207**, 150-62.

Pradeep, A., Sharma, C., Sathyanarayana, P., Albanese, C., Fleming, J. V., Wang, T. C., Wolfe, M. M., Baker, K. M., Pestell, R. G. and Rana, B. (2004). Gastrin-mediated activation of cyclin D1 transcription involves beta-catenin and CREB pathways in gastric cancer cells. *Oncogene* **23**, 3689-99.

Raftery, L. A. and Sutherland, D. J. (1999). TGF-beta family signal transduction in Drosophila development: from Mad to Smads. *Dev Biol* **210**, 251-68.

Ray, R. P. and Wharton, K. A. (2001). Context-dependent relationships between the BMPs gbb and dpp during development of the Drosophila wing imaginal disk. *Development* **128**, 3913-25.

Riese, J., Yu, X., Munnerlyn, A., Eresh, S., Hsu, S. C., Grosschedl, R. and Bienz, M. (1997). LEF-1, a nuclear factor coordinating signaling inputs from wingless and decapentaplegic. *Cell* **88**, 777-87.

Rocheleau, C. E., Yasuda, J., Shin, T. H., Lin, R., Sawa, H., Okano, H., Priess, J. R., Davis, R. J. and Mello, C. C. (1999). WRM-1 activates the LIT-1 protein kinase to transduce anterior/posterior polarity signals in C. elegans [In Process Citation]. *Cell* **97**, 717-26.

Roose, J., Huls, G., van Beest, M., Moerer, P., van der Horn, K., Goldschmeding, R., Logtenberg, T. and Clevers, H. (1999). Synergy between tumor suppressor APC and the beta-catenin-Tcf4 target Tcf1. *Science* **285**, 1923-6.

Rousset, R., Mack, J. A., Wharton, K. A., Jr., Axelrod, J. D., Cadigan, K. M., Fish, M. P., Nusse, R. and Scott, M. P. (2001). Naked cuticle targets dishevelled to antagonize Wnt signal transduction. *Genes Dev* **15**, 658-71.

Rulifson, E. J. and Blair, S. S. (1995). *Notch* regulates *wingless* expression and is not required for reception of the paracrine *wingless* signal during wing margin neurogenesis in *Drosophila*. *Development* **121**, pp. 2813-1824.

Rulifson, E. J., Micchelli, C. A., Axelrod, J. D., Perrimon, N. and Blair, S. S. (1996). wingless refines its own expression domain on the Drosophila wing margin. *Nature* **384**, 72-4.

Schweizer, L., Nellen, D. and Basler, K. (2003). Requirement for Pangolin/dTCF in Drosophila Wingless signaling. *Proc Natl Acad Sci U S A* **100**, 5846-51. Epub 2003 May 1.

Segal, D. and Gelbart, W. M. (1985). Shortvein, a new component of the decapentaplegic gene complex in Drosophila melanogaster. *Genetics* **109**, 119-43.

Shi, Y. and Massague, J. (2003). Mechanisms of TGF-beta signaling from cell membrane to the nucleus. *Cell* **113**, 685-700.

Shi, Y., Hata, A., Lo, R. S., Massague, J. and Pavletich, N. P. (1997). A structural basis for mutational inactivation of the tumour suppressor Smad4. *Nature* **388**, 87-93.

Shibuya, H., Yamaguchi, K., Shirakabe, K., Tonegawa, A., Gotoh, Y., Ueno, N., Irie, K., Nishida, E. and Matsumoto, K. (1996). TAB1: an activator of the TAK1 MAPKKK in TGF-beta signal transduction. *Science* **272**, 1179-82.

Shin, T., Yasuda, J., Rocheleau, C., Lin, R., Soto, M., Bei, X., davis, R. and Mello, C. (1999). MOM-4, a MAP kinase kinase kinase-related protein, activates WRM-1/LIT-1 kinase to transduce anterior/posterior polarity signals in *C. elegans*. *Mol. Cell* **4**, 275-280.

Shirakabe, K., Yamaguchi, K., Shibuya, H., Irie, K., Matsuda, S., Moriguchi, T., Gotoh, Y., Matsumoto, K. and Nishida, E. (1997). TAK1 mediates the ceramide signaling to stress-activated protein kinase/c-Jun N-terminal kinase. *J Biol Chem* **272**, 8141-4.

Simpson, P. and Carteret, C. (1989). A study of shaggy reveals spatial domains of expression of achaete-scute alleles on the thorax of Drosophila. *Development* **106**, 57-66.

Smit, L., Baas, A., Kuipers, J., Korswagen, H., van de Wetering, M. and Clevers, H. (2004). Wnt activates the Tak1/Nemo-like kinase pathway. *J Biol Chem* **279**, 17232-40. Epub 2004 Feb 11.

Spencer, F. A., Hoffmann, F. M. and Gelbart, W. M. (1982). Decapentaplegic: A gene complex affecting morphogenesis in Drosophila melanogaster. *Cell* **28** 451-461.

Spiegelman, V. S., Slaga, T. J., Pagano, M., Minamoto, T., Ronai, Z. and Fuchs, S. Y. (2000). Wnt/beta-catenin signaling induces the expression and activity of betaTrCP ubiquitin ligase receptor. *Mol Cell* **5**, 877-82.

Strigini, M. and Cohen, S. M. (1997). A Hedgehog activity gradient contributes to AP axial patterning of the Drosophila wing. *Development* **124**, 4697-705.

Strutt, D., Weber, U. and Mlodzik, M. (1997). The role of RhoA in tissue polarity and Frizzled signaling. *Nature* **387**, 292-295.

Tajima, Y., Goto, K., Yoshida, M., Shinomiya, K., Sekimoto, T., Yoneda, Y., Miyazono, K. and Imamura, T. (2003). Chromosomal region maintenance 1 (CRM1)-dependent nuclear export of Smad ubiquitin regulatory factor 1 (Smurf1) is essential for negative regulation of transforming growth factor-beta signaling by Smad7. *J Biol Chem* **278**, 10716-21.

Takaesu, G., Kishida, S., Hiyama, A., Yamaguchi, K., Shibuya, H., Irie, K., Ninomiya-Tsuji, J. and Matsumoto, K. (2000). TAB2, a novel adaptor protein, mediates activation of TAK1 MAPKKK by linking TAK1 to TRAF6 in the IL-1 signal transduction pathway. *Mol Cell* **5**, 649-58.

Takaesu, G., Surabhi, R. M., Park, K. J., Ninomiya-Tsuji, J., Matsumoto, K. and Gaynor, R. B. (2003). TAK1 is critical for IkappaB kinase-mediated activation of the NF-kappaB pathway. *J Mol Biol* **326**, 105-15.

Tanimoto, H., Itoh, S., ten Dijke, P. and Tabata, T. (2000). Hedgehog creates a gradient of DPP activity in Drosophila wing imaginal discs. *Mol Cell* **5**, 59-71.

Teleman, A. A. and Cohen, S. M. (2000). Dpp gradient formation in the Drosophila wing imaginal disc. *Cell* **103**, 971-80.

ten Dijke, P. and Hill, C. S. (2004). New insights into TGF-beta-Smad signalling. *Trends Biochem Sci* **29**, 265-73.

Theisen, H., Haerry, T. E., O'Connor, M. B. and Marsh, J. L. (1996). Developmental territories created by mutual antagonism between Wingless and Decapentaplegic. *Development* **122**, 3939-48.

Thorpe, C. J., Moon, R. T., Kanei-Ishii, C., Ninomiya-Tsuji, J., Tanikawa, J., Nomura, T., Ishitani, T., Kishida, S., Kokura, K., Kurahashi, T. et al. (2004). nemo-like kinase is an essential co-activator of Wnt signaling during early zebrafish development

Tolwinski, N. S. and Wieschaus, E. (2001). Armadillo nuclear import is regulated by cytoplasmic anchor Axin and nuclear anchor dTCF/Pan. *Development* **128**, 2107-17.

Townsley, F. M., Cliffe, A. and Bienz, M. (2004). Pygopus and Legless target Armadillo/beta-catenin to the nucleus to enable its transcriptional co-activator function. *Nat Cell Biol* **6**, 626-33.

Tsuneizumi, K., Nakayama, T., Kamoshida, Y., Kornberg, T. B., Christian, J. L. and Tabata, T. (1997). Daughters against dpp modulates dpp organizing activity in Drosophila wing development. *Nature* **389**, 627-31.

Tsuneizumi, K., Nakayama, T., Kamoshida, Y., Kornberg, T. B., Christian, J. L. and Tabata, T. (1997). Daughters against dpp modulates dpp organizing activity in Drosophila wing development. *Nature* **389**, 627-31.

van de Wetering, M., Cavallo, R., Dooijes, D., van Beest, M., van Es, J., Loureiro, J., Ypma, A., Hursh, D., Jones, T., Bejsovec, A. et al. (1997). Armadillo coactivates transcription driven by the product of the Drosophila segment polarity gene dTCF. *Cell* **88**, 789-99.

van de Wetering, M., Oosterwegel, M., Dooijes, D. and Clevers, H. (1991). Identification and cloning of TCF-1, a T lymphocyte-specific transcription factor containing a sequence-specific HMG box. *Embo J* **10**, 123-32.

van Noort, M. and Clevers, H. (2002). TCF transcription factors, mediators of Wnt-signaling in development and cancer. *Dev Biol* **244**, 1-8.

Verheyen, E. M., Mirkovic, I., MacLean, S. J., Langmann, C., Andrews, B. C. and MacKinnon, C. (2001). The tissue polarity gene *nemo* carries out multiple roles in patterning during Drosophila development. *Mech. Dev.* **101**, 119-132.

Verheyen, E. M., Purcell, K. J., Fortini, M. E. and Artavanis-Tsakonas, S. (1996). Analysis of dominant enhancers and suppressors of activated *Notch* in *Drosophila*. *Genetics* **144**, 1127-1141.

von Bubnoff, A. and Cho, K. W. (2001). Intracellular BMP signaling regulation in vertebrates: pathway or network? *Dev Biol* **239**, 1-14.

Waltzer, L. and Bienz, M. (1998). Drosophila CBP represses the transcription factor TCF to antagonize Wingless signalling. *Nature* **395**, 521-5.

Wang, C., Deng, L., Hong, M., Akkaraju, G. R., Inoue, J. and Chen, Z. J. (2001). TAK1 is a ubiquitin-dependent kinase of MKK and IKK. *Nature* **412**, 346-51.

Wharton, K. A., Cook, J. M., Torres-Schumann, S., de Castro, K., Borod, E. and Phillips, D. A. (1999). Genetic analysis of the bone morphogenetic protein-related gene, gbb, identifies multiple requirements during Drosophila development. *Genetics* **152**, 629-40.

Wharton, K. A., Thomsen, G. H. and Gelbart, W. M. (1991). Drosophila 60A gene, another transforming growth factor beta family member, is closely related to human bone morphogenetic proteins. *Proc Natl Acad Sci U S A* **88**, 9214-8.

Willert, K., Logan, C. Y., Arora, A., Fish, M. and Nusse, R. (1999). A Drosophila Axin homolog, Daxin, inhibits Wnt signaling. *Development* **126**, 4165-73.

Williams, J. A., Paddock, S. W. and Carroll, S. B. (1993). Pattern formation in a secondary field: a hierarchy of regulatory genes subdivides the developing Drosophila wing disc into discrete subregions. *Development* **117**, 571-84.

Wisotzkey, R. G., Mehra, A., Sutherland, D. J., Dobens, L. L., Liu, X., Dohrmann, C., Attisano, L. and Raftery, L. A. (1998). Medea is a Drosophila Smad4 homolog that is differentially required to potentiate DPP responses. *Development* **125**, 1433-45.

Wnt-1 signal induces phosphorylation and degradation of c-Myb protein via TAK1, HIPK2, and NLK

Wnt Homepage, http://www.stanford.edu/~rnusse/wntwindow.html.

Wu, J. and Cohen, S. M. (1999). Proximodistal axis formation in the Drosophila leg: subdivision into proximal and distal domains by Homothorax and Distal-less. *Development* **126**, 109-17.

Wu, J. and Cohen, S. M. (2000). Proximal distal axis formation in the Drosophila leg: distinct functions of teashirt and homothorax in the proximal leg. *Mech Dev* **94**, 47-56.

Wu, J. and Cohen, S. M. (2002). Repression of Teashirt marks the initiation of wing development. *Development* **129**, 2411-8.

Xiao, Z., Watson, N., Rodriguez, C. and Lodish, H. F. (2001). Nucleocytoplasmic shuttling of Smad1 conferred by its nuclear localization and nuclear export signals. *J Biol Chem* **276**, 39404-10.

Xing, Y., Clements, W. K., Kimelman, D. and Xu, W. (2003). Crystal structure of a beta-catenin/axin complex suggests a mechanism for the beta-catenin destruction complex. *Genes Dev* **17**, 2753-64.

Xu, T., and G.M. Rubin. (1993). Analysis of Genetic Mosaics in Developing And Adult Drosophila Tissues. *Development* **117**, 1223-1237.

Yamada, M., Ohkawara, B., Ichimura, N., Hyodo-Miura, J., Urushiyama, S., Shirakabe, K. and Shibuya, H. (2003). Negative regulation of Wnt signalling by HMG2L1, a novel NLK-binding protein. *Genes Cells* **8**, 677-84.

Yamada, M., Ohkawara, B., Ichimura, N., Hyodo-Miura, J., Urushiyama, S., Shirakabe, K. and Shibuya, H. (2003). Negative regulation of Wnt signalling by HMG2L1, a novel NLK-binding protein. *Genes Cells* **8**, 677-84.

Yamaguchi, K., Shirakabe, K., Shibuya, H., Irie, K., Oishi, I., Ueno, N., Taniguchi, T., Nishida, E. and Matsumoto, K. (1995). Identification of a member of the MAPKKK family as a potential mediator of TGF-beta signal transduction. *Science* **270**, 2008-11.

Yang, X., van Beest, M., Clevers, H., Jones, T., Hursh, D. A. and Mortin, M. A. (2000). decapentaplegic is a direct target of dTcf repression in the Drosophila visceral mesoderm. *Development* **127**, 3695-702.

Yasuda, J., Yokoo, H., Yamada, T., Kitabayashi, I., Sekiya, T. and Ichikawa, H. (2004). Nemo-like kinase suppresses a wide range of transcription factors, including nuclear factor-kappaB. *Cancer Sci* **95**, 52-7.

Yost, C., Torres, M., Miller, J. R., Huang, E., Kimelman, D. and Moon, R. T. (1996). The axis-inducing activity, stability, and subcellular distribution of beta-catenin is regulated in Xenopus embryos by glycogen synthase kinase 3. *Genes Dev* **10**, 1443-54.

Yu, K., Srinivasan, S., Shimmi, O., Biehs, B., Rashka, K. E., Kimelman, D., O'Connor, M. B. and Bier, E. (2000). Processing of the Drosophila Sog protein creates a novel BMP inhibitory activity. *Development* **127**, 2143-54.

Yu, K., Sturtevant, M. A., Biehs, B., Francois, V., Padgett, R. W., Blackman, R. K. and Bier, E. (1996). The Drosophila decapentaplegic and short gastrulation genes function antagonistically during adult wing vein development. *Development* **122**, 4033-44.

Yu, X., Riese, J., Eresh, S. and Bienz, M. (1998). Transcriptional repression due to high levels of Wingless signalling. *Embo J* **17**, 7021-32.

Zecca, M., Basler, K. and Struhl, G. (1996). Direct and long-range action of a wingless morphogen gradient. *Cell* **87**, 833-44.

Zeng, W., Wharton, K. A., Jr., Mack, J. A., Wang, K., Gadbaw, M., Suyama, K., Klein, P. S. and Scott, M. P. (2000). naked cuticle encodes an inducible antagonist of Wnt signalling. *Nature* **403**, 789-95.

Zeng, Y. A. and Verheyen, E. M. (2004). Nemo is an inducible antagonist of Wingless signaling during Drosophila wing development. *Development* **131**, 2911-2920.

Zhang, J. and Carthew, R. W. (1998). Interactions between Wingless and DFz2 during Drosophila wing development. *Development* **125**, 3075-85.